Fabrication of Biocompatible Microstructures to Support Tissue Regeneration

By

Perla Ayala

A dissertation submitted in partial satisfaction of the

requirements for the degree of

Joint Doctor of Philosophy

with the University of California, San Francisco

in

Bioengineering

in the

Graduate Division

of the

University of California, Berkeley

Committee in charge:

Professor Tejal A. Desai
Professor Sanjay Kumar
Professor Ting Xu

Fall 2011

Abstract

Fabrication of Biocompatible Microstructures to Support Tissue Regeneration

Perla Ayala

Joint Doctor of Philosophy in Bioengineering
with the University of California, San Francisco,

University of California, Berkeley

Professor Tejal A. Desai, Chair

Cardiac fibrosis is considered to be an independent risk factor in the outcome of congestive heart failure. Heart transplantation is the only treatment for patients who are at the end stage of this condition. Shortage of donor organs has created a need for therapeutic alternatives. This dissertation investigates new strategies for cardiac repair systems that could reduce pathological fibrosis and promote growth of myocytes at the site of injury. Design of successful engineered therapies for tissue regeneration relies on discerning how cell behavior can be modulated by chemical and physical cues. Recent studies have shown that external physical cues such as stiffness and geometry can affect cell morphology and function. In this work, the combinatorial effect of stiffness and micro-scale topographical cues on proliferation and gene expression is investigated in 2D and 3D. The 2D system consists of fibroblasts grown on "micropegged" polydimethylsiloxane (PDMS) substrates of different stiffness. The 3D system consists of fibroblasts encapsulated with poly(ethylene glycol) dimethacrylate (PEGDMA) "microrods" of different stiffness in matrigel to create a 3D culture with micro-scale cues of defined mechanical properties in the physiological range.

Fibroblasts cultured on micropegged substrates have reduced collagen expression compared to fibroblasts cultured on flat substrates. Cells on stiffer micropegged substrates exhibit down regulation of important regulators of ECM synthesis but there is no down-regulation of these markers when cells are cultured on the softer micropegged substrates. Similarly, three-dimensional cultures with stiffer microrods show reduced fibroblast proliferation and down-regulation of collagen and other important regulators of ECM synthesis, but three dimensional cultures with soft microrods do not show significant difference on fibroblast proliferation and expression of some ECM regulators compared to cultures with no microrods.

To determine whether microrods can influence myocardial repair and remodeling *in vivo,* adult female Sprague-Dawley rats undergo left anterior descending (LAD) artery occlusion for thirty minutes followed by reperfusion. Microrods suspended in PBS are injected into the left ventricle (LV) two days after myocardial infarction (MI). Five weeks after the injections echocardiography reveals an increase in ejection fraction (EF) in the microrod group compared to the PBS control. Histology analysis shows a trend on decreased amount

of scar formation and increased wall thickness of the microrod treated group compared to the PBS control.

Furthermore, it is shown that microrods can be utilized as growth factor delivery devices. Mechano growth factor (MGF) is expressed rapidly after tissue damage and prevents apoptosis in the myocardium; thus is considered a suitable therapeutic candidate for cardiac repair. Here, it is shown that microrods can be loaded with MGF and that the peptide can be eluted from the microrods for a period of days. Bioactivity of MGF is confirmed by analyzing stem cell migration and myoblast proliferation. Interestingly, it is also observed that myoblast's interaction with microrods can enhance proliferation even after seven days of culture. These studies indicate that microrods protect rapid degradation of MGF, promote stem cell migration and enhance myoblast proliferation.

Results from this work will help create more tunable *in vitro* tissue engineered platforms and develop new therapeutic approaches for *in vivo* tissue regeneration.

DEDICATION

I thank God for all the blessings in my life including the opportunity to pursue my dreams and for guiding me through the process.

This dissertation is dedicated to my grandparents Gustavo and Ramona Martos, to my parents Gonzalo and Martha Ayala, to my siblings Angelica, Gonzalo, Jose Manuel and Juan Carlos, and to my husband Jose Luis Ramirez all who unconditionally love me and believe in me.

TABLE OF CONTENTS

LIST OF FIGURES

LIST OF TABLES

ACKNOWLEDGEMENTS

I want to give special thanks to my research advisor, Professor Tejal Desai for her support, guidance, and mentoring during my research tenure in her lab. I believe innovative research is accomplished in an open and collaborative environment and her lab is certainly characterized by that atmosphere. I would also like to thank other professors who have also supported and mentored me during this process: Sanjay Kumar, Jeff Lotz, Randall Lee, Lydia Sohn, Ting Xu, and David Schaffer.

I would like to thank the members of the Lee Lab that provided time and training during the course of the in vivo experiments especially Kim Du, Jiashing Yu, Richard Sievers and Qizhi Fang. I would also like to thank Jose I. Lopez and the members of the Weaver lab who helped me with AFM measurements.

I am very grateful for all those who have shared their time and insight in topics from personal to scientific: Kristy Aisnlie, Rahul Thakar, James Norman, Jose I. Lopez, Azucena Rodriguez, Aliza Allon, Alana Lerner, Lily Peng, Kayte Fischer, Adam Mendelosohn, Lalitha Muthusubramanian, Kelly Chavez, Rachel Lowe, Rob Tucker, Jennifer Wade, James Pinney and all the past and present members of the Desai Lab.

I am also very grateful for the fellowships and scholarships that supported me through my PhD tenure including a National Science Foundation graduate research fellowship, a University of California Berkeley Chancellor's fellowship, and a UC Berkeley College of Engineering Macchi Fellowship & McCamish Scholarship.

This dissertation includes work that has been previously published and co-authored. Chapter 2 was previously published as *Chapter 24: Fabrication of Cell Mircrointegrated Tissues* in The Handbook of Enabling Technologies for Regenerative Medicine by CRC/Taylor and Francis in 2010 and was co-authored with Dan Bernards, Rahul G. Thakar, Kristy Ainslie, and Tejal A. Desai. Chapter 3 was previously published as *Integrin α3 blockade enhances microtopographical down-regulation of α-smooth muscle actin: Role of microtopography on ECM Regulation* in the journal of Integrative Biology in 2011 and was co-authored with Tejal A. Desai. Chapter 4 was previously published as *Microtopographical cues in 3D Attenuate Fibrotic Phenotype and Extracellular Matrix Deposition: Implications for Tissue Regeneration* in the Journal of Tissue Engineering in 2010 and was co-authored with Jose I. Lopez, and Tejal A. Desai. Chapter 5 is based on work currently in preparation co-authored with Jiashing Yu, Kim Du, Richard Siever, Qizhi Fang, James Pinney, Randall Lee, and Tejal A. Desai. Chapter 6 is based on work also currently in preparation and co-authored with Tamara Los, Brenda Russell, and Tejal A. Desai.

Chapter 1: Introduction

1.1. Myocardial Infarction and Heart Failure

Since 1900 cardiovascular disease (CVD) has remained a leading cause of death in the United States. CVD claims more lives each year than the next four leading causes of death combined, which are cancer, chronic lower respiratory diseases, accidents, and diabetes mellitus.[1] A great number of patients with CVD are afflicted with ischemic heart disease. Approximately nineteen million people worldwide sustain a cardiac event annually. In the United States it is estimated that 1.2 million Americans have a new or recurrent heart attack a year. About sixty percent of the patients who experience a heart attack survive in a given year.[2] Acute Myocardial Infarction (MI) is defined as death or necrosis of myocardial cells due to prolonged ischemia.[3] This occurs when plaque ruptures forming a thrombus that blocks a coronary vessel, resulting in severe reduction of blood supply to the myocardium.[4] The loss of about 25% of the approximately 4 billion cardiomyocytes can lead to congestive heart failure.[5] After cardiomyocyte death, the necrotic tissue is removed by macrophages and replaced with granulation tissue that ultimately results in a collagenous scar. During this process, the infarcted wall thins, the left ventricular (LV) chamber dilates and interstitial fibrosis and cardiomyocyte hypertrophy appear in the infarcted and non-infarcted regions of the ventricle. These changes are linked with the cardiac dysfunction that leads to heart failure. Cardiac fibrosis has been considered to be an independent risk factor in the outcome of heart failure and no effective treatment exists to alleviate this problem.[6-7]

1.2 Current Treatments

Current treatments for surviving patients include anti-thrombotic drugs such as Aspirin and Heparin, angiotensin-converting enzyme (ACE) inhibitors and beta-adrenergic blockers, angioplasty, coronary artery bypass, mechanical devices (artificial hearts and constraint devices) and ultimately heart transplantation, but there is no treatment to restore the function of the damaged myocardium.

1.3 Cardiac Remodeling

Following cardiomyocyte necrosis, a greatly regulated process of repair and remodeling takes place. There is an initial activation of matrix metalloproteinases (MMPs), which main function is to degrade the present extracellular matrix (ECM).[8] This proteolytic activity declines after the first week with an increased expression of MMP inhibitors, known as tissue inhibitors of MMPs (TIMPs).[9] Inflammatory response peaks at week two with inflammatory cells including macrophages and neutrophils migrating into the infarct area. This process takes place for about 3 weeks when these cells begin to apoptose. In addition, there is increased activation of transforming growth factor (TGF-B1) a key initiator of fibrogenesis. Fibrosis is found not only in the infracted myocardium, but in remote sites as well. The principal cells responsible for the formation of fibrous tissue are transformed fibroblasts known as myofibroblasts which are characterized by expressing α-smooth muscle actin (SMA). Myofibroblasts appear in the first days after MI and remain abundant for months. They are co-localized with accumulated collagen and persist in the infarct scar for years where they can continue to promote fibrosis.[10] Collagen types I and III have been shown to be over expressed in the myocardium after MI,[11] and recently it was

shown that collagen type VI also appears after MI and can play a significant role during fibrosis in the heart and other organs.[12-15] Increased fibrosis leads to stiffening of the myocardium which in turn loses its ability to relax and properly pump blood to the body. Studies have shown that the elastic modulus of the myocardium in healthy rats is about 18 kPa, but increases threefold (60 kPa) in the infarcted myocardium.[16] In addition, the overproduced extracellular matrix has been linked to the onset of arrhythmias since this tissue does not have the required electrical properties.

1.4 Intrinsic Mechanisms of Repair: Cardiac Progenitor Cells

The human heart possesses a very limited capacity to regenerate when compared to other tissues such as liver, skeletal muscle, lung, gut, bladder, bone or skin. Recently, researchers[17] have identified a pool of multipotent cardiac stem cells (CSCs) in the heart of rats. They reported the existence of Lin^- $c\text{-}kit^+$ cells with properties of stem cells and showed that the human heart contains a population of CSCs that can divide and differentiate into myocytes, and smooth muscle cells and endothelial cells. [18] Urbanek et *al*. showed that cardiac stem cells, identified by c-kit, MDR1, Sca-1, were involved in myocardial regeneration after a heart attack. [19] The CSC population increases acutely after infarction, but decreases in chronic heart failure.[20] Even when new myocytes are created, the capacity of the heart to grow is harshly limited and the intrinsic mechanisms of repair are insufficient for reconstitution of the injured myocardium. Therefore, other strategies to treat the failing heart are needed.

1.5 Therapeutic Approaches for Cardiac Repair

Since 1967 heart transplantation has been the only therapeutic solution for patients with end stage heart failure. The shortage of donor organs has resulted in a quest for other therapeutic alternatives that include the use of cardiomyoplasty, biomaterials, growth factor delivery, or combinatorial therapy. Various cell types (embryonic stem cells, induced pluoripotent stem cells, cardiac progenitor cells, bone marrow stem cells, and skeletal myoblasts)[21-25] have been proposed to treat MI. Although cell transplantation has been found to be beneficial the main challenges are cell retention after injection and cell integration with the host tissue, additionally the main obstacles in the use of embryonic stem cells are immunological rejection and the propensity of teratoma formation. Recent research has shown that the use different biological materials such as fibrin, alginate, matrigel, collagen, chitosan, decellularized ECM, and other natural and synthetic polymers could be beneficial for cardiac repair because they could provide mechanical support or promote cell migration.[26-27] The challenge is to have a system that could be simple to deliver, that would degrade over a long period of time as new tissue is produced, and that would integrate with the host tissue. Another approach is to encapsulate cells in a biocompatible material or to engineer cardiac tissue *in vitro*; the challenge with this approach is to acquire a robust number of appropriate cells and to design a successful platform that would be delivered through a minimally invasive process.[28-29] Growth factor delivery could also aid in the cardiac repair process, but the main challenge is protein degradation. To overcome this problem researchers are also investigating the use of materials as growth factor delivery systems.[30-31] Although many challenges remain in the fields of tissue engineering and regenerative therapy, these studies can eventually lead to successful therapies to treat or prevent heart failure.

1.6 Motivation

The approach of injectable therapies is very appealing from the clinical perspective since delivery of the therapy would be minimally invasive. One way to achieve this goal is to develop material-based therapeutics at the micro-scale. This requires not only the ability to fabricate biocompatible materials and tissues at this scale, but also an understanding of how physical cues such as stiffness and topography from the material can influence cell behavior.

1.7 Research Goals

The goals of this research were to investigate the effect of microtopographical cues on 2D and 3D culture systems in relation to fibroblast proliferation and gene expression, to fabricate substrates with microtopography of different stiffness, to create biocompatible tunable microstructures to investigate microtopography in 3D culture, to evaluate the encapsulation, delivery and bioactivity of a desired growth factor from "microrods", and to investigate the effect of injecting microrods in the left ventricle after myocardial infarction. The findings could help in the creation of improved therapeutic platforms not just for cardiac repair, but other organs as well.

Chapter 2. Introduction to Microfabricating Tissues

2.1 Tissue Engineering and Microfabrication

Microfabrication takes advantage of integrated-circuit manufacturing technology to pattern materials with dimensions ranging from micrometers to millimeters.[32] The ability to design and control features at the micrometer scale provides biologists and engineers with an essential tool in the development of complex tissue engineering constructs. Tissue engineering is a field that integrates principles of engineering and life sciences for tissue development that restores or maintains a whole organ or a damaged tissue.[33] The ultimate goal of tissue engineering is to create functional tissues that can be delivered *in vivo* to a site of repair or dysfunction. In one method to achieve this goal, cells are placed on an implantable scaffold that provides mechanical support and tissue specific orientation.

Tissue engineered scaffolds should model or mimic the physiological cellular microenvironment. *In vivo*, the extracellular matrix (ECM) is the scaffold that provides structural support to the cells. Primarily the ECM is composed of polysaccharides, proteoglycans, and proteins, such as collagen, laminin, fibronectin.[34] The ECM plays a critical role in controlling cellular organization, proliferation and differentiation, migration and motility.[35-36] Indeed, numerous studies have shown that the mechanical matrix rigidity of the ECM affect cellular phenotype, migration and differentiation.[37-38] In addition to providing contact guidance for cell growth and maintenance, the ECM mediates biochemical signaling. *In vitro* microenvironments that are biologically accurate and simulate *in vivo* conditions are required for these studies.

The design and development of novel strategies for tissue engineering and regenerative therapies requires a general understanding of how both chemical and physical cues in the biological microenvironment affect cellular behavior. Microfabricated systems provide a platform to study how chemical and physical cues affect cell behavior in a controlled manner. With the ever increasing capability to develop more physiologically accurate scaffolds, tissue engineers can also use microfabrication methods to create complex tissues with microintegrated channels for nutrients and blood supply.[39-41] The utilization of microfabrication technologies can provide an array of tools for the development of the next generation of tissue engineering scaffolds.

2.2 Microfabricated Technologies

Microfabrication, a collection of techniques that develop materials on the microscale, can be used to create physiologically relevant materials that mimic the scale cells experience *in vivo.*[42-44] Parameters such as cell alignment and organization can be engineered to mimic the *in vivo* environment through microfabrication techniques. In addition, microfabrication allows for control and replication of topography and substrate stiffness. The geometric control of spacing and arrangement between and among cell types can be used to regulate the microenvironment to engineer cell growth, protein expression, proliferation and migration.[45] Furthermore, with microfabrication it is possible to systematically control the discrete presentation of biochemical molecules, and therefore the differential adhesion of cells to substrates.[43,46] Molecule functionalization,[47-48] drug release kinetics[49-50] and surface passivation[51] can be manipulated in conjunction with aspect ratio, management of shape and spacing through one or more microfabrication techniques. The small size of microfabricated devices also offers limitless possibilities for

application *in vivo*. The relative size of microfabricated elements correlates to the original application for the techniques: semiconductor processing. Techniques such as chemical etching and photo- and soft- lithography have been adopted beyond their initial use in silicon to have application in epoxy-based, hydrogel and biodegradable polymers (Figure 1). Silicon or polymer based devices can be further functionalized through techniques like surface chemistry to create patterned microenvironments with nanoscale features.

One challenge in the development of microfabricated tissues however, is adapting microfabrication techniques to create biocompatible substrates and scaffolds. The engineering and fabrication of biocompatible and biodegradable biomaterials with microintegrated cues can provide an innovative way to create cell loaded constructs that mimic *in vivo* cellular microenvironments.

2.2.1 Materials

2.2.1.1 Silicon

Silicon is the most traditional material for microfabrication due to its use historically in integrated circuit development. In biomedical applications, many silicon-based devices, such as implantable sensors,[52-53] devices for drug delivery[54-56], and electrical stimulation,[57-59] are already under consideration for use within the human body. Micro- and nano-structured silicon, such as porous and nanowired silicon, has previously been employed as a foundation for sensor technologies,[60-68] Silicon is not only a user-friendly material, but also can be formulated to be biocompatible and not invoke a significant immune response.[69]

2.2.1.2 Glass

Like silicon, glass or silicon oxide is available in a variety of sizes and compositions, such as fused silica and borosilicate wafers. Of these two materials, silica offers ease in microscopic imaging.[32] Additional microfabrication techniques are being developed continuously to enhance the role of micro- and nano-structured glass.[70-71] The use of glass in microfabricated implants is not as universal as silicon, but its use is increasing as micro- and nano-scale technology develops new fabrication methods. The immunogenicity of glass has been observed with immune cells on both flat and nanostructured surfaces. Studies have reported that a difference was not observed between the adherence of cells on textured versus flat glass.[72] With the increasing development of micro-structured glass surfaces, as well as the proven biocompatibility of such surfaces, the application of these surfaces for implanted devices is certain.

2.2.1.3 Polymers

Often the most economical and appropriate substrate material for microfabrication of living systems is polymer based. Many traditional polymer manufacturing techniques, such as injection molding and embossing, can be carried over into the microfabrication realm at a much smaller scale.[32] Polymers can be introduced through photolithographic techniques. The most common photolithographic polymers commercially available are SU-8 and poly(methyl methacrylate) (PMMA). Patterning of additional polymers can be accomplished using micro-molding of SU-8, PMMA, or silicon fabricated masters. The range of polymers available adds an additional design element to the microfabrication

process by allowing the developer to tailor specific material properties such as hydrophobicity, biodegradability, and biocompatibility. Furthermore, features such as drug release kinetics, biodegradability, and cell incorporation can be altered with variables such as molecular weight, chemical structure, and/or cross-linking density. A variety of biocompatible polymers are currently used in medical applications, including poly(ethylene) glycol (PEG) polyglycolic, acid (PGA), polylactic acid (PLA), polycaprolactone (PCL), poly(glycerol-sebacate) (PGS) and poly(DL-lactide-co-glycolide) (PLGA). Chen *et al.* reviews some of these polymers and presents average degradation rates and tensile modulus.[73]

2.2.2 Microfabrication Methods

In addition to scaffold formation, cell patterning is a common desired component for tissue engineering and for fundamental cell biology studies. Microfabrication techniques such as photolithography and chemical etching have provided scientists with the ability to control micrometer features on cell culture substrates. Additionally, techniques referred to as soft lithography, have been developed for biological studies and tissue engineering applications. These techniques include: microcontact printing (μCP) and microfluidic patterning (Figure 2.1). Microfabrication methods provide the advantage of creating tissue platforms in a reproducible manner that is relatively rapid and facile.

2.2.2.1 Photolithography

The most commonly applied microfabrication technique is photolithography. The process of photolithography involves the transfer of a pattern from a mask to a thin film via the localization of light. In this process photoresist layers are selectively exposed to ultraviolet (UV) light through a photomask that contains a desired pattern. The photoresist is typically spin coated onto a flat substrate and forms a uniform film. To generate the pattern, the substrate is exposed to UV light under a photomask, the uncross-linked areas of the photoresist are then developed in an organic solvent. By combining steps of masked exposure and thin film application, multi-layered resists can be formulated with high aspect ratios. Higher resolution photolithographic techniques, such as x-ray and e-beam lithography, can lead to smaller feature size as well as more intricate topography. Photolithography can also be combined with other microfabrication methods such as etching to add more complexity to the patterns.

2.2.2.2 Etching

Etching can be either wet, with acids and bases, or dry, commonly with plasmas, and removes material from the bulk surface. Etching can be isotropic (etching in all directions equally) or anisotropic (etching is directional). Chemical etching can be more selective than physical etching but is amenable to fewer materials.[32] One disadvantage of etching and photolithography is that they are not always applicable to biological systems. Many of the steps in these technologies involve exposure to organic solvents, plasmas, and harsh chemical conditions that can be deleterious to cells and denature bioactive molecules.

2.2.2.3 Soft lithography

Microfabrication has been increasingly adopted by biomedical and biological researchers in large part due to a set of alternative fabrication techniques known as soft

lithography. The term "soft lithography" is given because it uses a patterned elastomeric polymer as a mask, stamp or mold, to pattern "soft materials" (for example, polymers, gels and organic monolayers, typically on surfaces like silicon and glass).[74] Soft lithography utilizes stamps, molds and membranes to generate channels, grooves, islands, as well as other microscale features.[75] The most common soft lithographic techniques used for cell patterning are μCP and microfluidic patterning. The patterning of these microscale features on culture substrates provides a stage where the microenvironment of growing cells can be controlled and selectively studied.

An important step in soft lithography is creating a mold, which consists of a master with features to be transferred to a polymer. The patterned elastomer is generated from a master, generally a silicon wafer that had been previously fabricated by photolithographic techniques.[76] The pattern of the master can be replicated through techniques like injection molding, hot embossing, and plastics casting.[77] Polydimethylsiloxane (PDMS) is generally the polymer used because it is easy to use, inexpensive, and nonreactive. Once polymerized, the PDMS is hardened and can be cut from the silicon mold, cleaned, and is ready for use. Though PDMS is extremely hydrophobic (contact angle ~ 110°), exposure to plasma, usually an oxygen plasma, yields a high free energy surface (contact angle ~ 10°) that is negatively charged.[78-79] A useful advantage of soft lithography is that several replicas of the inverse pattern, in a secondary polymer such as biodegradable PLGA or PCL, can be produced from a single PDMS master. These techniques can be used to create *in vitro* culture substrates and implantable microintegrated tissues.

2.2.2.3.1 Microcontact printing

μCP is most commonly recognized as a stamping procedure (Figure 2.1). Usually, the patterned component is an ECM molecule in solution, like collagen, gelatin, or fibronectin. The protein can be covalently bound to the surface through a self-assembled monolayer (SAM), usually comprised of silanes or thiols. SAMs are a self assembled organized organic monolayer films that allow for surface functionalization.[75-76] The terminal group of an SAM can posses a variety of functional groups, making it possible to control the properties of the surface either by covalently binding compounds such as proteins or passivation layers, like poly(ethylene glycol).

2.2.2.3.2 Microfluidic Patterning

The elastomeric polymer PDMS has also been used for fabricating microfluidic channels and networks. Microfluidic channel are created by placing a sheet of PDMS with channels embossed on the surface in contact with a flat surface. The channels formed by conformal contact contain a weak physical seal between the two layers of material (the PDMS and a glass slide).[76,80] The ability to generate and sustain parallel streams of different solutions in microchannels provides a unique opportunity to pattern cells and their environments. An important characteristic of fluids flowing in microfluidic channels is that the flow is laminar due to the small diameter of the channel. As two or more streams at a low Reynolds number (Re) join into a single stream at a low Re, the combined streams flow parallel to each other with mixing only by diffusion. This ability to create and sustain parallel streams of different solutions provides the opportunity to pattern the substrate and the location of the cells.[81-82]

2.3 Microintegrated Tissues

Organs of the human body have distinct organization and specific function as do the tissues that comprise them. Each living tissue is intricate and possesses microscale structure and organization that renders it functional for a defined purpose. To accomplish this purpose tissues have precisely arranged cells with features generally on the micrometer scale. These tissue-specific characteristics should be addressed both when studying cell behavior and when developing new tissue scaffolds. Microfabrication offers the opportunity to design structures at a scale close to those of living tissues. Numerous microfabricated scaffolds have been designed for tissue engineering applications in a variety of systems including vascular, cardiac, hepatic, ocular, and neural.

2.3.1 Vascular

The vascular system consists of three lamellar layers: adventitia, media, and intima. The three layers are diversified in cell type, extracellular matrix composition, and functional properties. The adventitia is mainly composed of fibroblasts in a collagen I matrix and comprises the outermost layer of vascular tissue. The media is composed of smooth muscle cells surrounded by laminin layers and provides both mechanical strength and modulation of blood pressure through contraction and relaxation. The intima, the most luminal layer that is in direct contact with the blood, is comprised of confluent endothelial cell layer and a basement membrane which prevents blood clotting and produces cytokines to help modulate smooth muscle cell contraction.[83]

The creation of tissue-engineered vascular grafts is critical for vessel replacement therapies. In a vessel wall, smooth muscle cells are aligned in distinct configurations that result in specific vasocontraction patterns. The complex orientation of vascular cells requires parallel alignment of cells layered orthogonal to each other. Commonly used microfabrication techniques, such as photolithography can be applied to orient the cell layer in such a fashion to mimic the cell layers observed *in vivo*. For example, Sarkar *et al.* microfabricated thin film PCL scaffolds for vascular tissue engineering using soft lithography techniques (Figure 2.2). They found that micro-grooved topographical cues significantly enhanced vascular smooth muscle cells aspect ratio and alignment, in addition to remodeling of the underlying extracellular matrix. This study suggests that topographical patterning of tissue scaffolds can influence cellular and matrix spatial organization and provide a framework for achieving the required organization and physical properties for blood vessels.[84]

Vascular smooth muscle cells (VSMCs) have also been aligned by PDMS[84] and PLGA[84-85] constructed microchannels. By incorporating extra cellular matrix proteins in gels, with microfabricated channels, the three main cellular components of vessel walls (fibroblasts, VSMCs and endothelial cells) were patterned in co-culture to create a vessel wall model.[86] Each microfabricated layer was tailored to orient each particular cell type and then semi-porous surfaces were layered to recreate the layered structure of the tissue. Similarly, human umbilical vein endothelial cells (HUVECs) can be also be aligned when constrained by PEG coated channels.[51,87] The relocation of endothelial cells into the microfabricated channels was shown to be twice as fast when vascular endothelial growth factor (VEGF) was introduced into the channel.[88] The ultimate goal is to scale up these technologies to a full 3D system to create a complete blood vessel.

2.3.2 Cardiac

The complex architecture of cardiac tissue is maintained by three-dimensional ECM networks composed of collagen, laminin, fibronectin, and proteoglycans. This ECM network orients the myocytes, mechanically couples them and provides elastic support during ventricular filling.[89] Cardiomyocytes are generally 10–15 μm in diameter and up to 100 μm in length. The ECM in cardiac tissue is more than an *in vivo* scaffold it provides microstructural cues that regulate cardiac muscle cell morphogenesis, as well as myocardial function.[89]

The replication of *in vivo* geometry, size scale and topography is critical in cardiac tissue engineered constructs for the long term maintenance of an *in vivo* cell phenotype. Physical control of muscle cells by extracellular matrix is an important regulator of myofibrillar organization. Parker *et al.* engineered the shape of neonatal rat ventricular myocytes by culturing them on microfabricated fibronectin islands. The myocytes spread and assumed the shape of the island. Additionally, myofibrillogenesis was studied spatially and temporally, and the assembly of actin networks was predicted by the given shape of the island.[89] Khademhosseini *et al*. used microfluidic patterning of hyaluronic acid (HA) on glass as a method to fabricate 3D cardiac organoids. Cardiomyocytes elongated and aligned along the pattern direction. After 3 days in culture, the linearly aligned myocytes detached from the surface and formed contractile cardiac organoids, providing an inexpensive way to create *in vitro* cardiac tissue models.[90]

In addition to microfabricated technologies used to replicate cardiac tissue *in vitro*, therapeutic applications have been developed to treat disease states such as what occurs after myocardial infarction. Acute Myocardial Infarction (MI) is defined as death or necrosis of myocardial cells due to prolonged ischemia.[3] After myocardial infarction cardiomyocyte death leads to an inflammatory and wound healing response that result in fibrous tissue formation. Ideally the heart muscle would be restored with minimal scarring. The successful creation of cardiac tissue engineering constructs will rely on an understanding of how physical cues guide behavior of different cell types, mainly myocytes and fibroblasts.

Surface topography has a large impact not only on cardiomyocyte shape, but also on gene expression and protein distribution. Deutsch *et al.* have shown that three-dimensional surface topography of culture substrates significantly affects *in vitro* cardiac myocyte orientation. Cardiac myocytes plated on these substrates exhibited a more *in vivo* like cellular phenotype: they displayed greater attachment and cell height compared to conventional culture substrates.[91] Myocytes in contact with micropeg or microgroove features showed an increase in myofibrillar height and a decrease in cell area compared those grown on a flat substate.[92] In addition to microtopography affecting a singular cell type, it can elucidate distinct results on different cells. On similarly pegged surfaces, scar-tissue forming fibroblasts displayed reduced proliferation while cardiomyocytes had similar proliferation to flat controls.[93] The same trend in reduced fibroblast proliferation was observed with microrods of similar dimension in a three-dimensional culture.[94] Norman *et al*. observed that SU-8 microrods suspended in Matrigel™ with fibroblasts significantly inhibit the proliferation of fibroblasts as compared to a three-dimensional Matrigel ™ culture without microrods.[94] These examples display that researchers in the

tissue engineering field can take advantage of microfabricated technologies for the creation of the next generation of complex scaffolds for cardiac regeneration.

2.3.3 Ocular

The cornea is a specialized transparent tissue located at the front of the eye. It consists of three tissue layers: the outer epithelium, the inner endothelium, and the intermediate stroma. The stroma makes up 90% of the corneal thickness and is composed of collagen fibers which are arranged in bundles referred to as lamellae. The orthogonal arrangement of the lamellae as well as the uniform spacing of the fibers result in "destructive interference" of incoming light rays, thereby reducing scatter and promoting corneal transparency.[95] The successful creation of a tissue engineered cornea will require *in vivo*-like cell alignment and organization, which could be accomplished through microfabrication. Corneal epithelial cells on microfabricated silicon nanochannels elongated along the length of the channels and were mostly round on smooth substrates.[96-97]

In addition to the tissue engineering of corneal tissue, the repair of the retina is growing in importance with an increasing older generation. Retinal degeneration resulting in the loss of photoreceptors is the leading cause of blindness.[98] Previous tissue replacements have failed to integrate the implanted tissue into the host retina.[99] This lack of donor tissue integration could be due to deficiencies in structural support for transplanted cells as well as loss of supporting architecture in the host tissue.[100] Microfabricated tissue replacements with desired architecture could be developed to provide support for the newly implanted tissue. Retinal progenitor cells (RPCs) grown on microfabricated poly(methyl methacrylate) (PMMA) displayed signs of cell differentiation and when implanted *in vivo*, the RPCs migrated off the surface of the scaffold and inserted into the tissue layer. Tao *et al.* used both photolithography and reactive ion etching to create PMMA thin films for retinal progenitor cell ocular implantation (Figure 2.3).[101] In the creation of the scaffold, photolithography is used to create a resist mask for the etching process. The resist and PMMA are then etched to create circular holes in PMMA. The original PMMA scaffold has been microfabricated with biodegradable poly(glycerol-sebacate) to further develop this novel retinal tissue engineering scaffold.[102] Microfabricated scaffolds that support cell viability and accurate architectural organization will be crucial in the creation of functional eye implants.

2.3.5 Hepatic

Hepatocytes are the cells that carry out most of the metabolic and biosynthetic processes in liver, and reside in convoluting layers surrounded by endothelial and other cells. Primary hepatocytes can be difficult to maintain in culture since *in vitro* they rapidly lose liver-specific functions. Although a variety of culture methods have been used to maintain hepatocyte phenotype, not all liver functions can obtained at the desired level.[103] In order to maintain functional hepatocytes *in vitro* and develop devices for therapeutic. applications, the complex *in vivo* microenvironment of the liver must be recreated. Microfabrication techniques can be used to achieve spatial control desired to engineer hepatic tissue.

To investigate the role of increasing fibroblast density on hepatic function, Bhatia *et al.* employed μCP to co-cultures hepatocytes and fibroblasts (Figure 2.4).[104] It was shown

that fibroblast number modulates hepatocellular response through homotypic fibroblast interactions. Also, Powers *et al.* developed three dimensional scaffolds by deep reactive ion etching of silicon wafers creating an array of channels (through-holes) with cell-adhesive walls. Scaffolds were combined with a cell-retaining filter and supported in a reactor housing designed to deliver a continuous perfusion across the top of the array and through the 3D tissue mass in each channel. It was demonstrated that this system enables the formation of hepatocellular aggregates which maintained their structure and viability at least two weeks in bioreactor culture, providing a promising platform for the studies of *in vivo* physiology and pathology in an *in vitro* environment.[105] Park *et al.* used photolithographic techniques to fabricate microgrooves onto an underlying glass substrate. The microgrooved-substrate in the bioreactor decreased the damaging effects of shear stress on the hepatocytes while also providing adequate oxygenation. This illustrates a critical aspect in tissue engineered constructs for liver regeneration: the incorporation of blood supply. Using standard photolithography techniques, Kaihara *et al*. fabricated templates with trench patterns similar to the branched architecture of vascular and capillary networks on silicon and Pyrex surfaces. Hepatocytes and endothelial cells were cultured and subsequently lifted off as single-cell monolayers from these two-dimensional molds. Both cell types were viable and proliferative, and hepatocytes maintained liver-specific albumin production.[106] Microfabrication technology facilitated the development of branched vascular networks from two-dimensional templates that may be combined with layers of hepatocytes to form three dimensional vascularized tissues. These studies have provided important microfabricated tools and considerations towards the engineering of liver tissues and supports.

2.3.6 Neural

Neurons are highly specialized for processing and transmitting cellular signals. Neuron morphology consists of a soma, an axon, and dendrites.[107] Recent efforts have focused on creating a cooperative environment for regeneration as well as providing an interface between the central nervous system (CNS) and the peripheral nervous system (PNS). The design of "nerve conduits" or "nerve guidance channels" is a key factor for both CNS and PNS repair.[108] Biomimetic microenvironments based on microfbabrication technologies can provide the platform for *in vitro* cell manipulation of soma orientation and axon growth guidance.

Controlling neuronal cell position and outgrowth is of critical interest in the development of tissue engineering applications.[108] In order to manipulate the growth of neuronal cells, microfabrication techniques can be utilized to provide guiding structures on the device substrate.[109-111] To more accurately mimic natural repair in the body, recent studies have focused on the use of various advanced approaches to create ideal nerve guidance channels that combine multiple stimuli. Microfluidic devices offer specific control of the microenvironment surrounding individual cells, and the delivery of biochemical or physical cues to neural networks or single neurons. To that end, Taylor *et al*. reported a microfluidic multi-compartment neuronal culturing device that can be used for a number of neuroscience research applications (Figure 2.5).[111] Through engineering of microfluidic compartmentalization, areas of neuronal attachment and neurite outgrowth can be fluidically isolated.[111] Micropatterned substrates have also been created for neurite elongation studies *in vitro* and for tissue engineering applications.[112-114] Schmalenberg *et*

al. utilized μCP to locate laminin in microfabricated grooves and then seeded rat Schwann cells on the substrates. The micropatterns provided physical guidance, laminin provided chemical cues, and Schwann cells provided biological cues for axon growth.[113] The use of microfabricated elements can be used to provide contact guidance cues for the development of neuronal tissue engineering constructs.

2.4 Conclusion

Design and development of successful regenerative therapies requires an in-depth understanding of fundamental biology and the ability to accurately manipulate cells. A major challenge for building a functional engineered tissue is the arrangement and organization of cells in the appropriate scaffold. All tissues *in vivo* contain a hierarchical structure that must be replicated in order to better duplicate living systems. Microfabrication techniques have allowed the creation of *in vivo*-like microenvironments for *in vitro* studies. Applications of techniques like photolithography, soft-lithography and chemical etching can be used to create tissue engineering scaffold that mimic cellular organization *in vivo*. Such scaffolds have been applied in a variety of systems including vascular, cardiac, ocular, hepatic, and neuronal, displaying the flexibility of these microfabrication techniques.

In addition to the ubiquitous use of microfabrication methods to develop two-dimensional scaffolds, these techniques have more recently been applied to develop three-dimensional scaffolds. To address this challenge, researchers have searched for biocompatible materials that can be microfabricated for clinical applications. Numerous groups have reported the application of microfabrication techniques for the micropaterning of cell-laden hydrogels.[115-121] These cell-laden hydrogels provide a three-dimensional environment that has been shown to increase hepatocyte specific metabolites and cell viability. As of yet, these three-dimensional scaffolds provide few organizational cues to mimic the desired *in vivo* hierarchy, but certainly this emerging application of microfabricated technologies will have additional application in other tissues.

In addition to three-dimensional scaffolds, microfabricated elements can provide spatial and temporal control of cell growth and stimuli to help understand niche interactions with stem cells, thus leading to novel stem cell therapies. Studies have demonstrated that mechanical cues that embody cell shape, cytoskeletal tension, and RhoA signaling, are integral to the commitment of stem cell fate.[122] Microfabricated elements can help elucidate the link of these mechanical cues with respect to stem cell differentiation and proliferation. Knowledge from these and similar studies plays a critical role in the design and creation of new scaffolds and regenerative therapies to enhance stem cell modulation *in vitro* and *in vitro*.

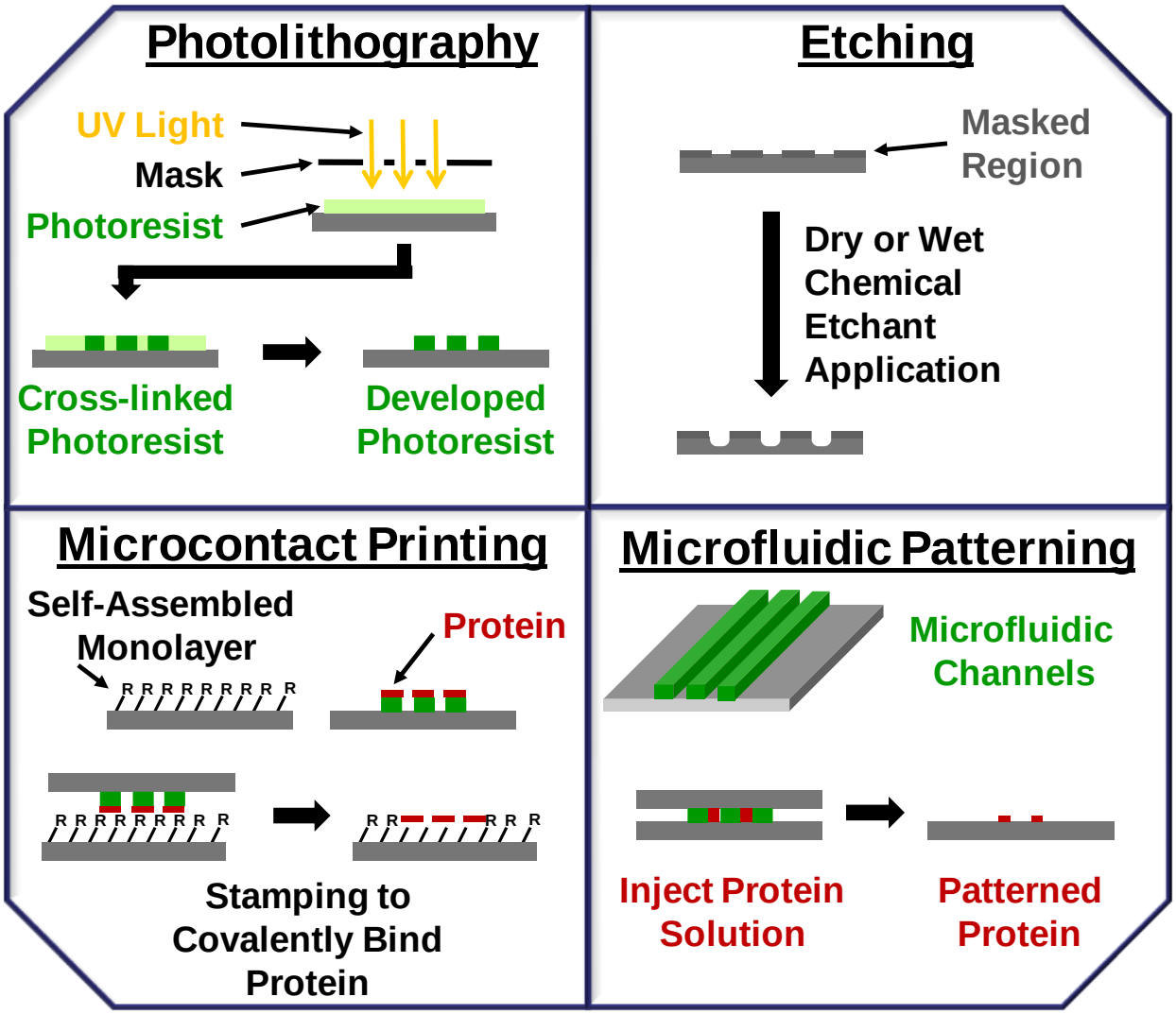

Figure 2.1 Common microfabrication techniques.

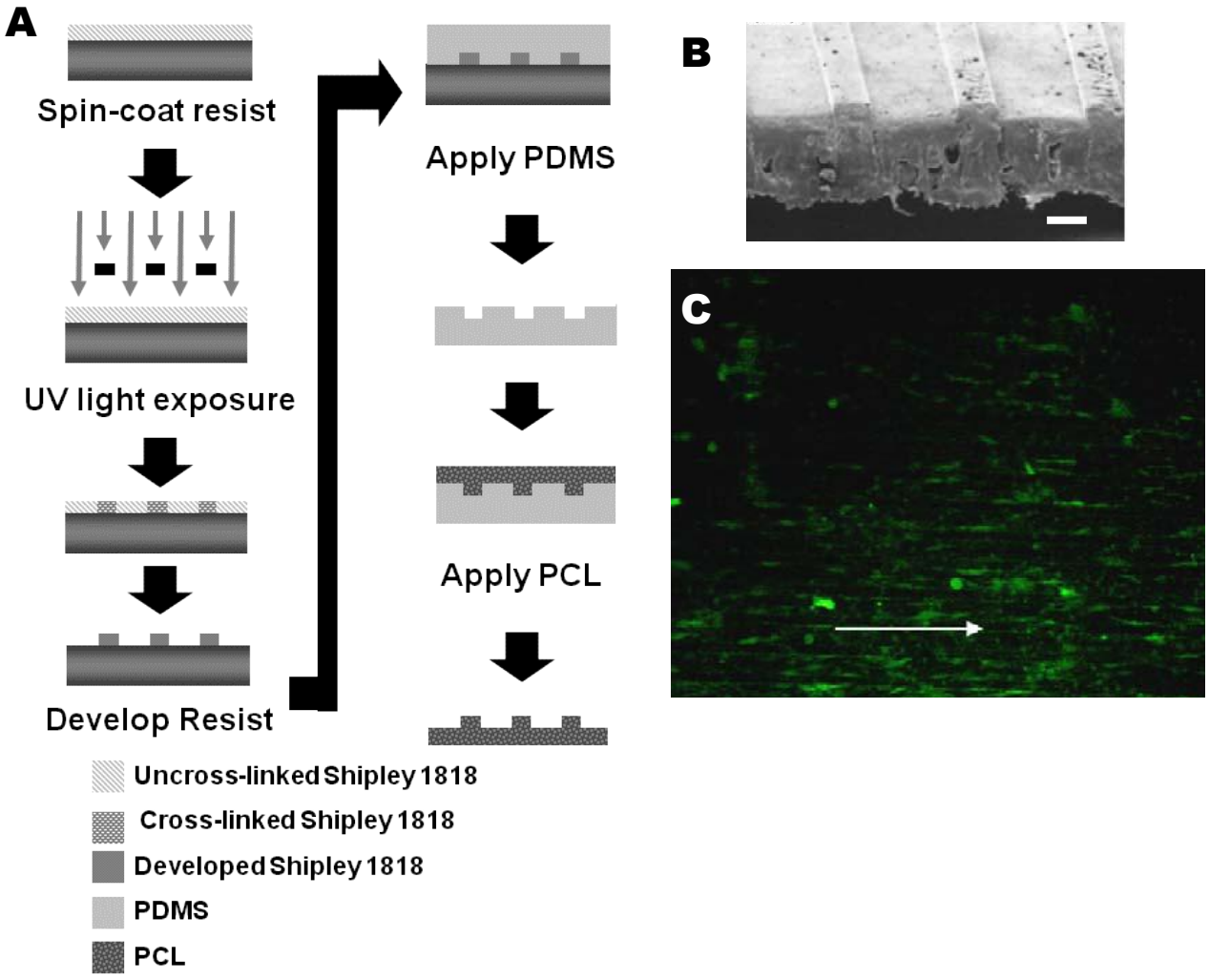

Figure 2.2 Micromolding fabrication of PCL tissue engineering scaffolds. (A) Process flow diagram for development of micro-fabricated PCL films. Adapted from Sarkar *et al.*[84-85] (B) Scanning electron micrograph of non-porous PCL scaffold. The scale bar represents 10 microns. (C) Vascular smooth muscle cells cultured on patterned PLGA leached PCL.

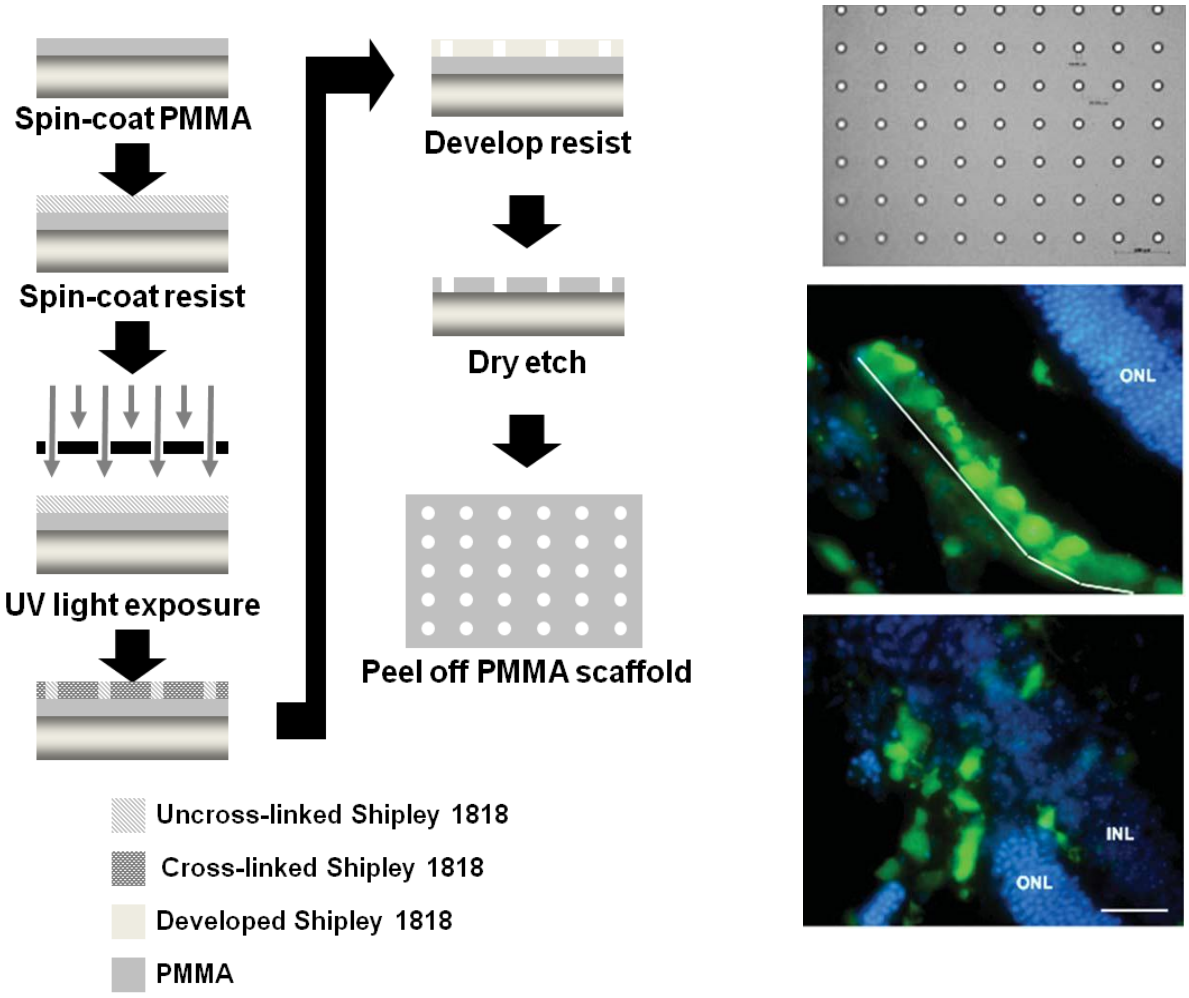

Figure 2.3 PMMA scaffold for retinal progenitor cell implantation. (A) Process flow diagram of thin film construction. Adapted from Tao *et al.* (B) Optical micrograph of PMMA scaffold, 6 μm thick, which contains pores approximately 11 μm in diameter and spaced 63 mm apart. Scale bar = 100 μm. (C) Green fluorescent protein (GFP) positive cells implanted into the host retina on porous PMMA membrane. The white line approximates the contours of the membrane. ONL – outer-nuclear layer (D) GFP positive cells migrating into the photoreceptor (ONL) and inner nuclear layer (INL) of the host retina. Nuclei of the host retinal layers are stained blue. Scale bar equals 50 μm. (Adapted from: S. Tao *et al*[101]).

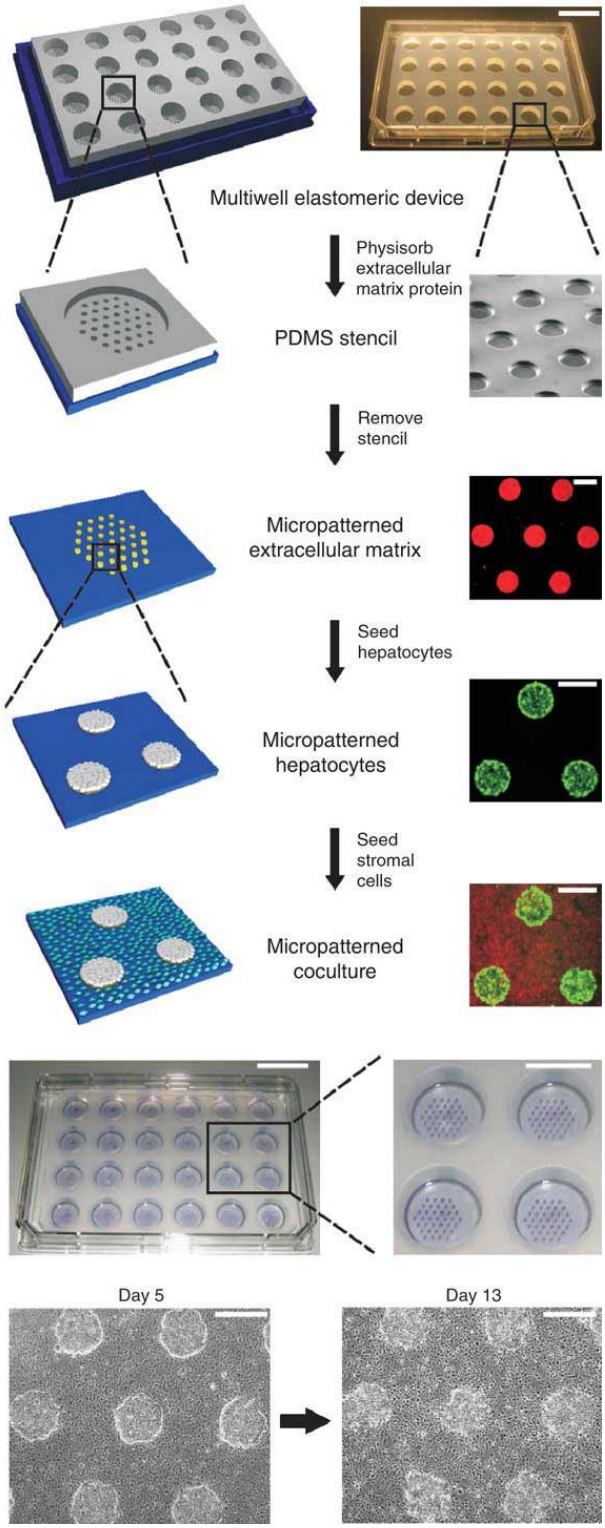

Figure 2.4 Flow process schematic used by Bhatia and co-workers to microcontact print extracellular matrix protein to pattern fibroblasts and hepatocytes. Hepatocytes are arranged in 500-micron collagen-coated islands and surrounded by fibroblasts. Scale bars represent 500-micron.[123]

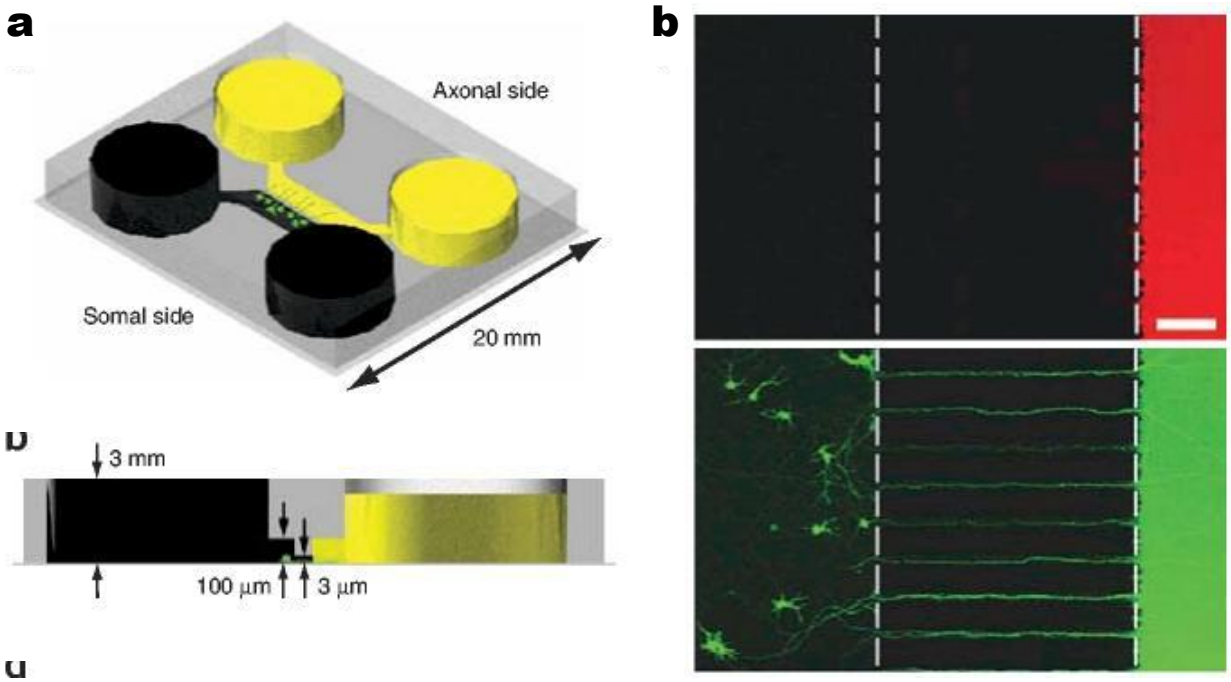

Figure 2.5 Schematic of microfluidic-based culture platform for the growth and alignment of central nervous system neurons. (a) Culture system comprised of two PDMS molded reservoirs with microgrooves between. (b) Demonstration of fluidic isolation of Texas red dextran (top panel). CellTracker Green (middle panel) labeled isolated axons.[111]

Chapter 3. Role of Microtopography and Stiffness on ECM Regulation on 2D Cultures

Abstract

Development of functional engineered matrices for regenerative therapies can benefit from an understanding of how physical cues at the microscale affect cell behavior. In this work, we use microfabricated systems to study how stiffness and microscale topographical cues in the form of "micropegs" affect extracellular matrix synthesis. Previous work from our lab has shown that microtopographical cues in 2D and 3D systems decrease cellular proliferation and regulate matrix synthesis. In this work, the combined role of stiffness and topography on ECM synthesis is investigated in a 2D micropeg system. These studies show that fibroblasts cultured on Polydimethylsiloxane (PDMS) substrates with micropegs have reduced expression of collagen type I (Col 1) and collagen type VI (Col VI) compared to fibroblasts cultured on flat substrates. In addition, cells on micropegged substrates exhibit down regulation of other important regulators of ECM synthesis such as alpha smooth muscle actin (α-SMA), and integrin alpha 3 (Int α3). Interestingly, this effect is dependent on the contractility and adhesion of the cells. When cultured in the presence of RhoA kinase (ROCK) and myosin light chain kinase (MLCK) inhibitors, no significant differences in the expression of collagen, α-SMA, Int α3, and TGFB1 are observed. Additionally, disruptions in cell adhesion prevent microtopographical regulation of ECM synthesis. When using an antibody to block the extracellular domain of Int α3, no differences in the expression of collagen are observed and blocking Int α3 results in enhanced down-regulation of α-SMA on the stiffer micropegged substrates. These findings demonstrate that regulation of extracellular matrix production by cells on a synthetic substrate can be guided via physical cues at the microscale, and add to the body of knowledge on the role of integrin-mediated mechanotransduction.

3.1 Background

The major objective in the development of engineered tissues is to design and create scaffolds that will properly integrate with the host tissue to support the regenerative process. *In vivo* the microenvironment provides cells with the necessary chemical signals to modulate cell migration, proliferation, and differentiation. Likewise, biophysical signals and mechanical stresses from the extracellular matrix (ECM) can be converted into intracellular responses that regulate cell behavior and fate. The utilization of appropriate cues in tissue engineered platforms would ensure successful control of cellular behavior. Recent studies have highlighted the importance of physical properties on scaffolds where cells are guided towards the correct phenotype and suitable behavior.[124-129] On rigid ECM scaffolds brain tumor cells spread, form stress fibers, and migrate rapidly. On softer ECM scaffolds with rigidity comparable with normal brain tissue, tumor cells appear rounded and fail to migrate.[124] Muscle stem cells cultured on hydrogel substrates that mimic the elasticity of muscle (12 kPa) self-renew in vitro and contribute to muscle regeneration when transplanted into mice.[126] Microfabricated topography in a PCL thin film enhanced the attachment and organization of retinal progenitor cells and induced cellular differentiation compared to flat thin films.[128]

An important challenge in tissue regeneration by exogenous cells, engineered scaffolds, or combinatorial therapy is the ability to create an *in vivo* environment that is

receptive to treatment especially in aged, injured, and diseased tissues. The extracellular matrix in particular plays a critical role on cell behavior and vice versa the cell regulates the deposition of ECM molecules based on cues from this closed feedback loop. The ECM's inherent properties regulate several cellular functions including organization, proliferation, differentiation, and migration.[35-36,130-132] In particular, studies have shown that the elasticity of the ECM can significantly affect cellular phenotype, migration and differentiation.[37-38,133] An increase in tissue stiffness can be associated with the excess deposition of extracellular matrix proteins, a process known as fibrosis. This stiffening has been connected with pathological conditions including cancer and heart failure.[134-135]

The success of cardiac tissue regeneration approaches is highly dependent on the ability to generate an appropriate microenvironment that can restore myocardial function and support optimal healing, rather than over-expression of fibrous tissue. Major challenges for current approaches in stem cell regenerative therapy are cell survival and the formation of scar tissue that leads to differentiation of stem cells into unwanted phenotypes.[136] Providing a scaffold that could facilitate cell retention and would allow for healing without fibrosis could alleviate these problems. Controlling fibroblasts, the main producers of collagen and other ECM molecules, is an important step to support the intrinsic regenerative process.

Effective manipulation of the cues that cells encounter in their microenvironment can greatly impact cell phenotype. It is now evident that mechanical, topographical, and geometrical cues can be utilized to modulate cellular morphology and behavior in 2D and 3D systems.[37,45,137-143] Previous studies have revealed that microtopographical cues can play a significant role in fibroblast proliferation. Neonatal rat ventricular fibroblasts (NRVF) showed decreased proliferation when cultured on 2D surfaces with micropegs compared to flat surfaces.[137] This observation was correlated with a significant decrease in cyclin D1 expression indicating that cell proliferation was affected at the level of G1/S cell cycle transition.[137] Furthermore, it was observed that when fibroblasts from the 3T3 cell line were cultured on the micropeg substrates, the decrease in proliferation was dependent on local micropeg-cell interactions and was regulated by contractile mechanics.[144] It was also shown that micropegs enhanced cell-scaffold adhesive interactions without changing the cell's elasticity. Additionally, adhesion to micropegs increased the expression of RhoA GTPase, myosin heavy chain II (MYH2), and connexin 43 (Cxn 43) in myoblasts.[145]

How the microenvironment can alter the remodeling of the ECM is not as well understood. Studies have also highlighted the impact mechanical stretch can have on fibroblast phenotype and ECM synthesis.[146-149] In particular, it has been observed that tissue stretch can decrease soluble transforming growth factor beta1 and procollagen type I in mouse subcutaneous connective tissue after injury.[146] Myofibroblast phenotype can be reversed to fibroblast phenotype with decrease in collagen production after mechanical stretch.[148] However, regulation of cell phenotype, gene expression, and ECM synthesis using microtopographical cues has not been fully explored. An understanding of how cell adhesion and interaction to micro-fabricated scaffolds affects cell behavior will supply critical information for the rational design of tissue engineering scaffolds.

In this work, we utilize micropegged silicone scaffolds to determine if regulation of ECM synthesis can be accomplished by using micro scale topographical cues. In addition, we investigate the role of stiffness in microtopographical regulation of gene expression and

ECM synthesis. Knowledge of the role of topography in matrix remodeling can be used to design and develop improved engineered regenerative therapies.

3.2 Experimental Section

3.2.1 Fabrication of Polydimethyl siloxane (PDMS) substrates

PDMS Micropeg substrates were fabricated as reported previously. [144-145] The micropegs are 15 μm tall with 25 x 25 μm cross-sectional area, the spacing between micropegs is 125 μm from center to center of micropegs on one side and 50 μm spacing from center to center on the other side. To construct a photoresist mold, SU-8 2010 negative photoresist (Microchem, Newton, MA, USA) was spin-coated onto a single-crystal silicon wafer to a thickness of 15 μm and baked at 95°C for 3 minutes. Microscale holes were introduced by placing a patterned photomask over the coated wafer and exposing it to UV light for 30 s at an intensity of 5 mW cm^{-2}. The uncrosslinked photoresist was then removed by washing the wafer in SU-8 developer (Microchem, Newton, MA, USA) for 30 s, and then the SU-8 molds were baked at 95°C for 3 min. The dimensions of the resulting microscale holes were then verified by light microscopy and surface profilometry. To create PDMS (Sylgard 184, Dow Corning, MI, USA) micropeg arrays with different elastic moduli (1.79 MPa and 0.05MPa), the silicone elastomer base and the crosslinker were mixed thoroughly at different ratios (10:1 and 50:1, respectively) as previously reported.[138] The solution was degassed under vacuum, poured onto the SU-8 mold and spin-coated at 200 RPM for 1 min followed by 250 RPM for 30 s to achieve a thickness of 15 μm. The PDMS-wafer composite was then baked for 18 hr at 60°C. After the PDMS cured, the micropatterned PDMS membranes were peeled from the SU-8 masters. Unpatterned PDMS membranes were fabricated in an identical manner, except for the use of unpatterned, non-PR-coated silicon wafers as masters. Prior to use in cell culture experiments, the PDMS was rendered hydrophilic by exposure to oxygen plasma and then incubated with Dulbecco's Modified Eagle's Medium (DMEM) with 10% fetal bovine serum and 1% penicillin/streptomycin (Gibco-BRL, Grand Island, NY) for 1 hr before seeding cells.

3.2.2 Cell Culture

NIH 3T3 mouse fibroblasts were cultured in complete medium consisting of Dulbecco's Modified Eagle's Medium (DMEM) with 10% fetal bovine serum and 1% penicillin/streptomycin (Gibco-BRL, Grand Island, NY). Cell cultures were maintained in a humidity-controlled 5% CO_2 incubator at 37°C and were allowed to grow to ~90% confluence. Prior to seeding, cells were trypsinized and resuspended in complete medium. Cells were plated at a density of 10,000 cells cm^{-2} and washed after 1 hour to remove non-adherent cells.

3.2.3 Fluorescent Microscopy

Cells were fixed in 4% paraformaldehyde (Fisher Scientific, Pittsburgh, PA) for 15 minutes, permeabilized with 0.5% Triton X-100 (Sigma, St. Louis, MO) for 15 minutes, and blocked with 1% bovine serum albumin (BSA) (Sigma, St. Louis, MO) for 30 minutes. F-actin was stained using Alexa Fluor 563 phalloidin (Molecular Probes, Eugene, OR) for 30 minutes. To stain for α-SMA, cells were incubated with mouse anti-α-SMA IgG (Sigma, St.

Louis, MO) for 1.5 hr at room temperature, and incubated with Alexa 488-conjugated donkey anti-mouse IgG (Molecular Probes, Eugene, OR, USA) for 1 hr at room temperature. Nuclei were then stained with Hoechst 33258 (Molecular Probes, Eugene, OR, USA) for 5 minutes. Images were acquired using a Nikon TE2000E motorized inverted microscope or a Nikon C1si spectral confocal.

3.2.4 Quantitative PCR and mRNA Expression

RNA levels were quantified after five days of culture using a Fast SYBR® Green Cells-to-CT™ Kit (Applied Biosystems, Foster City, CA). Reverse transcription was performed on a Mastercycler S (Eppendorf, Hamburg, Germany). Quantitative PCR was performed using a StepOne Plus (Applied Biosystems, Foster City, CA). The primers used include: Col 1 forward primer 5'-GCACGAGTCACACCGGAACT-3' and reverse 5'-AAGGGAGCCACATCGATGAT-3'; Col VI forward primer 5'-ACCCGGGACCGGCTACT-3' and reverse 5'-CAGAACGTCCATCCGTAATGAC-3'; α-SMA forward primer 5'-TCCTGACGCTGAAGTATCCGATA-3' and reverse 5'-GGTGCCAGATCTTTTCCATGTC-3'; integrin α3 forward primer 5'-ATCATCCTCCTCTTGTGGAAGTG-3' and reverse 5'-GCCTTCTGCCTCTTAGCTTCATA-3'; GAPDH forward primer 5'-TGGCCTCCAAGGAGTAAGAAAC-3' and reverse 5'- GGGATAGGGCCTCTCTTGCT-3'; and TGFB1 forward primer 5'-GAGGTCACCCGCGTGCTA-3' and reverse 5'-TGTGTGATGTCTTTGGTTTTCTC-3'. Each sample was analyzed in triplicate, and results were normalized to glyceraldehyde 3-phosphatedehydrogenase (GAPDH) and the flat PDMS substrates (1.7 MPa). Note that lysate collected from micropegged scaffolds consists of mRNA from cells adhered to micropegs and cells adhered to the flat regions. Thus, comparative analysis results on a conservative underestimate of the effects of the micropegs on gene expression.

3.2.5 Western Blotting

Protein levels were determined by Western blot, with detection by HRP conjugated secondary antibodies (Santa Cruz Biotechnology, Inc.) and development using Novex ECL chemiluminescent substrate (Invitrogen). ImageJ was used to determine band intensity levels from the developed blots. All intensity levels were internally normalized to the loading control (GAPDH or α-tubulin) prior to calculating ratios of protein levels on micropeg-textured versus flat scaffolds. Note that lysate collected from micropegged scaffolds consists of protein from cells adhered to micropegs and cells adhered to the flat regions. Thus, comparative analysis results on a conservative underestimate of the effects of the micropegs on protein expression.

3.2.6 Time Lapse Imaging

To analyze the dynamics of fibroblasts interaction with the micropegs, cells were cultured on patterned PDMS substrates and allowed to grow for 3 days and then imaged for 15 h. Where indicated, the MLCK inhibitor ML-7, the ROCK inhibitor Y-27632 (Calbiochem, San Diego, CA), or the integrin α3 antibody were diluted in complete medium prior to addition to cultures.

3.2.7 Contractility Inhibition Studies

To investigate the impact of cellular contractility, Y-27632 was used to inhibit Rho-associated kinase (ROCK) and ML-7 was used to inhibit myosin light chain kinase (MLCK) (Calbiochem, San Diego, CA, USA). Both drugs were diluted to 25 μM in complete medium prior to addition to the cultures. In all cases, cells were seeded and allowed to attach and spread for 1 hour before application of the drug, and the drug was left in the culture for 5 days prior to analysis.

3.2.8 Adhesion Disruption Studies

To investigate the impact of disruptions on cellular adhesion, cells were treated with a functional antibody against the extracellular domain of integrin α3 (2μg/mL, Chemicon) in complete medium. In all cases, cells were seeded and allowed to attach and spread for 1 hour before application of the antibody. Cells were cultured for 5 days prior to analysis.

3.2.8 Statistical Analysis

A statistically significant difference among groups was detected by analysis of variance (ANOVA). Sequential Holm t-tests were then performed to identify differences between specific pairs of conditions.

3.3 Results

3.3.1 Fibroblasts actively interact with the micropegs forming a three-dimensional network

In this work Polydimethyl siloxane (PDMS) flat and micropegged scaffolds of different stiffness were created to determine if surface elasticity and microtopography can influence fibroblasts' production of extracellular matrix proteins. To prepare the substrates with different stiffness (1.79 MPa and 50 kPa) the elastomer to crosslinker ratio was varied based on a protocol by Brown et al.[138] Cells were seeded on PDMS substrates that had been oxygen plasma treated and incubated in media for at least 1 hr. Fibroblasts were cultured for five days to allow for cells to proliferate and synthesize their own ECM. To observe the interaction of fibroblasts with the micropegged substrates a time lapse video was obtained after three days of culture. Cells attached to substrates and actively interacted with the micropegs, aligning with a set of micropegs, attaching to a micropeg, or releasing micropeg to bring other cells to attach to the micropegs (Figure 3.1). After five days of culture, cells where fixed, stained, and imaged using confocal microscopy. Cells that maintained a close interaction with micropegs formed a three-dimensional network with the micropegged substrate. Cells preferentially attach to micropegs and interestingly also formed bridges across micropegs (Figure 3.2). Cells attach and display similar cytoskeleton organization on both, the 1.79 MPa and the 50 kPa substrates. Substrate elasticity did not affect cell morphology and cell interaction with micropegs as analyzed by image analysis of cell area and cell shape index (Figure 3.6).

3.3.2 Microtopography and stiffness influence collagen synthesis

To investigate how the mRNA expression of extracellular matrix and other known fibrotic markers is affected by microtopography and stiffness, fibroblasts were cultured for five days on flat and micropegged susbstrates with elastic moduli of either 1.79 MPa or 50

kPa. Cells were lysed and mRNA content was analyzed by doing qPCR analysis. It was found that fibroblasts on substrates with micropegs have reduced expression of collagen type I (Col 1), collagen type VI (Col VI), alpha smooth muscle actin (α-SMA), and integrin alpha3 (Int α3) compared to fibroblasts cultures in flat substrates (Figure 3.3A). No significant difference in mRNA expression of the genes investigated was observed between the cells cultured on the 1.79 MPa flat substrates and the cells cultured on the flat 50 kPa substrates. There was no statistically significant down-regulation on Col 1 and Int α3 expression when cells where cultured on the softer micro-pegs (50 kPa). These markers were chosen to be analyzed since they have been shown to be elevated after myocardial infarction.[150-151] The results for transforming growth factor beta 1 (TGFB1) follow the same trend of mRNA expression on the different substrates.

These findings suggest that micropeg stiffness impacts expression of these genes but stiffness of flat substrate in the range investigated does not have a significant impact. Immunoflurescence staining and western blot analysis was done to qualitatively determine changes at the protein level. There was a decrease in the production of procollagen type I (Figure 3.3B) and Col VI (Figure 3.7A) on the micropegged substrates compared to the flat substrates which is consistent with our qPCR analysis. Additionally, there was reduced expression of α-SMA (Figure 3.4B and Figure 3.7B) and Int α3 (Figure 3.3C and Figure 3.7C) in fibroblasts cultured on micropegged substrates compared to cells cultured on flat substrates.

3.3.3 Inhibition of cell contractility prevents micro-topographical regulation of gene expression

Fibroblasts were cultured on flat and micropegged PDMS substrates of different stiffness in the presence of pharmacological inhibitors for Rho kinase (ROCK) and myosin light chain kinase (MLCK) to determine how inhibiting cell contractility influences microtopographical regulation of mRNA expression. The fibroblasts' morphology was altered in the presence of both ROCK inhibitor (Y27632) and MLCK inhibitor (ML7). Cells cultured in the presence of ROCK inhibitor showed more elongated morphology and more cells were in contact with micropegs than in control (Figure 3.4B and Figure 3.8). Cells cultured in the presence on MLCK inhibitors showed slightly less elongation compared to ROCK inhibited cells (Figure 3.4B and Figure 3.8). Microtopographical regulation of gene expression was dependent on the contractility of the cells. Analysis of mRNA expression by qPCR showed no significant difference in gene expression on micropegged surfaces compared to flat surfaces when cells where culture in the presence of both ROCK inhibitor and MLCK inhibitor (Figure 3.4A). Additionally, immunofluorescence staining showed no changes in α-SMA expression (Figure 3.4B, Figure 3.9A and Figure 3.9B) in fibroblasts cultured on micropegged substrates compared to cells cultured on flat substrates. In contrast with ROCK inhibited cells, fibroblasts grown in the presence of MLCK inhibitors showed mRNA expression patterns which follow studies in the absence of inhibitors.

3.3.4 Integrin α3 blockade enhances microtopographical down-regulation of α-smooth muscle actin and prevents regulation of collagen expression by microtopography

To determine if down regulation of collagen and alpha smooth muscle actin by microtopograhy was dependent on cell adhesion and integrin mediated mechanotransduction, cell cultures were treated with a functional antibody against the extracellular domain of integrin α3. With the antibody present, cells grown on micropegged substrates seem to recover normal phenotype (Figure 3.8). Although cells cultured on micropegs displayed restored morphology compared to cells on flat substrates, disruptions in cell adhesion prevented microtopographical regulation of ECM. Interestingly, when the extracellular domain of integrin α3 was blocked, enhanced downregulation of α-SMA expression in cells cultured on the stiffer micropegged substrates was observed compared to cells cultured on the flat substrate, but no differences in the expression of Col 1, Col VI, and TGB1 were observed (Figure 3.5A). Immunofluorescence staining showed reduced expression of α-SMA in fibroblasts cultured on micropegged substrates compared to cells cultured on flat substrates in the presence of the integrin α3 blocking antibody (Figure 3.5B and Figure 3.9C).

3.4 Discussion

In this work we explored the incorporation of microtopographical cues in the form of micropegs on a 2D scaffold as a way to regulate expression of extracellular matrix molecules and other fibrotic markers. The critical role that fibroblasts have in myocardial remodeling has rendered them an attractive therapeutic target for the treatment of the failing heart and other fibrotic pathologies.[152-154] Myofibroblasts, which are activated fibroblasts with the novo expression of alpha smooth muscle actin (α-SMA)[155], are found at the infarct site after day 3-4 post infarction. Myofibroblasts are considered the main synthesizers of collagen and other ECM molecules after tissue injury, but in contrast with other tissues, cardiac myofibroblasts remain in the infarct site years after the myocardial infarction.[156-157]

Although there is a significant increase in collagen I, collagen III, and collagen VI production in cardiac pathology after myocardial infarction, recent studies have shown that collagen VI in particular plays an important role in myofibroblast expression, and the origin of fibrosis in the heart and in other diseased tissues as well.[12-15] In these studies, it was observed that fibroblasts' extracellular matrix synthesis is down-regulated by microtopography on two dimensional PDMS substrates. Micropegs also down-regulate the expression of α-smooth muscle actin, integrin α3, and TGFB1, however this effect seems to be dependent on micropeg stiffness. When cells where cultured on the softer micropegs (50 kPa), there was no statistically significant down-regulation on Col 1 and Int α3 expression. The expression of collagen type VI correlated with the expression of α-SMA which is in agreement with an earlier study which showed that collagen type VI induces the cardiac myofibroblast phenotype.[13]

Our previous studies have shown that micropegs reduced primary cardiac fibroblast proliferation,[137] and the interaction of 3T3 fibroblasts with the micropegs resulted in a decrease in BrdU incorporation compared to fibroblasts only contacting the flat areas of the substrate.[144] Moreover, when cardiac myocytes were cultured on similar

micropegged substrates they displayed *in vivo* like phenotype and had greater attachment and cell height compared to flat culture substrates.[158] Surface topography also had a significant impact on gene expression and protein distribution which resulted in an increase in myofibrillar height and a decrease in cell area.[92] Subsequently it was shown that microtopographical cues in a 3D system also inhibit fibroblast proliferation. SU-8 epoxy microrods suspended in matrigel significantly inhibited the proliferation of the fibroblasts as compared to a three-dimensional matrigel culture without microrods.[141] In contrast, these same microrods increased human mesenchymal stem cell proliferation and slowed osteogenic differentiation.[159] In addition, it was observed that polyethylene glycol dimethacrylate (PEGDMA) microrods of different stiffness could affect proliferation and differentially regulate extracellular matrix production with stiffer microrods having a greater effect. Here we show that microtopographical cues on a two dimensional scaffold also down regulate ECM synthesis and expression of fibrotic markers. Consistent with previous studies in a three dimensional system, stiffness of the microstructure is important in its ability to regulate gene expression.

These effects are dependent on the cell's ability to sense and interact with the microstructures through cell adhesion and contractility. An important mediator of cytoskeletal tension is the small GTPase RhoA. It plays a critical role in the assembly of actin stress fibers in response to various stimuli such as cell adhesion, shape, and cytoskeletal tension.[160] RhoA propagates downstream signals in effector proteins such as Rho associated Kinase (ROCK). Direct phosphorylation of myosin light chain (MLC) by ROCK can lead to contractile force generation. Independent from RhoA, phosphorylation of MLC can also be regulated by Ca^{2+} -dependent myosin light chain kinase (MLCK). In this work, when the fibroblasts' myosin based-contractility was inhibited by two different independent mechanisms (ROCK and MLCK) there was no down-regulation of collagen synthesis and other fibrotic markers on micropegged substrates compared to flat substrates. These observations are consistent with previous studies in 2D micropegged surfaces where modulation of cell proliferation was found to be contractility-dependent[144] and treatment with Y27632 and ML7 resulted in increased cell proliferation.[161] Inhibition of ROCK with Y27632 suppressed the micropegs' ability to regulate gene expression. Treating cells with ML7 resulted in attenuation of microtopographical regulation of mRNA expression since the mRNA expression trends remained similar to untreated cells. It was previously shown that cells on micropegged substrates displayed greater tether lengths compared to cells on flat substrates.[145] This difference in tether length was also observed after treatment with ML7 and cells on micropegged substrates displayed similar tether lengths to cells culture on untreated flat substrates suggesting micropegs could rescue contractility. Treatment with Y27632 prevented differences in tether length between cells on flat substrates and cells on micropegged substrates.[145] Taken together, these observations suggest that contractility inhibition with ML7 seems to only attenuate microtopographical regulation of cell proliferation and gene expression whereas inhibition with Y27632 results in suppression of microtopographical regulation. ML7 targets MLCK which only phosphorylates myosin light chain, while Y27632 targets ROCK which phosphorylates MLC, inhibits myosin light chain phosphatase (MLCP) and can also activate LIM Kinase (LIMK) which regulates actin cytoskeletal organization.[162] Previous studies indicate that MLCK is responsible for MLC phosphorylation at the periphery and ROCK regulates MLC phosphorylation in the center of cells which results on decreased focal

adhesion maturation in the center.[163] Cells cultured with ML7 have rescued contractility by ROCK activity in the center, and MLCK activity rescues contractility in the periphery when cells are treated with Y27632. This indicates that microtopographical regulation depends on cell contractile mechanics. Specifically, mechanotrasduction signals might be more closely dependent on the formation of focal adhesions in the center of the cell than at the periphery.

In addition, it was observed that blocking the extracellular domain of integrin α3 hindered the micropegs' ability to down-regulate the expression of collagen, and enhanced the down-regulation of α-SMA by the micropegs. Integrins are the main receptors that form transmembrane connections between the extracellular matrix and the actin cytoskeleton. In the infarcted myocardium integrin α3 is elevated 3 days post-MI and precedes the expression of myofibroblasts and collagen VI. It has been observed that both types collagen VI and collagen III interact with the integrin α3 receptor in cardiac fibroblasts.[150] In this work, fibroblasts cultured in the presence of the integrin α3 antibody displayed more rounded morphology and fewer cell to cell connections. These observations are consistent with earlier studies which showed that α3β1-deficient keratinocytes failed to polarize in the direction of the wound and instead scattered at random as individual cells rather than a cohesive monolayer.[164] In a different study it was observed that the inhibition of integrin α3 extracellular domain resulted in reduced myoblast adhesion and decreased of fusion index.[165] Morover, studies have shown that blocking functionality of α3 integrin receptor with an antibody can lead to an attenuation of type VI collagen induced myofibroblast differentiation.[150] And recently a study also showed that deletion of integrin α3 prevented epithelial-mesenchymal transition a source of myofibroblasts in lung fibrosis.[166] Thus, integrin α3 is implicated as an important regulator of cell phenotype, cell-cell interactions, and matrix deposition. Our studies indicate that expression of this molecule could be down-regulated by stiffer micro-pegs. Additionally blocking integrin α3 enhanced the down-regulation of α-smooth muscle actin by the microtopography, but disruption of cell adhesion abrogated regulation of ECM. These observations suggest that microtopographical regulation of ECM is cell adhesion dependent whereas α-SMA expression is closely regulated by integrin α3. Fibroblasts on micropegged substrates may have reduced Integrin α3 expression even in the presence of the blocking antibody, which results in enhanced α-SMA downregulation on these substrates. Future studies could focus on the temporal expression of these markers and the specific pathways involved in microtopographical regulation of gene expression.

3.5 Conclusion

The present study demonstrates that micro scale cues on a two dimensional scaffold affect gene expression, and extracellular matrix regulation. We utilized PDMS scaffolds of different stiffness with topographical cues in the form of micropegs to investigate the role of microtopographical cues on gene expression and extracellular matrix (ECM) synthesis. No differences in gene expression were observed on cells cultured on the flat substrates of different stiffness. Cells cultured on micropegged substrates showed reduced collagen synthesis and a decreased expression of other important markers elevated after myocardial infarction which are known to contribute to the remodeling process. Stiffer micropegged substrates had a greater effect than softer micropegged substrates. Morover,

microtopographical regulation of gene expression was found to be dependent on cell contractility and cell adhesion. When cells were cultured in the presence of contractility inhibitors, no significant differences in gene expression were observed. Functional blocking of Int $\alpha 3$ prevented regulation of ECM expression and enhanced microtopographical down-regulation of α-SMA. Overall, these studies add to the body of knowledge showing the critical role physical cues alone have on cell behavior and performance. These findings highlight the influence of micro-scale cues on gene expression and the critical role of integrins in mechanotransduction. In addition, this knowledge could be applied towards the design of novel therapeutic platforms that could provide a microenvironment for optimal tissue regeneration.

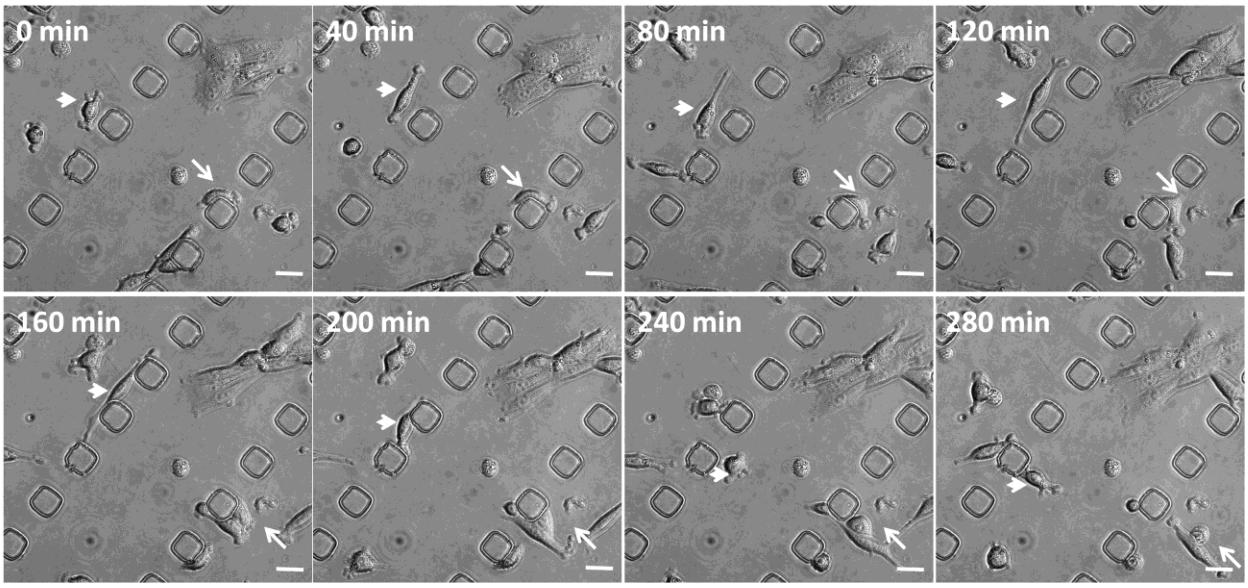

Figure 3.1 Fibroblasts actively interact with the micropegs. Time lapse bright field imaging of fibroblasts at day 3 interacting with the micropegs. Short arrows follow cell number 1 and long arrows follow cell number 2. Cells actively attach, align, and detach from the micropegs to bring other cells in contact with micropegs. Scale bar, 25 μm.

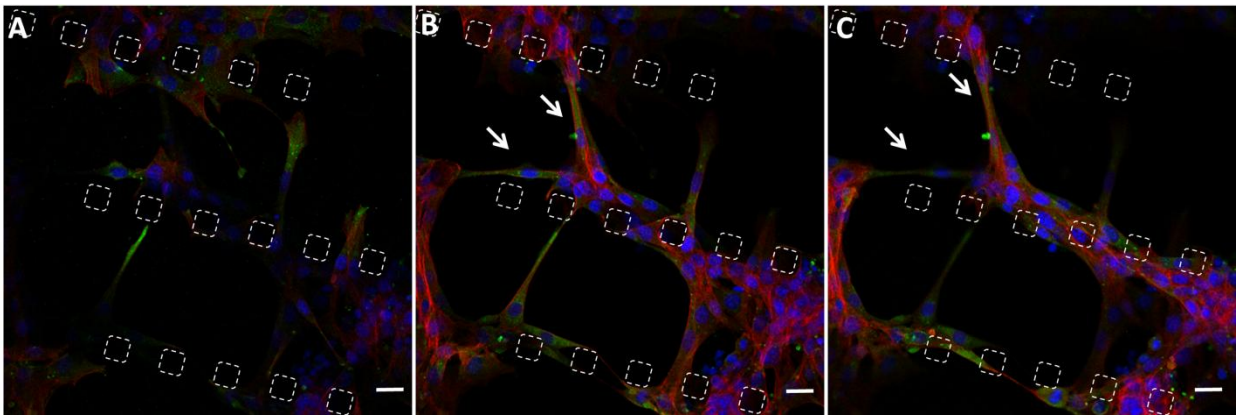

Figure 3.2 Fibroblasts form a three-dimensional network with the micropegged substrate. Confocal imaging at day 5 reveals cells interacting with the micropegs at the (A) bottom, (B) middle, and (C) top of the micropegs (50 kPa substrate). Arrows show cells bridging micropegs. Blue: Nuclei, Red: F-actin, Green: α-SMA. Scale bar, 25 μm.

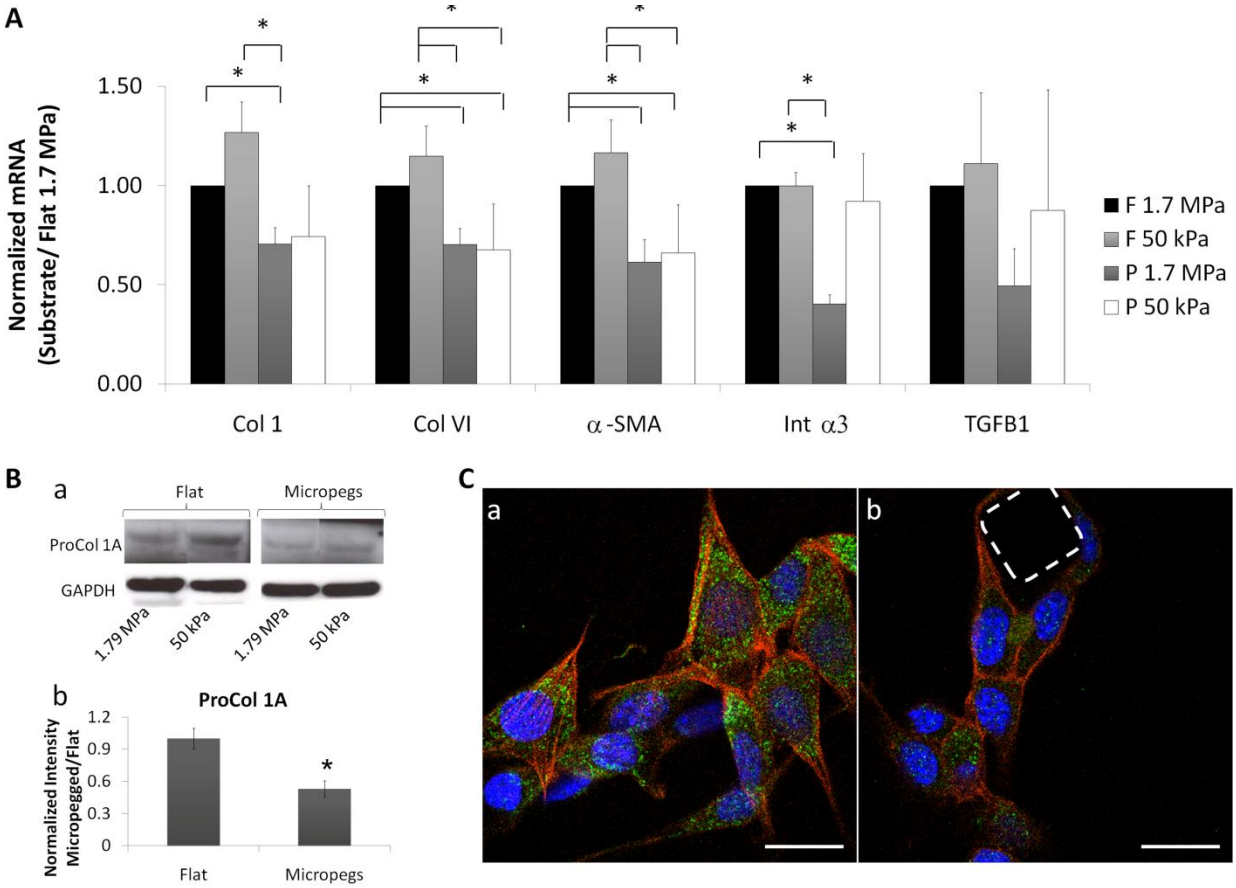

Figure 3.3 Microtopography and stiffness influence gene expression and collagen synthesis. (A) Fibroblasts on substrates with micropegs (P) have reduced expression of collagen type I and collagen type VI, α-SMA, and integrin α3 compared to fibroblasts cultures in flat substrates (F) as analyzed by qPCR. Data is normalized to GAPDH and 1.79 MPa flat substrate. Bars represent SEM and (*) indicates $p < 0.05$, (n = 5). (B) Fibroblasts on micropegged substrates have reduced collagen synthesis compared to cells on flat substrates as analyzed by a) Western Blot and b) Immunoflurescence staining. (C) Immunofluorescence staining shows decreased integrin α3 expression in cells cultured on micropegged substrates (b) compared to cells cultured on flat substrates (a). Dashed line indicates micropeg. Blue: Nuclei, Red: F-actin, Green: Integrin α3. Scale bar, 25 μm.

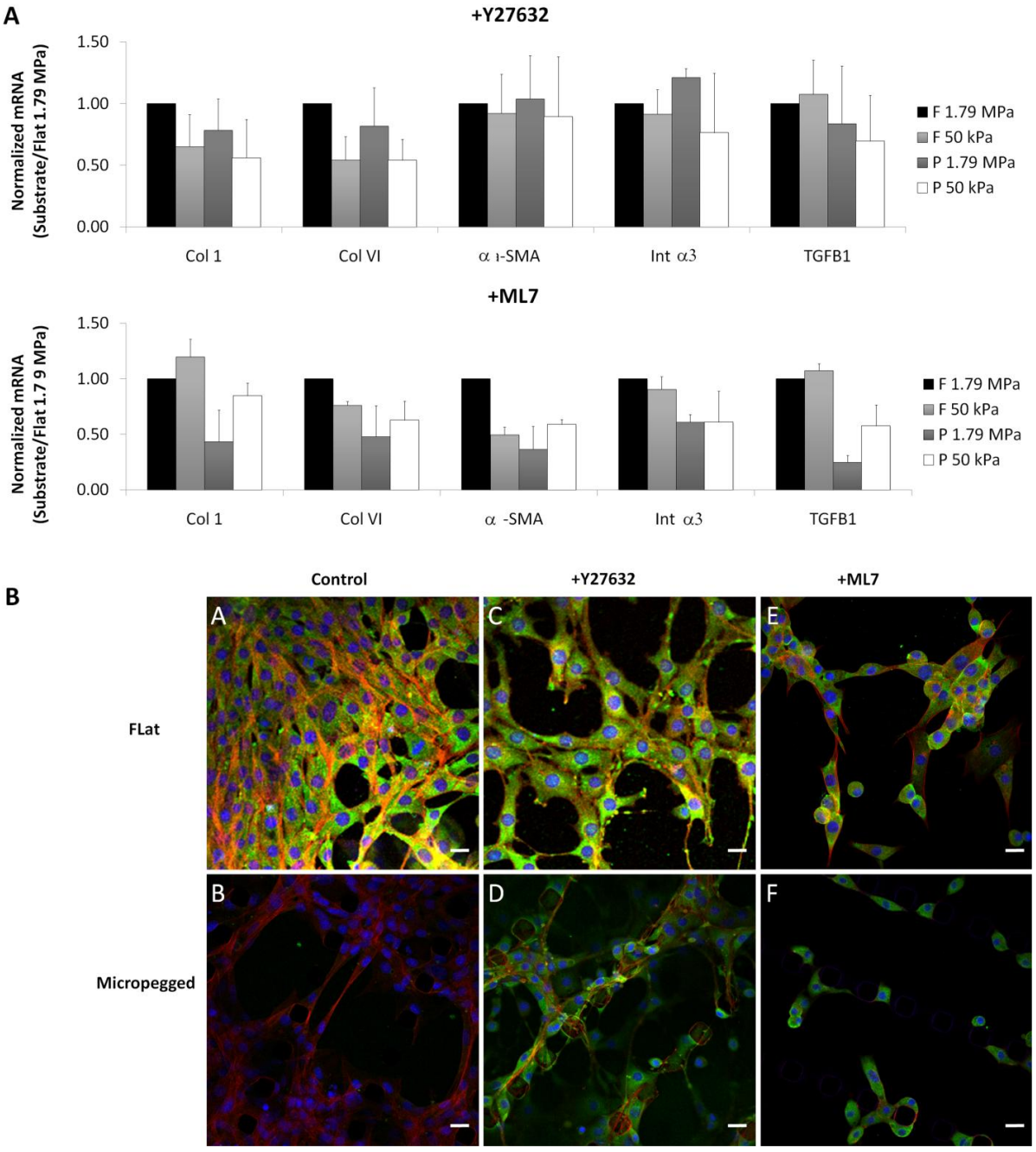

Figure 3.4 Inhibition of cell contractility prevents micro-topographical regulation of gene expression. A) When cells are cultured in the presence of ROCK inhibitor (Y27632) no differences in the expression of collagen, α-SMA, Int α3, and TGFB1 are observed among the different groups. In the presence of myosin light chain kinase inhibitor (ML7) microtopography regulation is attenuated but data did not reach statistical significance. Data is normalized to GAPDH and 1.79 MPa flat substrate. Bars represent SEM, (n = 3). B) Immunofluorescence staining of α-SMA on flat (top) and micropegged (bottom) on 1.79 MPa substrates at day 5. (a & b) control, and (c & d) treated with ROCK inhibitor (Y27632), and (e & f) treated with MLCK inhibitor (ML7). Blue: Nuclei, Red: F-actin, Green: α-SMA. Scale bar, 25 μm.

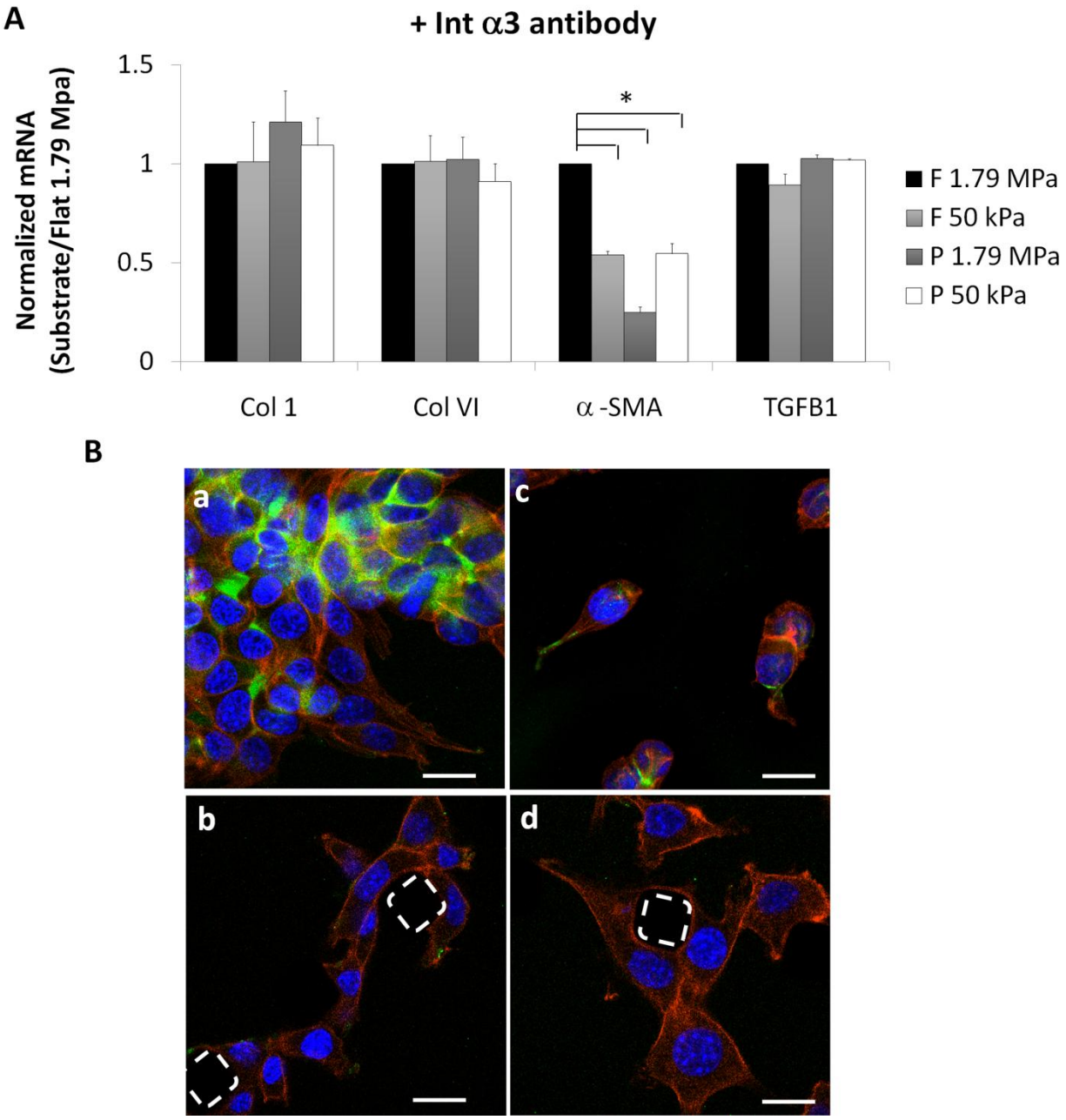

Figure 3.5 Integrin α3 blockade enhances microtopographical down-regulation of α-smooth muscle actin and prevents regulation of collagen expression by microtopography. A) When the adhesion molecule integrin α3 is blocked no differences in the expression of collagen type I, collagen type VI, and TGFB1 are observed. However blocking of integrin α3 enhances down-regulation of α-SMA on the micropegged substrates. Data is normalized to GAPDH and 1.79 MPa flat substrate. Bars represent SEM and (*) indicates $p < 0.01$, (n = 3). B) Immunofluorescence staining of α-SMA on flat (top) and micropegged (bottom) on 1.79 MPa substrates at day 3. (a & b) control, and (c & d) treated with integrin α3 antibody. Blue: Nuclei, Red: F-actin, Green: α-SMA. Scale bar, 25 μm.

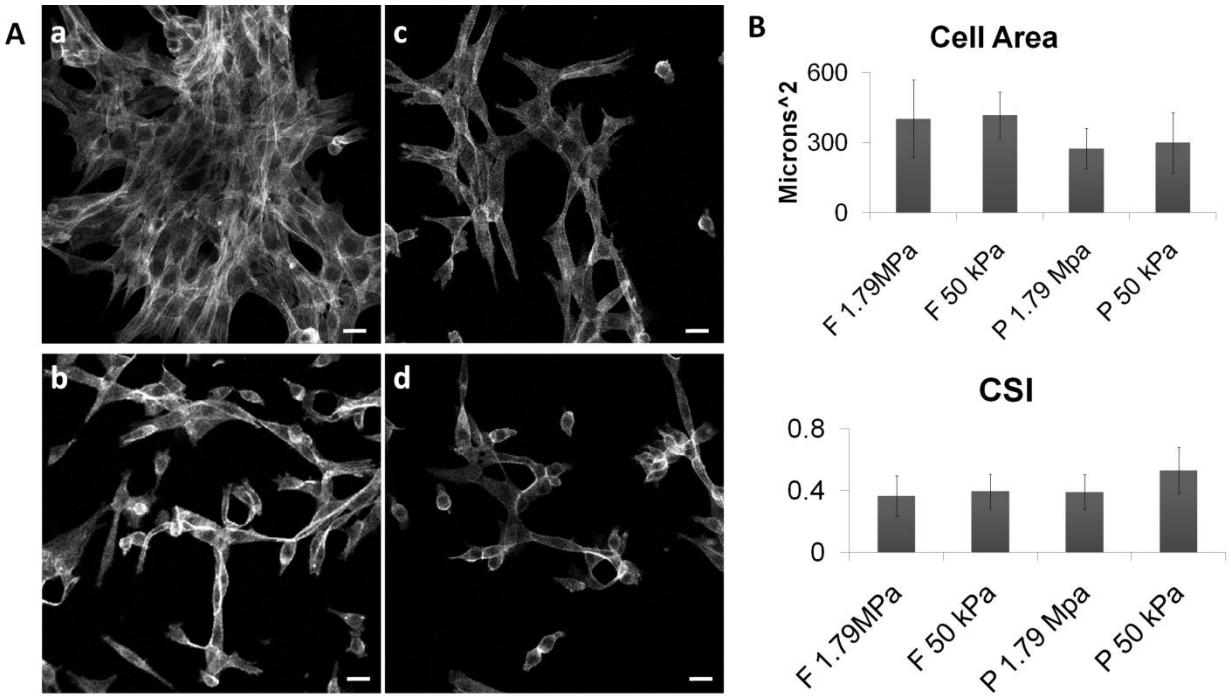

Figure 3.6 A) Fibroblasts on flat (top) and micropegged (bottom) substrates. (a-b) 1.79 MPa substrates, (c-d) 50 kPa substrates. F-actin. Scale bar, 25 μm. B) Cell area and cell shape index (CSI) did not significantly changed on the 1.79 MPa substrates compared to the 50 kPa substrates.

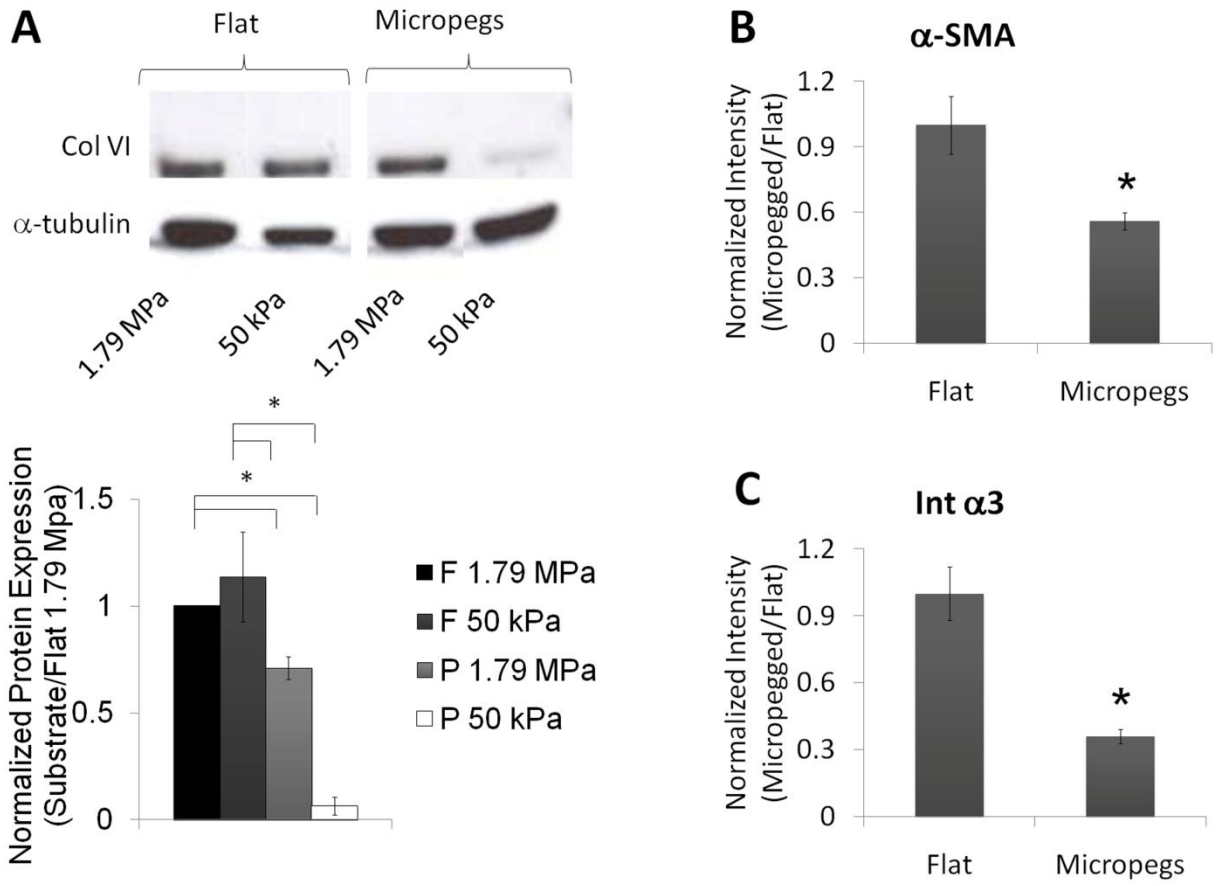

Figure 3.7 (A) Fibroblasts on substrates with micropegs (P) have reduced expression of collagen type VI compared to fibroblasts cultures in (F) flat substrates as analyzed by western blot. Fibroblasts on substrates with micropegs have reduced expression (B) α-SMA, and (C) integrin α3 compared to fibroblasts cultures in flat substrates as analyzed by immonoflurescence staining. Data is normalized to 1.79 MPa flat substrate. Bars represent standard deviation and (*) indicates $p < 0.05$.

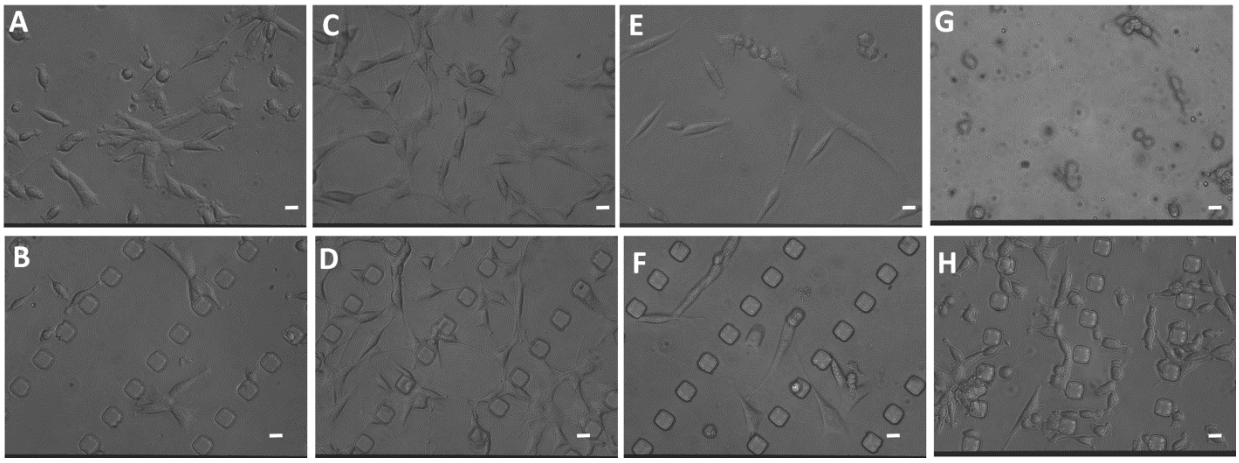

Figure 3.8 Bright field imaging of cells at day 3 on flat and micropeg substrates (A-B) control, (C-D) with ROCK inhibitor (Y27632), (E-F) with MLCK inhibitor (ML7), and (G-H) with integrin $\alpha 3$ antibody. Scale bar, 25 μm.

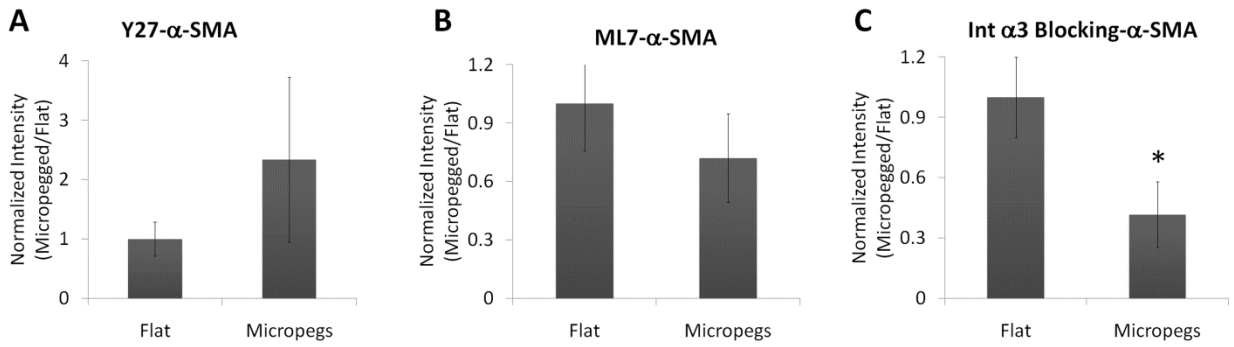

Figure 3.9 In the presence of (A) ROCK inhibitor (Y27632) or (B) myosin light chain kinase inhibitor (ML7) no difference in the expression of α-SMA, is observed between cells cultured on flat substrates and cells cultured on micropegged substrates. (C) Blocking of integrin α3 results in down-regulation of α-SMA on the micropegged substrates comapared to flat substrates as analyzed by immunofluorescence staining. Data is normalized to 1.79 MPa flat substrate. Bars represent standard deviation and (*) indicates $p < 0.05$.

Chapter 4. Biocompatible and Tunable Microstructures in 3D Culture

Abstract

Recent studies have highlighted the role of external biophysical cues on cell morphology and function. In particular, substrate geometry and rigidity in 2D has been shown to impact cell growth, death, differentiation, and motility. Knowledge of how these physical cues affect cell function in three dimensions is critical for successful development of novel regenerative therapies. In this work, the effect of discrete micromechanical cues in 3D on cell proliferation, gene expression and extracellular matrix (ECM) synthesis was investigated. PEGDMA hydrogel microrods were fabricated using photolithography and suspended in gel to create a 3D culture with microscale cues of defined mechanical properties in the physiological range (2kPa-50kPa). These microrods significantly affected fibroblast proliferation, matrix production, and gene expression. Cultures with stiff microrods reduced fibroblast proliferation and down-regulated expression of key ECM proteins involved in scar tissue formation. In addition, the contractility marker alpha smooth muscle actin (α-SMA) and adhesion molecule integrin $\alpha 3$ were also significantly down-regulated. Cultures with soft microrods had no significant difference on fibroblast proliferation and expression of Cyclin D1, α-SMA, and integrin $\alpha 3$ compared to cultures with no microrods. Here, we present a new platform of potentially injectable microrods with tunable elasticity; in addition we show that cell proliferation and gene expression are influenced by discrete physical cues in 3D.

4.1 Background

There is increasing evidence that the efficacy of tissue regeneration is likely dependent on creating a suitable microenvironment that can support cell function and decrease pathological healing. For example, recent findings have demonstrated that the functional improvements associated with the direct delivery of hematopoietic stem cells to the heart is not due to their capacity to differentiate into myocytes, but rather their secretion of factors that appear to be beneficial for angiogenesis.[167-169] One issue regarding cell retention or death may be due to defects of the microenvironment. An environment is needed which allows for perfect, rather than "suboptimal" healing, one in which the type and amount of extracellular matrix (ECM) synthesis is suitable for the tissue regeneration, rather than fibrous scarring. In the last several years, mechanical, topographical, and geometrical cues have been shown to modulate cellular morphology and behavior in 2D and 3D systems.[37,45,137-143] However, the potential to control fibroblast behavior and ECM synthesis using discrete microtopographical cues has not been fully explored. This knowledge could provide a better understanding of the role of topography in matrix remodeling, with the potential to enhance regenerative therapies.

In vivo, the intrinsic chemical and mechanical properties of the ECM play a critical role in controlling the organization, proliferation, differentiation, and migration of stem[132,170] and mature[35-36,130-131] cell populations. In particular, numerous studies have shown that the rigidity of the ECM can have a significant effect on cellular phenotype, migration and differentiation.[37-38,133] Mesenchymal stem cells (MSCs) differentiate to a specific lineage depending on the elasticity of the matrix in 2D[37] and fibroblasts preferentially proliferate in 3D rigid gels and migrate more in flexible ones.[171]

Furthermore, an increase of rigidity in the matrix could also be associated with pathological conditions such as cancer and heart failure.[134-135]

Stiffening of tissue can be directly attributed to fibrosis, the over deposition of extracellular matrix (ECM) proteins. Chronic forms of fibrotic diseases cause almost 45% of all deaths in the developed world.[172] Pathological production of extracellular matrix has been well recognized in the heart, liver, lung, kidney, bone marrow, cornea, spinal cord, skin, and even in the tumor stroma microenvironment.[12,134,153,172-174] A particular case where fibrosis prevents tissue regeneration can be observed in the myocardium following a heart attack. Studies have found an increase in collagen I, collagen III and collagen VI production in cardiac pathology after myocardial infarction.[9,150,157] Fibrous tissue appears in the infarcted and also non-infarcted myocardium.[9] The measured elastic modulus of myocardium in healthy rats yields E=18 kPa, while there is a threefold increase (E=60 kPa) for infarcted myocardium.[16] Tissue stiffness has been shown to have a critical effect on cardiomyocyte function with scar-tissue rigidity having an adverse effect on embryonic cardiomyocyte beating. Injected MSCs have been shown to reduce the stiffness of scar formation after myocardial infarction[16], while another study showed that injection of MSCs resulted in the generation of ossifications in the infracted myocardium.[136]

Fibroblasts are the main synthesizers of ECM, but after injury they acquire a contractile phenotype characterized by the expression of alpha smooth muscle actin (α-SMA).[155] Interstitial fibroblasts are responsible for collagen synthesis in the normal myocardium, while contractile fibroblasts, termed myofibroblasts, have been associated with fibrosis at the site of injury following a myocardial infarction. Controlling fibroblast numbers and aberrant collagen production is a critical step to sustain the intrinsic tissue regeneration process. By manipulating the cues that cells encounter in the microenvironment, it may be possible to guide cell behavior and support tissue regeneration. Previously, we have shown that microtopography plays an important role in fibroblast proliferation. Micropegs on a 2D surface decrease proliferation of fibroblasts compared to flat surfaces.[137] In addition, this was correlated with a significant decrease in cyclin D1 expression demonstrating that cell proliferation was affected at the level of G1/S cell cycle transition.[137] Furthermore, it was found that this effect was dependent on local micropeg-cell interactions and was regulated by contractile mechanics.[144] Subsequently we showed that microtopographical cues in a 3D system also inhibit fibroblast proliferation. SU-8 epoxy microrods suspended in matrigel significantly inhibited the proliferation of the fibroblasts as compared to a three-dimensional matrigel culture without microrods.[141] We have also shown that these stiff epoxy microrods could have an opposite effect on stem cells in a 3D culture. These same microstructures increased human mesenchymal stem cell proliferation and slowed osteogenic differentiation.[175]

Although there are some studies that have addressed the effect of mechanical stretching on fibroblast phenotype and ECM synthesis[146-149], little is known about the combined effect of substrate stiffness and microtopography on fibroblasts and ECM synthesis. Effective strategies to avert the development of fibrosis while allowing overall repair would represent a critical therapeutic innovation.[6] In this work, we develop a biocompatible microrod system with tunable mechanical properties to investigate the role of 3D micromechanical cues on fibroblast function.

4.2 Materials and Methods

4.2.1PEGDMA Microrod Fabrication

Microrods were fabricated using a precursor solution consisting of poly(ethylene glycol) dimethacrylate (PEGDMA) MW 750 (Sigma-Aldrich, St. Louis, MO), photo-initiator 2,2-dimethoxy-2-phenylacetophenone (Sigma-Aldrich, St. Louis, MO) dissolved in 1-vinyl-n-pyrrolidone (Sigma-Aldrich, St. Louis, MO) cross-linker (100 mg/mL), and 1X phosphate-buffered saline (PBS). Microrods were created with different magnitudes of stiffness by varying the PEGDMA (90%, 50%, 10% w/v) and the photoinitiator-crosslinker concentration (0.8%, 0.1%, 0.04% w/v). The hydrogel precursor solution was sonicated at room temperature (VWR Model 75T; West Chester, PA) for 15 minutes to ensure complete mixing of reagents.

Photolithography was used to create microrods designed to be 100μm long with a 15 x 15 μm cross section. Microrods were micro-fabricated in 3 inch silicon wafers. Each wafer was cleaned in piranha solution (3:1, H_2SO_4:H_2O_2) for 20 min, and rinsed with deionized water three times. Wafers were then rinsed with acetone, methanol and isopropanol and then baked at 200 ^oC for 2 min. The PEGDMA precursor solution was then spun onto each wafer to achieve a desired thickness of 15 μm. The wafer was exposed using a Karl Suss MJB3 mask aligner to a 405nm light source through the microrod patterned photomask at 9mW/cm^2 until crosslinking. The height of the microstructures was confirmed using an Ambios Technology XP-2 profilometer (Figure 2). Microrods on the wafer were then rinsed with isopropanol and dried with N_2 gas. Microrods were removed from the wafer by rinsing wafer with 70% ethanol and gently scraping microrods with a cell scraper. Collected microrods were centrifuged and rinsed in 70% ethanol three times. Microrods were then centrifuged and rinsed with sterile 1X phosphate-buffered saline (PBS) three times. Microrods were finally resuspended in cell culture media.

4.2.2 Cell Culture

NIH 3T3 mouse fibroblasts were cultured in complete medium consisting of Dulbecco's Modified Eagle's Medium (DMEM) with 10% fetal bovine serum and 1% penicillin/streptomycin (Gibco-BRL, Grand Island, NY). Cell cultures were maintained in a humidity-controlled 5% CO_2 incubator at 37°C and were allowed to grow to ~90% confluence. Prior to seeding, cells were trypsinized and resuspended in complete medium. For 2D cultures, the microrods remained attached to the surface and cells were plated at a density of 10,000 cells cm^{-2} and washed after 1 hour to remove non-adherent cells. Cultures were fixed after five days. For 3D cultures, cells were initially seeded at a concentration of 2,500 cells per 65 μL of low growth factor Matrigel (BD Biosciences, San Jose, CA) (4 mg/mL) either without microrods or with microrods at a seeding ratio of 1:5 number of microrods to number of cells into individual wells in a 96 well plate. This resulted in 2 mm-thick gels. The plate was incubated at 37 ^oC for 30 minutes to allow gels to solidify completely. Each gel was then covered with 200 μL of media and plate was placed in an incubator at 37 ^oC for five days.

4.2.3 Fluorescent Microscopy

Cells were fixed in 4% paraformaldehyde (Fisher Scientific, Pittsburgh, PA) for 15 minutes, permeabilized with 0.5% Triton X-100 (Sigma, St. Louis, MO) for 15 minutes, and blocked with 1% bovine serum albumin (BSA) (Sigma, St. Louis, MO) for 30 minutes. F-actin was stained using Alexa Fluor 488 phalloidin (Molecular Probes, Eugene, OR) for 30 minutes. Nuclei were then stained with Hoechst 33258 (Molecular Probes, Eugene, OR, USA) for 5 minutes. The Hoechst solution and the Alexa Fluor were also absorbed by the PEGDMA microrods allowing us to easily visualize the rods in 3D culture. Images were acquired using an Olympus BX 60 microscope, a Nikon TE2000E motorized inverted microscope or a Nikon C1si spectral confocal.

4.2.4 Scanning Electron Microscopy

Samples were dehydrated by adding and replacing a series of ethanol solutions in a graded series (35%, 50%, 70%, 95%, 100%). The final 100% ethanol solution was replaced with hexamethyldisilazane (HMDS) (PolySciences, Inc., Warrington, PA) for 10 minutes and removed rapidly. Samples were allowed to dry completely in vacuum overnight and analyzed in a Novelx *my*SEM (Lafayette, CA).

4.2.5 Proliferation Assay

Cellular proliferation was assessed at five days after initial seeding in the gels using an MTT (3-(4,5-Dimethylthiazol-2-yl)-2,5-diphenyltetrazolium bromide) assay (Sigma-Aldrich, St. Louis, MO). On the day of the assay, media was removed from the wells and was replaced with 100 μL of fresh growth media and 16.5 μL of the MTT reagent. The plate was then placed back in the incubator for 4 hours. After this time, the formazan crystals were dissolved with the solubilization solution and the absorbance was measured and compared to a standard curve to calculate the number of cells present.

4.2.6 Stiffness Characterization

Films of various PEGDMA concentration (90%, 50%, 10% w/v) and photoinitiator-crosslinker concentration (0.8%, 0.1%, 0.04% w/v) were prepared for stiffness characterization. For each hydrogel film, 100μL of the precursor solution were placed on a glass slide. The glass slide was exposed using a Karl Suss MJB3 mask aligner to a 365 light source at 9mW/cm^2 until crosslinking. The hydrogels were rinsed once with 1X phosphatase-buffered saline (PBS) and then soaked in 1X PBS for one week. Hydrated films of various PEGDMA and cross-linker concentrations were attached on a glass slide and mounted onto the stage of an Asylum MFP-3D atomic force microscope (Asylum Research, CA) coupled to a Nikon TE2000U epifluorescence microscope. Force measurements were obtained using Olympus silicon nitride cantilevers with nominal spring constants of 2.0 N/m. Displacement vs. position data was converted to force vs. indentation based on the estimated hard contact position, that was fitted to a Hertzian model to obtain Young's moduli. Force loading was applied to at least three sites in each sample.

4.2.7 RNA Isolation and Reverse Transcription

Total RNA was isolated from fibroblasts 5 days after culture. Trizol (Invitrogen) and Qiagen microRNA purification columns were used to isolate and purify RNA according to manufacturer's protocol. Genomic DNA contamination was removed by treating the

isolated RNA using RQ1 RNase-Free DNase (Promega, Madison, WI). RNA concentrations were quantified using a NanoDrop spectrophotometer (Thermo Scientific, Wilmington, DE). RNA was reverse transcribed using iScript cDNA (BioRad, Hercules, CA) and a thermal cycler Mastercycler S (Eppendorf, Hamburg, Germany) according to the manufacturer's protocol (5 minutes at 25°C, 30 minutes at 42°C, and 5 minutes at 4°C).

4.2.8 Quantitative PCR

Quantitative polymerase chain reaction (q-PCR) was performed with Power SYBR Green PCR Master Mix and a StepOne Plus Real-Time PCR System (Applied Biosystems, Foster City, CA). To ensure specificity of polymerase chain reaction (PCR), melt-curve analyses were performed at the end of all PCRs. The relative amount of target cDNA was determined from the appropriate standard curve and normalized by the amount of GAPDH cDNA present in each sample. Primers (Integrated DNA Technologies, San Diego, CA) are provided in Table 1. Each sample was analyzed in triplicate, and results were expressed relative to glyceraldehyde 3-phosphatedehydrogenase (GAPDH) as an endogenous control.

4.2.9 Contractility Inhibition Studies

To investigate the impact of cellular contractility, Y-27632 was used to inhibit Rho-associated kinase (ROCK) and ML-7 was used to inhibit myosin light chain kinase (MLCK) (Calbiochem, San Diego, CA, USA). Both drugs were diluted to 25 μM in complete medium prior to addition to the cultures. In all cases, cells were seeded and allowed to attach and spread for 1 hour before application of the drug, and the drug was left in the culture for 5 days prior to analysis. For contractility inhibition studies messenger RNA levels were quantified using a Fast SYBR® Green Cells-to-CT™ Kit (Applied Biosystems, Foster City, CA). Reverse transcription was performed on a Mastercycler S (Eppendorf, Hamburg, Germany). Quantitative PCR was performed using a StepOne Plus (Applied Biosystems, Foster City, CA). Each sample was analyzed in triplicate, and results were expressed relative to glyceraldehyde 3-phosphatedehydrogenase (GAPDH) as an endogenous control.

4.2.10 Statistical Analysis

A statistically significant difference among groups was detected by analysis of variance (ANOVA). Sequential Holm t-tests were then performed to identify differences between specific pairs of conditions.

4.3 Results

In this work, the mechanical properties of PEGDMA hydrogels were altered by both varying the monomer concentration while maintaining a set cross-linker concentration and changing cross-linker concentration while keeping monomer concentration constant. The elastic modulus of PEGDMA hydrogel films of various monomer and crosslinker concentration were analyzed by atomic force microscopy (Figure 4.1). For the hydrogels analyzed in these studies, changing the crosslinker concentration in PEGDMA hydrogels yielded greater elastic moduli range (2-50 kPa) than varying the monomer concentration (1.5-20 kPa).

Photolithography was used to create microrods of (H=15 μm, W=15 μm L=100 μm) with physiological stiffness[133] (2-50 kPa) by varying cross-linker concentration while

keeping the monomer concentration constant (Figure 4.2). This allowed for the development of microrods with very similar chemical composition but different mechanical properties in the physiological stiffness range. The length and width of the microrods is controlled by the mask, whereas the height of the microrod is controlled by the spin rate. By maintaining the monomer concentration, the viscosity of the precursor solution was unchanged allowing the spin rate to be consistent, thus enabling the fabrication of reproducible sized microrods with a range of elastic moduli.

To ensure that microrods were not toxic and to examine the interaction of fibroblasts with these hydrogel microstructures, fibroblasts were cultured on 2D surfaces with attached PEGDMA microrods (100 μm x 100 μm spacing). We observed that cells closely interacted with microrods of all stiffness in 2D. Interestingly they formed a distinct ordered architecture when in contact with the microrods even when not functionalized with adhesive ligands. Cells not only grow in the presence of the microrods but are able to attach, align and organize their cytoskeleton with the microrod-topography (Figure 4.3).

For 3D studies, cells were seeded within Matrigel scaffolds, a solubilized basement membrane rich in extracellular matrix proteins that mimic a natural ECM environment.[176-177] To elucidate the impact of micromechanical and topographical cues on cell proliferation within a 3D microenvironment, 3T3 fibroblasts were cultured in Matrigel with PEGDMA microrods of different stiffness (2 kPa, 20 kPa, and 50 kPa) at an initial microrod to cell ratio of 1:5 in a 3D matrigel gel for five days. This range of microrod stiffness was investigated since it is physiological relevant to both, a healthy myocardium (18 kPa) and an infarcted myocardium (>50 kPa).[16] Fluorescent microscopy shows 3T3 fibroblasts cultured with microrods in a 3D matrigel directly interact and stretch along and across microrods (Figure 2.4) in a similar manner as seen in 2D cultures (both aligning and bridging with microrods). An MTT assay was used to assess proliferation of fibroblasts in matrigel gels. An absorption standard curve was determined for fibroblasts growing in 3D Matrigel. This allowed for the determination of the linear range of absorption for experimental cell concentrations. The inclusion of microrods at the concentrations used did not cause changes in the absorbance. Therefore, changes in absorbance were only attributed to differences in cell number. In addition, we had previously shown that the incorporation of stiff microrods in the composite matrigel did not change its mechanical properties compared to matrigel without microrods.[141] Our data show that gels with stiffer microrods (20 kPa and 50 kPa) significantly down-regulated fibroblast proliferation compared to gels with no microrods (Figure 4.5). Soft microrods (2 kPa) appear to have a lesser effect (not statistically different) on fibroblast proliferation. The greatest effect in cell number was observed with the 20 kPa microrods. The percent cell number difference after five days in culture between the gels with no microrods and gels with microrods was 29%, 34%, and 23% for 50 kPa, 20 kPa, and 2kPa microrods respectively.

We also investigated whether local microscale domains could cause alterations in Cyclin D1, an important regulator of the G/S cell cycle transition, and in collagen type I (Col I) and collagen type VI (Col VI) expression. The expression of α-SMA and integrin α3, two cell markers that are also elevated post myocardial infarction[150] was also investigated. Expression of these genes was analyzed by quantitative PCR. In our study collagen type I and collagen type VI were down-regulated in cell populations cultured with all three stiffness microrods, suggesting that microstructures can be used to modulate ECM

synthesis. Not only was collagen down-regulated in all three microrod cultures, we also found that microstructure stiffness has profound effects on other fibrotic cell markers (Figure 6). Cultures with soft microrods showed no significant difference on the expression of Cyclin D1, α-SMA, and integrin α3 compared to cultures with no microrods. However, fibroblasts seeded with stiffer microrods (20 kPa and 50 kPa) showed down-regulation of Cyclin D1, the contractility marker α-SMA, and integrin alpha 3 with the most pronounced effect being observed in the 20 kPa microrod system (Figure 4.6). This response to the stiffer microstructures suggests that a reduction in cell proliferation may be associated with an alteration in mechanotransduction; cells attached to stiffer microrods generate a mechanical force that results in changes in cell proliferation.

To investigate if down regulation of collagen by the microrods was dependent on the cells' ability to "sense" the microrods through changes in contractiltity, we pharmacologically inhibited both Rho A kinase (ROCK) and myosin light chain kinase (MLCK) in cells grown in gels without microrods and in gels with 50 kPa microrods. Direct phosphorylation of myosin light chain (MLC) by ROCK leads to contractile force generation. Independent from RhoA, phosphorylation of myosin light chain can also be regulated by MLCK. When cultured in the presence of ROCK inhibitor Y27632, or MLCK inhibitor ML7, fibroblasts showed no change in collagen type I expression in the presence of microrods compared to gels with no microrods (Figure 4.7).

4.4 Discussion

Previous studies on substrate stiffness and microtopograpy have been done utilizing polyacrylamide, polydimethylsiloxane (PDMS) and SU-8 (epoxy polymer) substrates among others.[37,137-138,141-142] Although these materials are useful for *in vitro* experiments, they do not offer the necessary biocompatibility and mechanical/geometrical tunability for therapeutic purposes. In this study, a polyethylene glycol acrylate (PEGDMA) was utilized because it can be cross-linked in the presence of UV light allowing for the size and geometry to be easily controlled by photolithograpy. In addition, the mechanical properties of PEG acrylates can be tuned by varying PEG molecular weight, monomer concentration, and crosslinking density.[143,178-179]

Previous studies have also focused on the effects of 2D substrate stiffness or 3D homogeneous matrix properties.[180-182] In contrast, this PEGDMA microrods system was developed to investigate the effect of micromechanical domains on cell proliferation and gene expression in 3D. Fibroblasts were cultured in Matrigel with microrods of different stiffness (2 kPa, 20 kPa, and 50 kPa). It was found that these microrods attenuate the production of collagen from fibroblasts and that cells respond most dramatically to cues that have muscle-like stiffness values. The effect of these micromechanical domains on cell behavior is striking considering the microrods structures account for only 0.017% of the total 3D matrix. The expression of α-SMA in fibroblasts has been shown to be influenced by the mechanical microenvironment and the organization and the rigidity of the ECM.[155] In addition, studies have shown that mechanical stretching can influence collagen production.[146,148,183] In our studies, both collagen and α-SMA were regulated by the micromechanical domains in 3D culture.

Although many collagen types are expressed in the myocardium, it was recently shown that collagen type plays a significant role on cell behavior.[13,184-185] In particular, it

has been shown that collagen VI plays a critical role in the origin of fibrosis in the heart and other diseased tissues.[12-15] Interestingly, in our studies the expression of collagen type VI correlates with the expression of α-SMA, and integrin α3 in the different culture conditions. This association is in agreement with previous observations on myofibroblast studies, where it has been shown that type VI collagen induces the cardiac myofibroblast phenotype[13] and that collagen type VI interacts with the α3 integrin receptor in fibroblasts.[150] Blockade of the α3 integrin receptor has been correlated to an attenuation of type VI collagen induced myofibroblast differentiation.[150] A recent study has also shown that deletion of integrin α3 prevented epithelial-mesenchymal transition a source of myofibroblasts in lung fibrosis.[166] These results also implicate integrin α3 as an important regulator of cell phenotype and matrix deposition. Our studies show that expression of this molecule could be down-regulated by stiffer microrods with greatest effect observed when fibroblasts where seeded amongst 20 kPa microrods. Soft microrods (2 kPa) do not significantly down regulate Cyclin D1, α-SMA or integrin α3. We speculate that microrods of muscle-like stiffness (~20 kPa) direct fibroblasts to behave more like interstitial fibroblasts, whereas softer microrods seem to direct cells to more myofibroblastic behavior.

Interestingly, when fibroblasts' myosin based-contractility was inhibited by two different independent mechanisms (ROCK and MLCK) there was no down-regulation of collagen synthesis, suggesting that the actual interaction with the microrod and subsequent changes in contractility are responsible for the differences in collagen synthesis. This is consistent with previous observations in 2D micropeg surfaces where modulation of cell proliferation was found to be contractility-dependent.[(35)]

In vivo, lack of matrix support could be associated with initial collagen deposition as seen in the first days after myocardial infarction, with stiffer matrix formation occurring after long term fibrosis. This correlates with the presence of myofibroblasts and Col VI after myocardial infarction, where there is an elevation within the first week with reduced expression after two weeks, but persist after twenty weeks.[13,150] Myocardial regeneration requires migration and growth of cardiac progenitors and myocytes in the infarct area, a system capable of maintaining low fibroblasts while promoting muscle regeneration will be a critical step toward this goal. Our data suggests that microrods could provide structural support that prevents fibroblasts from acquiring a more fibrotic state, therefore limiting deposition of matrix molecules.

The present study demonstrates the ability of discrete topographical cues to affect cell proliferation, gene expression, and matrix production in a three dimensional system. To our knowledge this is the first study that investigates the effect of discrete micro-scale cues of different stiffness on cell function in 3D. The results from these studies have promising implications not only for tissue engineered constructs but also for stem cell studies in three dimensional systems *in vitro* and *in vivo.*

4.5 Conclusion

We fabricated a new microrod scaffold system from polyethylene glycol dimethacrylate that is biocompatible, mechanically tunable, and compatible with photolithographic processing. We created a scaffold system consisting of polymeric microrods of different stiffness embedded in a 3D matrix to investigate the role of discrete

micromechanical cues on cell proliferation, gene expression and extracellular matrix (ECM) synthesis. Microrods that were seeded with fibroblasts in a 3D biopolymer matrix effected cell behavior in terms of proliferation and gene expression. Stiffer microrods reduce fibroblast proliferation, collagen deposition and fibrotic phenotype expression where as softer microrods showed no significant effect. These microstructures offer numerous possibilities for *in vitro* studies involving the effect of discrete mechanical cues on stem cells, progenitor cells or even terminal cells such as myocytes in 3D cultures. The microrods can potentially also be used as injectable microscaffolds to influence tissue regeneration *in vivo*.

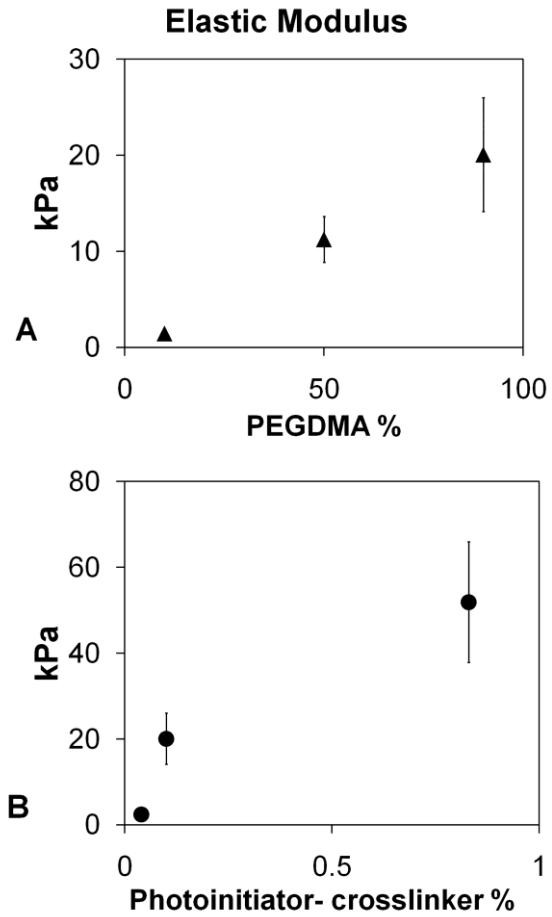

Figure 4.1 The elastic modulus of PEGDMA hydrogels can be controlled by varying the monomer and cross-linker concentration. A) Photoinitiator-crosslinker concentration 0.1% (w/v). B) PEGDMA concentration 90% (w/v). Bars indicate standard deviation.

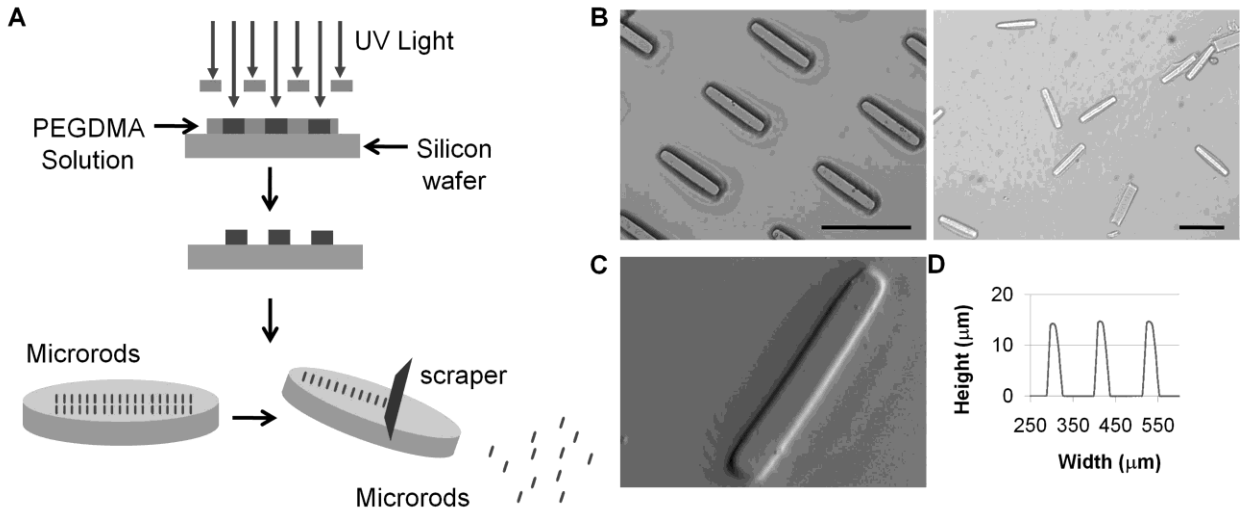

Figure 4.2 A) Schematic of PEGDMA microscaffold fabrication by photolithography. B) Bright field images of microrods attached and microrods released from substrate. C) SEM image of polyethylene glycol dimethacrylate (PEGDMA) microrods. D) Profile graph of microrods. Bar scale = 100μm.

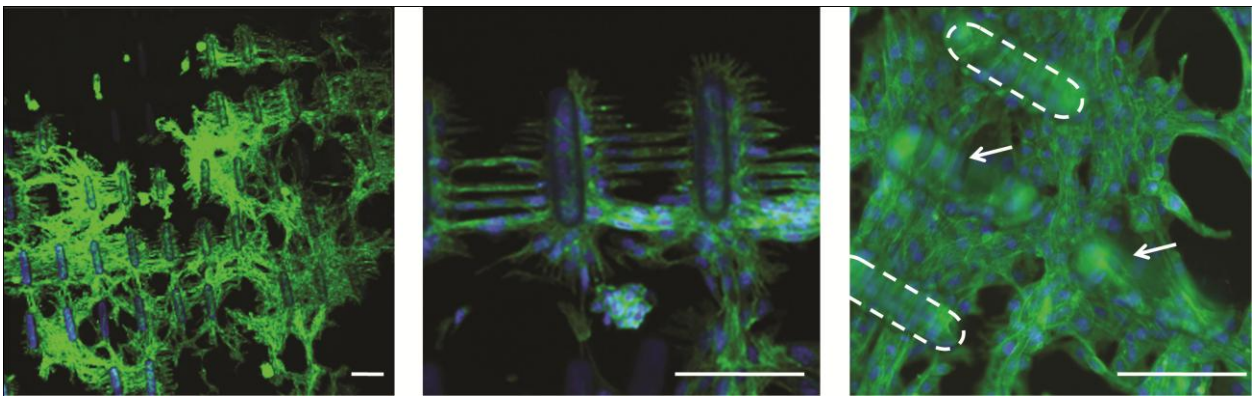

Figure 4.3 Fibroblasts on 2D surface bridge and align with PEGDMA microrods (50 kPa). F-actin (green), microrods and cell nuclei (blue). Arrow and dashed lines indicate microrods. Bar scale = 100μm.

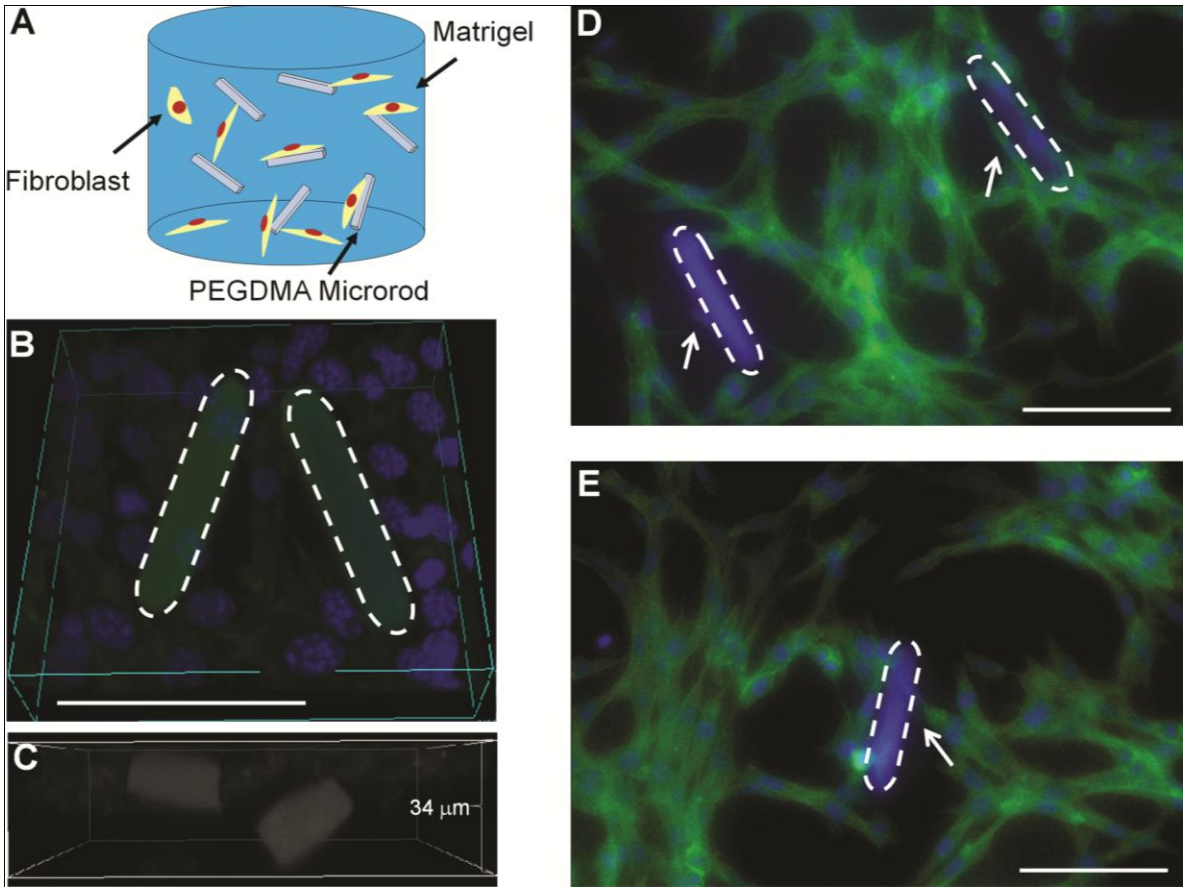

Figure 4.4 A) Schematic of 3D system. Fibroblasts and microrods encapsulated within Matrigel. B) 3D Reconstruction of fibroblasts and PEGDMA microrods in matrigel. C) Microrods in different z-planes within the gel. D, E) Fibroblasts attach and link PEGDMA microrods (50kPa) in 3D cultures. F-actin (green), cell nuclei (blue), and microrods (blue). Dashed lines indicate microrods. Arrows indicate cells attaching to microrods. Bar scale = 100μm.

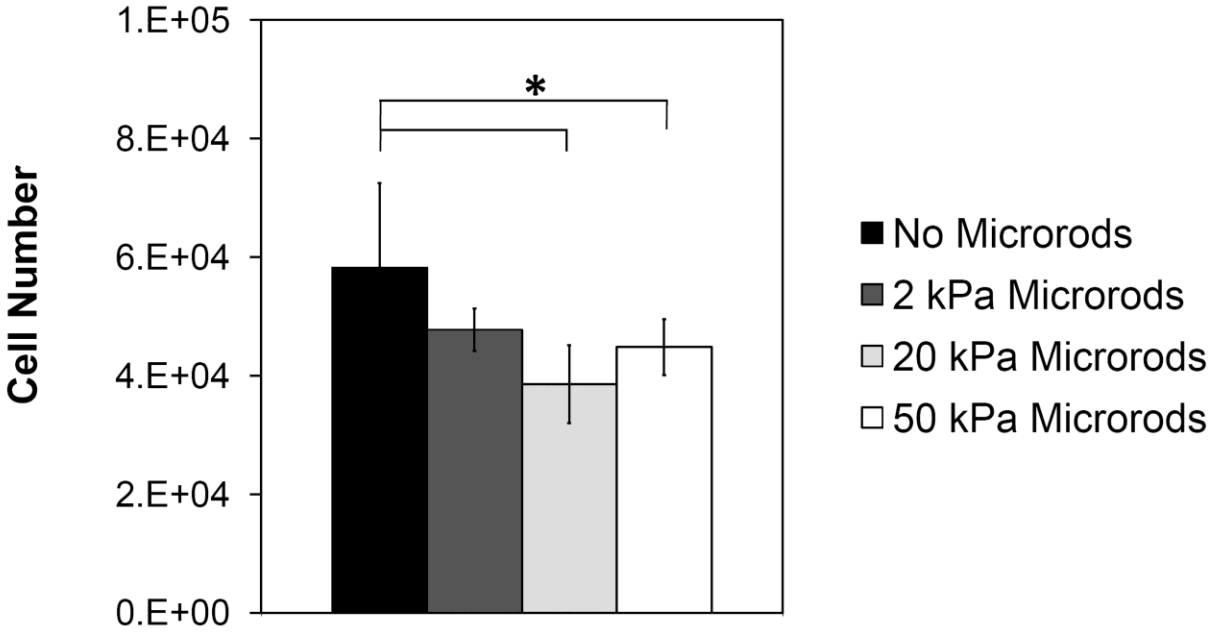

Figure 4.5 Fibroblast proliferation was significantly reduced in gels with microrods of higher stiffness (20 kPa, 50 kPa), but no significant difference was found with softer microrods (2 kPa) as analyzed by MTT assay. Bars indicate standard deviation and (*) indicates $p < 0.05$, (n = 6).

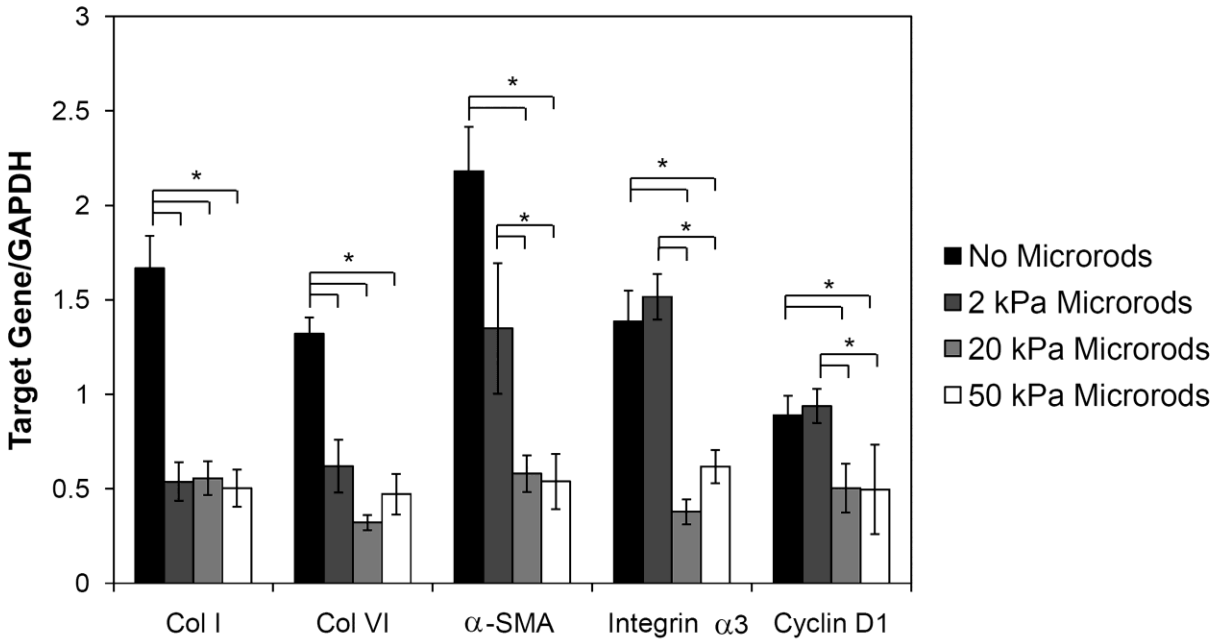

Figure 4.6 PEGDMA microrods of different stiffness have a varied response on ECM synthesis and gene expression in 3D gels. Collagens I and VI were down-regulated in all microrod cultures. Fibroblasts with stiffer microrods showed down-regulation of Cyclin D1, contractility marker α-SMA, and integrin α3. Cultures with soft microrods showed no significant difference on the expression of Cyclin D1, α-SMA, and integrin α3 compared to cultures with no microrods. Bars indicate SD and (*) indicates $p < 0.05$, ($n = 6$).

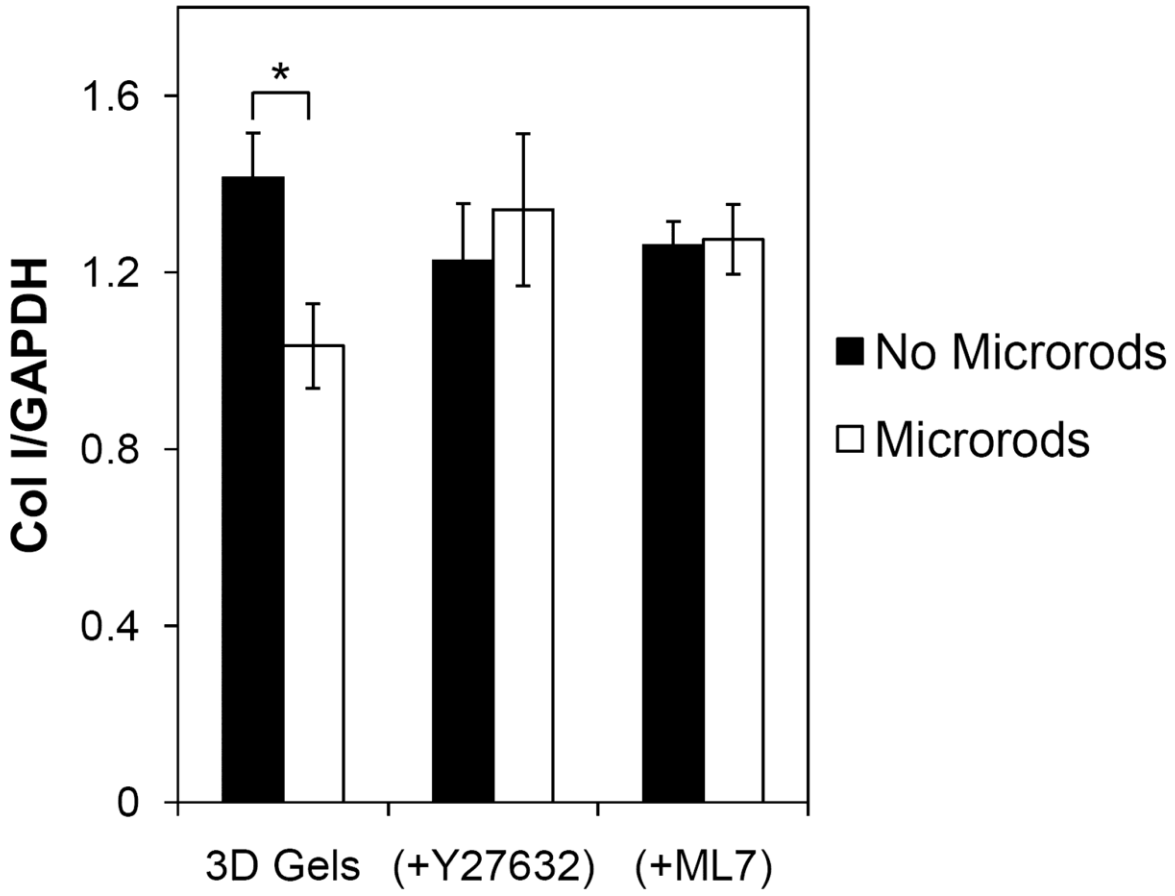

Figure 4.7 Fibroblast cultured in the presence of ROCK inhibitor Y27632, or MLCK inhibitor ML7, showed no change in collagen type I expression in the presence of microrods (50kPa) compared to gels with no microrods. Bars indicate SD and (*) indicates $p < 0.05$.

Gene	Primer Sequence (5'-3')
GAPDH	F: TGGCCTCCAAGGAGTAAGAAAC
	R: GGGATAGGGCCTCTCTTGCT
Col I	F: GCACGAGTCACACCGGAACT
	R: AAGGGAGCCACATCGATGAT
Col VI	F: ACCCGGGACCGGCTACT
	R: CAGAACGTCCATCCGTAATGAC
α-SMA	F: TCCTGACGCTGAAGTATCCGATA
	R: GGTGCCAGATCTTTTCCATGTC
INT α3	F: ATCATCCTCCTCTTGTGGAAGTG
	R: GCCTTCTGCCTCTTAGCTTCATA
Cyclin D1	F: AGCCAGCTGCAGTGCTGTAG
	R: CTGGTGGTGCCCGTTTTG

Table 4.1 qPCR Primers.

Chapter 5. Injection of Microrods in the Rat Model after Myocardial Infarction

Abstract

The utilization of polymer scaffolds for cardiac tissue engineering has been broadly investigated. However, many natural and synthetic polymers can be difficult to inject and little is known about the effect of injected micro-scale materials on myocardium remodeling after myocardial infarction. We have previously reported that poly(ethylene glycol) dimethacrylate (PEGDMA) microrods (15x15x100 μm) of different stiffness reduce fibroblast proliferation and down-regulate extracellular matrix production in an *in vitro* 3D environment. Stiffer microrods (50 kPa) had a greater effect than softer microrods (2 kPa) suggesting that a reduction in cell proliferation may be associated with an alteration in mechanotransduction. Indeed, when Rho kinase (ROCK) and myosin light chain kinase (MLCK), important regulators of cell contractility, were pharmacologically inhibited no differences were observed between the microrod group and the control. In this work, the role of microrods' size and stiffness was investigated *in vitro* and *in vivo*. Adult left ventricular fibroblasts were isolated from adult female rats and cultured with microrods in 3D matrigel. To investigate to role of size, two microrods sizes were fabricated. All microrods had a cross section are of 15 X 15 μm^2 but they were either 100 μm long, or 15 μm long. Microrods of different stiffness (2 kPa-50 kPa) were created as previously described. It was observed that stiffer microrods reduce fibroblast proliferation, collagen deposition and fibrotic phenotype expression where as softer were not as effective. Additionally, shorter microrods influenced fibroblasts only when seeded at similar volumes of longer microrods. To investigate the effect microrods on myocardial repair and remodeling *in vivo*, adult Sprague-Dawley female rats underwent LAD artery occlusion for 30 min followed by reperfusion. Microrods were injected into the LV two days after MI. Five weeks after the injections, echocardiography revealed an increase in EF and anterior wall thickness in the microrod group compared to the PBS control. Histology analysis demonstrated a trend on decrease scar formation and increase in wall thickness of the microrod treated group compared to the PBS control.

5.1 Background

Cardiac repair remains a critical challenge in the fields of tissue engineering and regenerative therapies. Ideally, therapeutic strategies for myocardial regeneration should promote migration and growth of myocytes in the infarct area, and slow down or reduce pathological fibrosis. The purpose of this study was to determine whether polyethylene glycol dimethacrylate (PEGDMA) microrods can influence myocardial repair and remodeling *in vivo*.

5.2 Materials and Methods

5.2.1 Microrods Fabrication

Microrods were fabricated as previously published, briefly using a precursor solution consisting of poly(ethylene glycol) dimethacrylate (PEGDMA) MW 750 (Sigma-Aldrich, St. Louis, MO), photo-initiator 2,2-dimethoxy-2-phenylacetophenone (Sigma-Aldrich, St. Louis, MO) dissolved in 1-vinyl-n-pyrrolidone (Sigma-Aldrich, St. Louis, MO)

cross-linker (100 mg/mL), and 1X phosphate-buffered saline (PBS). Microrods were created with different magnitudes of stiffness (50 kPa, 20 kPa, 2 kPa) by varying the PEGDMA the photoinitiator-crosslinker concentration (0.8%, 0.1% 0.04% w/v respectively). The hydrogel precursor solution was sonicated at room temperature (VWR Model 75T; West Chester, PA) for 15 minutes to ensure complete mixing of reagents. Photolithography was used to create microrods designed to be 100 μm or 15 μm long with a 15 x 15 μm cross section. Microrods were micro-fabricated in 3 inch silicon wafers. Each wafer was cleaned in piranha solution (3:1, H_2SO_4:H_2O_2) for 20 min, and rinsed with deionized water three times. Wafers were then rinsed with acetone, methanol and isopropanol and then baked at 200 ^oC for 2 min. The PEGDMA precursor solution was then spun onto each wafer to achieve a desired thickness of 15 μm. The wafer was exposed using a Karl Suss MJB3 mask aligner to a 405nm light source through the microrod patterned photomask at 9mW/cm^2 until crosslinking. The height of the microstructures was confirmed using an Ambios Technology XP-2 profilometer (Figure 2). Microrods on the wafer were then rinsed with isopropanol and dried with N_2 gas. Microrods were removed from the wafer by rinsing wafer with 70% ethanol and gently scraping microrods with a cell scraper. Collected microrods were centrifuged and rinsed in 70% ethanol three times. Microrods were then centrifuged and rinsed with sterile 1X phosphate-buffered saline (PBS) two times. Microrods were finally resuspended in PBS before injection.

5.2.2 Adult Rat Ventricular Fibroblasts Isolation

Adult left ventricular fibroblasts were isolated from the hearts of adult female Sprague-Dawley rats. Briefly, heart were excised from anesthetized adult female rats, rinsed in cold serum free media, and briefly perfused with isolation media. The left ventricles were isolated, minced, and digested with collagenase type 2 (2mg/ml) (Worthington Biochemical, Lakewood, NJ). The collagenase medium containing the ventricular fibroblasts was centrifuged for 2 min at 50 g to remove cell debris. The supernatant was then centrifuged for 5 min at 300 *g* and cells were resuspended in DMEM with 10% FBS. Cells were plated and allowed to attach for 30 min before the first media change, which removed weakly adherent cells, including myocytes and endothelial cells. Ventricular fibroblasts were used only at early passages (<P3).

5.2.3 In Vitro encapsulation of LVFs with microrods in 3D matrigel

Adult rat left ventricular fibroblasts were cultured in complete medium consisting of Dulbecco's Modified Eagle's Medium (DMEM) with 10% fetal bovine serum and 1% penicillin/streptomycin. Cell cultures were maintained in a humidity-controlled 5% CO_2 incubator at 37°C and were allowed to grow to ~90% confluence. Prior to seeding, cells were trypsinized and resuspended in complete medium. Cells were seeded at a concentration of 2,500 cells per 65 μL of low growth factor Matrigel (BD Biosciences, San Jose, CA) (4 mg/mL) either without microrods or with microrods at a seeding ratio of 1:5 number of microrods to number of cells into individual wells in a 96 well plate. This resulted in 2 mm-thick gels. The plate was incubated at 37 ^oC for 30 minutes to allow gels to solidify completely. Each gel was then covered with 200 μL of media and plate was placed in an incubator at 37^oC for 10 days.

5.2.4 Proliferation Assay

Cellular proliferation was assessed at five days after initial seeding in the gels using an MTT (3-(4,5-Dimethylthiazol-2-yl)-2,5-diphenyltetrazolium bromide) assay (Sigma-Aldrich, St. Louis, MO). On the day of the assay, 100 μL media was removed from the wells and 16.5 μL of the MTT reagent were added to each well. The plate was then placed back in the incubator for 4 hours. After this time, the formazan crystals were dissolved with the solubilization solution and the absorbance was measured.

5.2.5 mRNA Isolation and qPCR

Total RNA was isolated from fibroblasts 10 days after culture. Trizol (Invitrogen) and Qiagen microRNA purification columns were used to isolate and purify RNA according to manufacturer's protocol. Genomic DNA contamination was removed by treating the isolated RNA using RQ1 RNase-Free DNase (Promega, Madison, WI). RNA concentrations were quantified using a NanoDrop spectrophotometer (Thermo Scientific, Wilmington, DE). RNA was reverse transcribed using iScript cDNA (BioRad, Hercules, CA) and a thermal cycler Mastercycler S (Eppendorf, Hamburg, Germany) according to the manufacturer's protocol (5 minutes at 25°C, 30 minutes at 42°C, and 5 minutes at 4°C). Quantitative polymerase chain reaction (q-PCR) was performed with Power SYBR Green PCR Master Mix and a StepOne Plus Real-Time PCR System (Applied Biosystems, Foster City, CA). The relative amount of target cDNA was determined from the appropriate standard curve and normalized by the amount of GAPDH cDNA present in each sample. Primers (Integrated DNA Technologies, San Diego, CA) are provided in Table 5.1. Each sample was analyzed in triplicate, and results were expressed relative to glyceraldehydes 3-phosphatedehydrogenase (GAPDH) as an endogenous control.

5.2.6 Myocardial Infarction Surgery

The animal protocol was approved by the Committee for Animal Research of the University of California San Francisco and was performed in accordance with the recommendations of the American Association for Accreditation of Laboratory Animal Care. The rat model of ischemia reperfusion myocardial infarction (MI) is a well established model described previously.[186-188] Briefly, adult Sprague-Dawley female rats underwent 30 min of left anterior descending artery occlusion followed by reperfusion. The chest was then closed and the animal was allowed to recover for 2 days before treatments.

5.2.7 Microrods Injection

At two days post MI, the rats were injected with 50 μL of 100μm long 50 kPa microrods in PBS (1.25×10^6 microrods/mL) (n=11), 100 μm long 2 kPa microrods in PBS (1.25×10^6 microrods/mL) (n=5), 15 μm long, 50 kPa microrods (8.33×10^6 microrod/mL) (n=5), or just PBS (n=6). Closed chest echocardiography guided injections were performed.

5.2.8 Echocardiography

Transthoracic echocardiography was performed before injection as a baseline echocardiogram, and at 5 weeks post injection. The method of examination used in the study was based on established methods in the rat[189-190] and has been performed with reproducibility in our previous studies.[191] Briefly, the animals were placed in a slightly

lateral position and then a layer of acoustic coupling gel was applied to the thorax. Echocardiography was performed using a 30-MHz linear array transducer system Vevo660 (VisualSonics, Toronto, Canada). Left ventricular ejection fraction was calculated as: EF (%) = [(EDV - ESV)/EDV]. An echocardiographer blinded to the treatment group acquired the images and performed the data analysis.

5.2.9 Histology

Following echocardiogram at 5 weeks, animals were humanely sacrificed under general anesthesia. Hearts were arrested in diastole with injection of concentrated KCl and the hearts immediately excised and fresh frozen in O.C.T. freezing medium (Sakura Finetek). The hearts were cryosectioned into 10 μm thickness on glass slides. Ten representative slides of every interval from apex to base covering the entire infarcted area were selected for hematoxylin and eosin (H&E) and Masson's trichrome stain (Accustain, Sigma). Morphological assessment of infarct size was quantified based on planimetry on Masson's trichrome stained slides with Photoshop software (Adobe Photoshop CS3). Collagen deposition was measured in pixels and LV was traced. Collagen percent was calculated by dividing scar area by the LV area.

5.3 Results and Discussion

In this work, the role of microtopographical cues' size and stiffness on primary cells cultured in 3D Matrigel was investigated. Adult left ventricular fibroblasts were isolated from female rats and cells were used at early passages. To investigate to role of size, two microrods sizes were fabricated. All microrods had a cross section area of 15 X 15 μm^2 and they were either 100 μm long, or 15 μm long (Figure 5.1). Microrods (H=15 μm, W=15 μm, L=100 μm) of different stiffness were created as previously described.[192] It was observed that stiffer microrods were more effective in causing a reduction on cell proliferation as analyzed by MTT assay (Figure 5.2). These results are similar to previous studies done with 3T3 fibroblasts. This indicates that microstructures are able to influence immortalized cell line fibroblasts as well as primary cardiac fibroblasts. Shorter microrods were not effective at influencing proliferation when seeded at the same density as longer microrods, but when seeded at similar overall volumes (6.6 times as many) as the longer microrods they also influenced cell proliferation (Figure 5.2). Gene expression of fibrotic targets demonstrated similar trends (Figure 5.3). Collagen I, collagen VI and α-smooth muscle action (α-SMA) expression was downregulated on fibroblasts cultured with stiffer and longer microrods (50 kPa, 100 μm) compared to the no microrods group. Shorter microrods seeded at same density as the 100μm long microrods were not effective in regulating gene expression. Shorter microrods seeded at same volume density as longer microrods influenced down regulation of collagen I and α-SMA mRNA expression. These results indicate that some cell contact with the microrods is necessary to influence cell behavior. Softer microrods (2 kPa) influenced collagen I and collagen VI, but were not effective on influencing α-SMA expression. Cyclin D1 expression followed similar trends, but data was not statistically significant. Overall these results co-relate with previous work[144-145,192-193] that indicates that cell contact and the ability of the cells to effectively interact with the microtopography are important factors in eliciting a cell response.

To investigate if microrods could influence cardiac repair, adult female rats underwent left anterior descending artery ligation for 30 min followed by reperfusion. Two days after MI rats' hearts were echo-guided injected with microrods in the infarct area. Right before treatment, heart function was analyzed by echocardiography. Hearts were analyzed five weeks after by echocardiography and then they were excised and analyzed by histology. Analysis showed a trend on decreased fibrosis and increase in wall thickness of the microrod treated group compared to the PBS control (Figures 5.4, 5.5, 5.6). Five weeks after the injections, echocardiography revealed an increase in EF in the microrod group compared to the PBS control (Figure 5.7). These results indicate that injection of microrods can affect cardiac function, but amount of microrods delivered would need to be optimized. Although 50 μL of solution were injected, the final volume of microrods delivered was 1.4 μL. This represents approximately only 0.3% of volume of the left ventricle. Depending on size of infarct this could represent only 1.2% of the damaged area. The potential of these microdevices for therapeutic repair could also be enhanced by incorporation of a growth factor that would recruit stem cells to infarct area.

5.4 Conclusion

Microrods from polyethylene glycol dimethacrylate of different stiffness and size were microfabricated utilizing photolithographic techniques. Cardiac fibroblasts were encapsulated with the microrods in a 3D matrix to investigate the role of discrete microtopographical cues on cell proliferation, and gene expression. Microrods that were seeded with fibroblasts in 3D Matrigel influenced cell behavior in terms of proliferation and gene expression. Stiffer microrods reduce fibroblast proliferation, collagen deposition and fibrotic phenotype expression whereas softer microrods were not as effective. Shorter microrods influenced cells only when seeded at similar volumes of longer microrods. The microrods were injected in rats two days after MI. All animals survived after injection. The microrod group showed increased ejection fraction compared to the control group. Histology showed a trend on decreased collagen production in the hearts treated with microrods. These results suggest that microrods could provide regeneration support by reducing the fibrotic response.

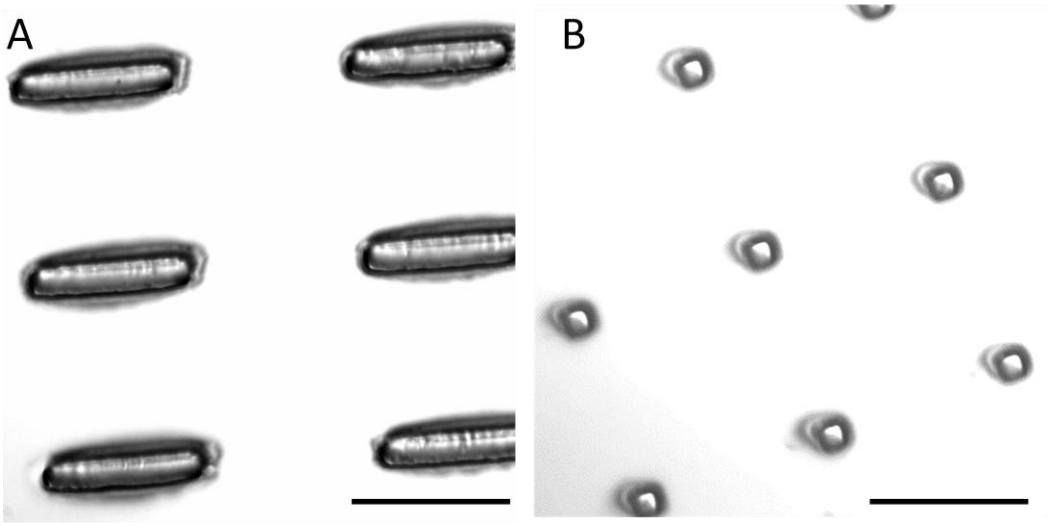

Figure 5.1 Bright field image of microrods (A) 100 μm long and (B) 15 μm long. Scale bar is 100 μm.

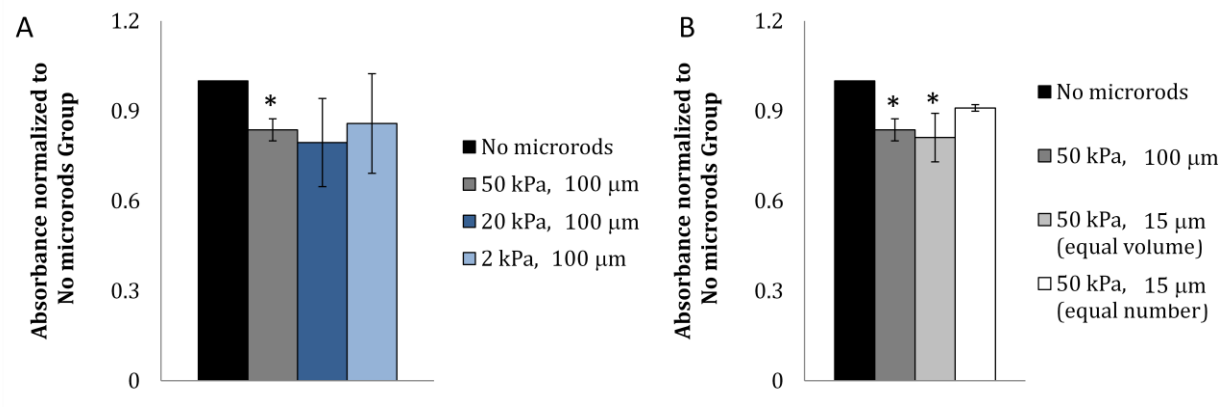

Figure 5.2 Cell number normalized to no microrods group and assessed by MTT assay. (A) Cardiac fibroblasts' proliferation was reduced in gels with microrods of higher stiffness (50 kPa), but no significant difference was found with softer microrods (2 kPa, 20 kPa). (B) Shorter microrods influenced cells only when seeded at similar volumes of longer microrods. Bars indicate standard deviation and (*) indicates $p < 0.05$.

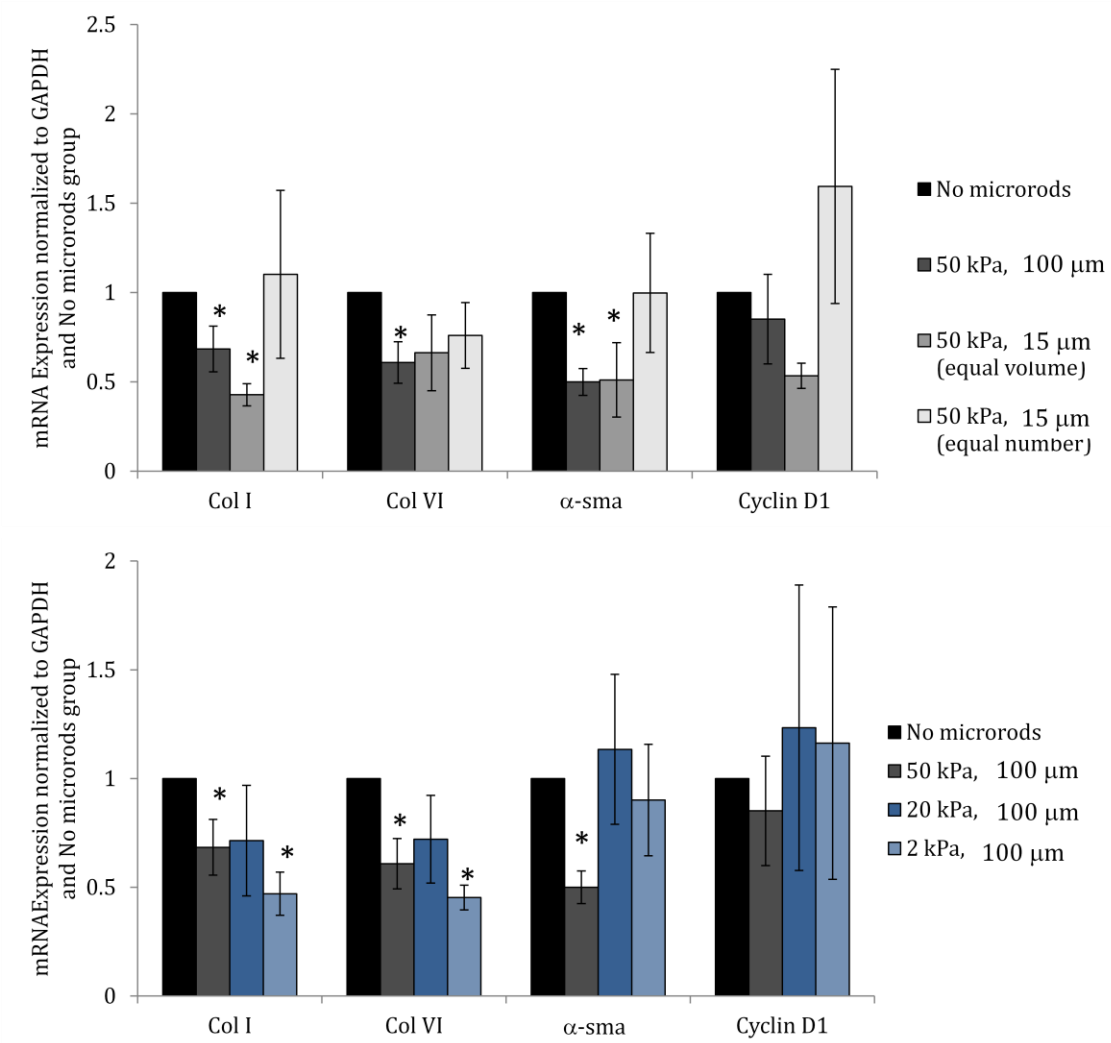

Figure 5.3 Gene expression of cardiac fibroblasts cultured with microrods in three dimensional matrigel. Collagen I, collagen VI and α-smooth muscle action (α-SMA) expression was down-regulated on fibroblasts cultured with stiffer and longer microrods (50 kPa, 100 μm) compared to no microrods group. Shorter microrods seeded at same volume density as longer microrods influenced down regulation of collagen I and α-SMA mRNA expression. Bars indicate standard error of the mean and (*) indicates $p < 0.05$ compared to control.

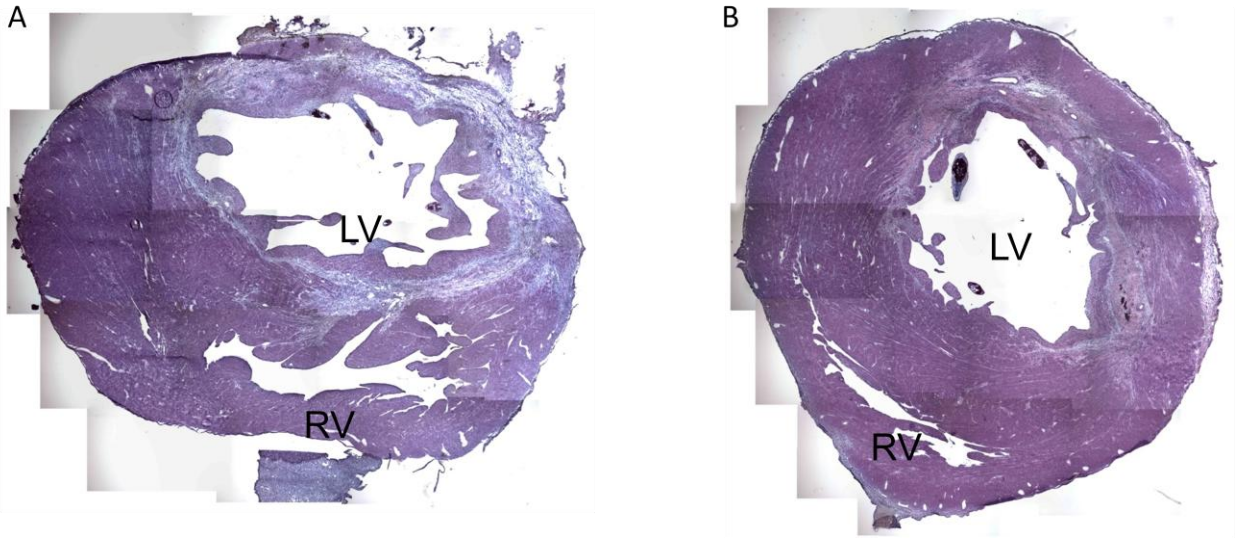

Figure 5.4 H and E staining of heart cross-section. (A) Control group. (B) Microrods group (50 kPa, 100 μm). LV stands for left ventricle and RV stands for right ventricle.

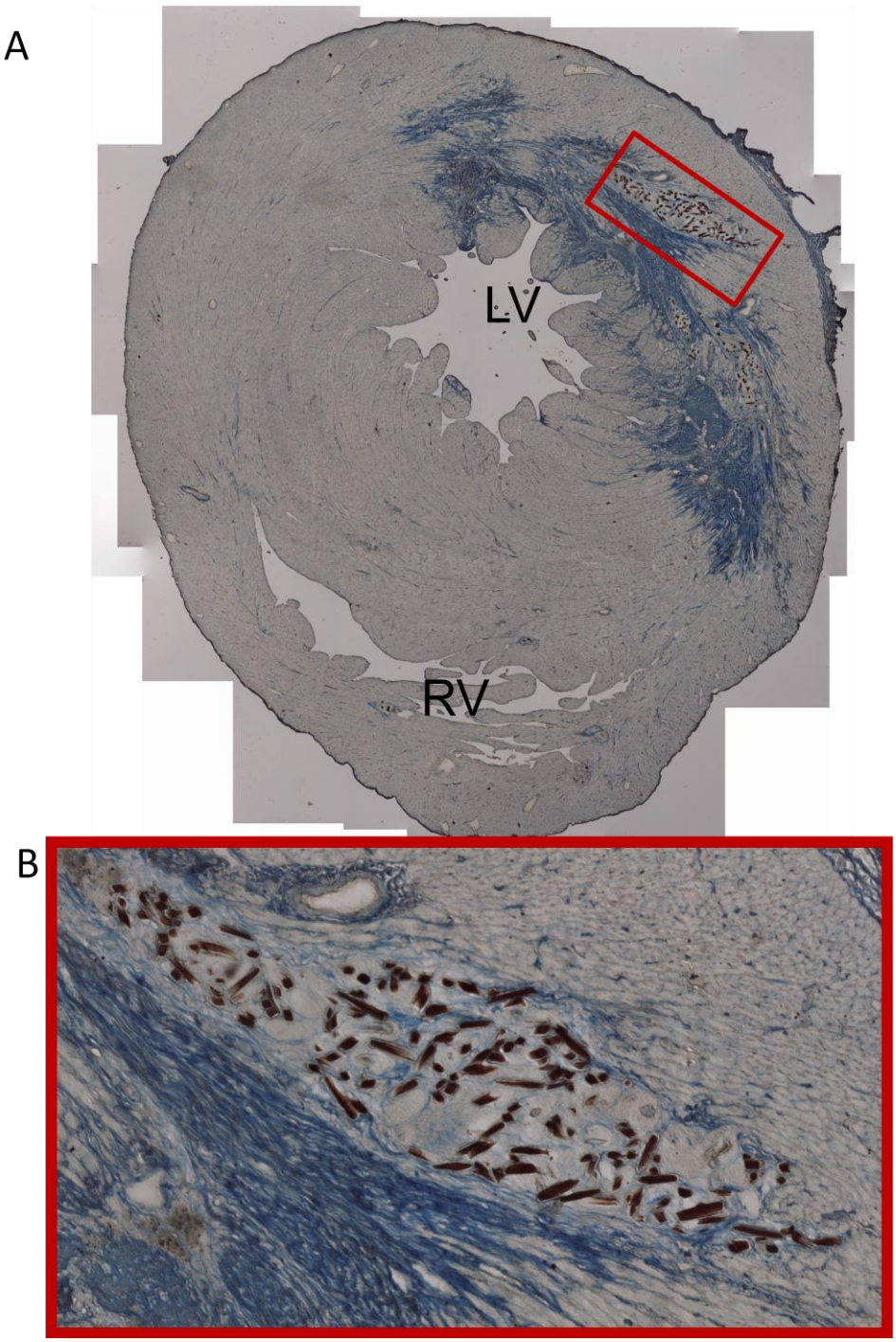

Figure 5.5 Masson's staining showing microrods in left ventricle. (A) Slice of heart cross-section. (B) Magnified area of heart-cross section. LV stands for left ventricle and RV stands for right ventricle. Collagen is blue, myocardium is brown, microrods are dark brown.

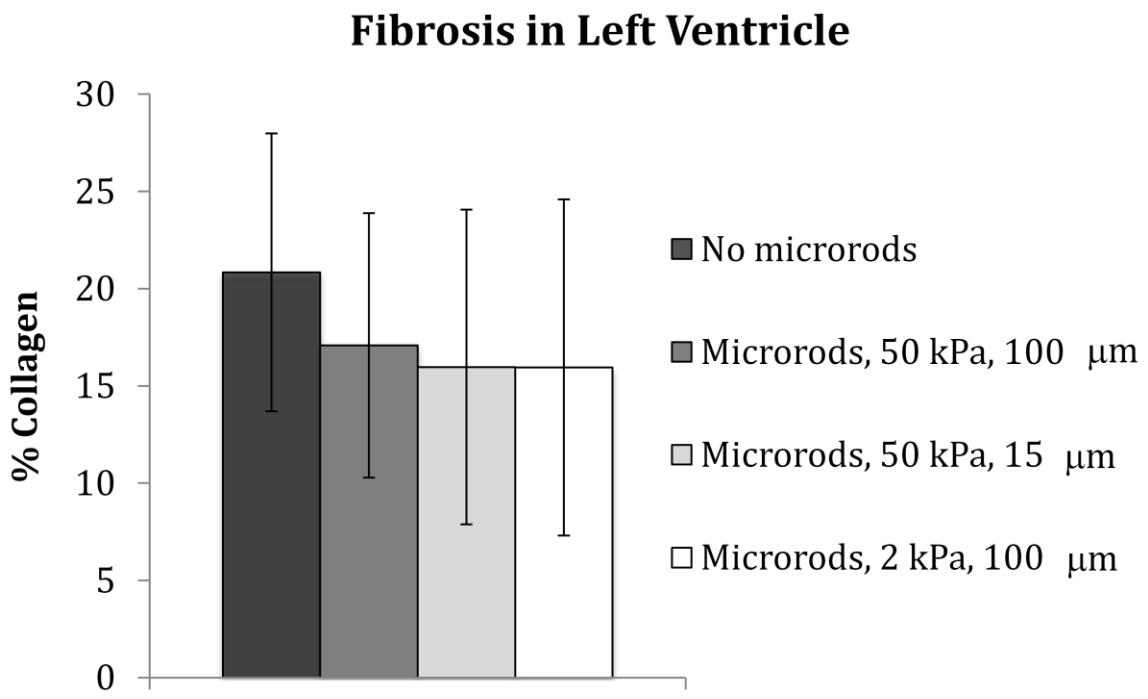

Figure 5.6 Percent collagen content in the left ventricle after 5 weeks post injection. Bars indicate standard deviation.

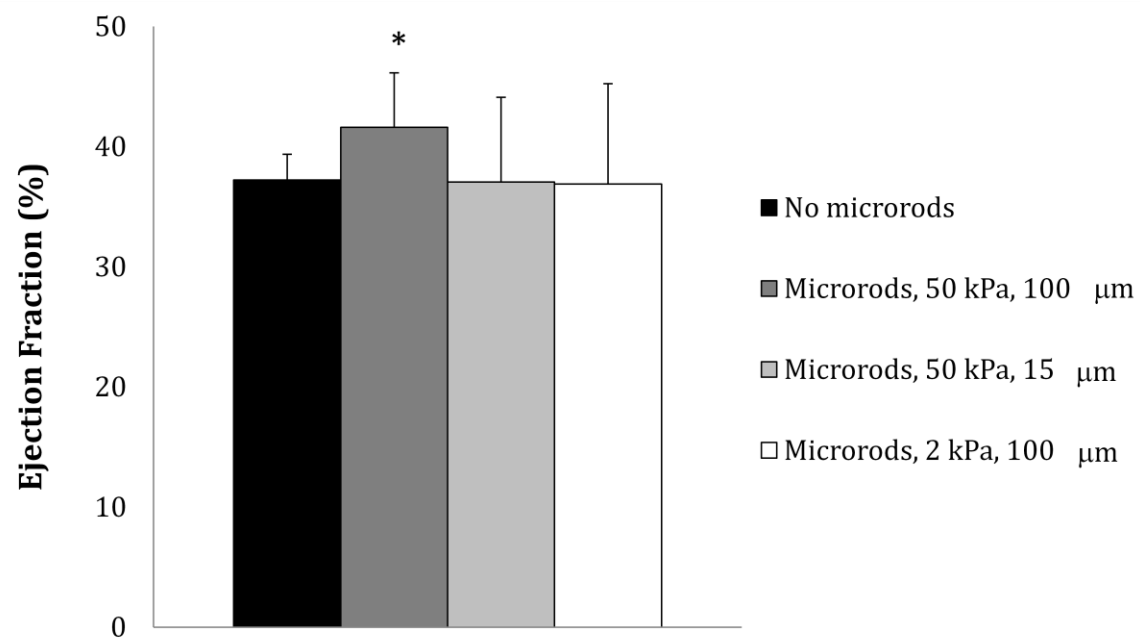

Figure 5.7 Ejection Fraction after 5 weeks post injection. Bars indicate standard deviation and (*) indicates $p < 0.05$ compared to control.

Gene	Primer Sequence (5'-3')
GAPDH	F: AAC CCA TCA CCA TCT TCC AG R: TAC TCA GCA CCA GCA TCA CC
α-SMA	F: TTC AAT GTC CCT GCC ATG TA R: CAT CTC CAG AGT CCA GCA CA
Col I	F: AGG CAT AAA GGG TCA TCG TG R: ACC GTT GAG TCC ATC TTT GC
Cyclin D1	F: AGC CAT CCA AAC TGA GGA AA R: ACA GAA AGG CAG AGC CAG AG
Col VI	F: ACT CAG CGG GAC ACT ACA CC R: ACA AAG CCA AAC ACA TCC TTG

Table 5.1 qPCR Primers

Chapter 6. Mechano Growth factor Delivery from PEGDMA Microrods

6.1 Introduction

Mechano growth factor is a splice variant of the insulin-like growth factor (IGF-I) domain, and it is also known as IGF-IEb domain in rodents and IGF-IEc in humans.[194] Mechano growth factor (MGF) releases naturally after mechanical overload or injury, strengthens surviving myocytes, blocks apoptosis of vulnerable myocytes, and attracts progenitor cells to the site of injury.[194-195] It is known that the myocardium expresses higher levels of IGF-I following ischemia or mechanical overload as detected using a general IGF-I antibody. However MGF is the type of IGF-I expressed in these conditions. [194] *In vivo* studies of ischemia and mechanical overload indicate that MGF reduces the size of the permanently damaged area of the myocardium. [195] This correlates with the finding that MGF is expressed rapidly after tissue damage and that it prevents apoptosis in the myocardium[194] making it a therapeutic candidate for cardiac repair. It was recently demonstrated that MGF increased the migratory response of human mesenchymal stem cells.[196]

The objectives of this study were to fabricate mechano growth factor E domain peptide (MGF-E) loaded microrods and to determine the elution profile and bioactivity of MGF-E from the microrod delivery device. Elution was investigated through a custom-made ELISA and the bioactivity of the peptide after elution was investigated by analyzing stem cell migration and skeletal myoblast (C2C12 cell line) proliferation.

6.2 Materials and Methods

6.2.1 Fabrication of microrods and MGF loaded microrods

Microrods were fabricated as previously published, briefly using a precursor solution consisting of poly(ethylene glycol) dimethacrylate (PEGDMA) MW 750 (50% w/v) (Sigma-Aldrich, St. Louis, MO), photo-initiator 2,2-dimethoxy-2-phenylacetophenone (Sigma-Aldrich, St. Louis, MO) dissolved in 1-vinyl-n-pyrrolidone (Sigma-Aldrich, St. Louis, MO) cross-linker (100 mg/mL) at final concentration of 0.8% w/v, and 1X phosphate-buffered saline (PBS). MGF loaded microrods were fabricated similarly, briefly using a precursor solution consisting of poly(ethylene glycol) dimethacrylate (PEGDMA) MW 750 (50% w/v) (Sigma-Aldrich, St. Louis, MO), photo-initiator 2,2-dimethoxy-2-phenylacetophenone (Sigma-Aldrich, St. Louis, MO) dissolved in 1-vinyl-n-pyrrolidone (Sigma-Aldrich, St. Louis, MO) cross-linker (100 mg/mL) at final concentration of 0.8% w/v, MGF dissolved in 60% acetonitrile (5mg/mL) at a final concentration of 450 μg/mL, and 1X phosphate-buffered saline (PBS). The hydrogel precursor solution was sonicated at room temperature (VWR Model 75T; West Chester, PA) for 15 minutes to ensure complete mixing of reagents. Photolithography was used to create microrods designed to be 100μm or 15μm long with a 15 x 15 μm cross section. Microrods were micro-fabricated in 3 inch silicon wafers. Each wafer was cleaned in piranha solution (3:1, H_2SO_4:H_2O_2) for 20 min, and rinsed with deionized water three times. Wafers were then rinsed with acetone, methanol and isopropanol and then baked at 200 ^oC for 2 min. The PEGDMA precursor solution was then spun onto each wafer to achieve a desired thickness of 15 μm. The wafer was exposed using a Karl Suss MJB3 mask aligner to a 405 nm light source through the

microrod patterned photomask at 9mW/cm^2 until crosslinking. The height of the microstructures was confirmed using an Ambios Technology XP-2 profilometer. Microrods on the wafer were then rinsed with DI water, isopropanol and dried with N_2 gas. Microrods were removed from the wafer by rinsing wafer with 70% ethanol and gently scraping microrods with a cell scraper. Collected microrods were centrifuged and rinsed in 70% ethanol three times. Microrods were then centrifuged and allowed to dry overnight in a sterile environment and are re-suspended in media right before cell studies.

6.2.2 Peptide Assay

Varying concentrations of microrods were used so that the predicted MGF delivery would be 30, 60 and 120ng if all the loaded peptide were fully eluted. A custom-made MGF-E antibody was used in an enzyme-linked immunoabsorbent assay (ELISA) on Immobilized-Amino plates and directly conjugated HRP- Primary rabbit aMGF antibody. The assay was calibrated for 0.1-120ng MGF-E peptide. Peptides were incubated for 2h at 37^{o}C, and antibodies were incubated for 1h at 37^{o}C. Elution of MGF-E peptide was compared to unloaded (empty) microrods. Elution of MGF-E was analyzed at 2.5, 4, and 22 hours.

6.2.3 Stem Cell Migration

Cell migration was done using human mesenchymal stem cells (HMSC) and mouse cardiac progenitor stem cells (mCP) isolated from MGF treated mice provided by Dr. Paul Goldspink. Cells were cultured overnight (22 hours) at 37^{o}C, 5% CO_2 against varying MGF concentrations (30-120ng) and a plating density of 5000 cells/well. Calcein-AM stain was used to visualize the extent of migration.

6.2.4 C2C12 Myoblasts Cultures

C2C12 myoblasts were cultured in complete medium consisting of Dulbecco's Modified Eagle's Medium (DMEM) with 10% fetal bovine serum and 1% penicillin/streptomycin (Gibco-BRL, Grand Island, NY). Cell cultures were maintained in a humidity-controlled 5% CO_2 incubator at 37°C and were allowed to grow to ~90% confluence. Prior to seeding, cells were trypsinized and resuspended in complete medium. Cells were cultured on 24 transwell plates for 7 days. MGF peptide, micorods, MGF-microrods, or no drug was added to an insert placed in each well. Microrods or MGF-microrods were also seeded with the myoblasts on other trasnwells. MGF peptide or MGF peptide loaded in microrods was used at a concentration of 60ng/mL (120ng per well).

6.2.5 CyQUANT proliferation assay

Cyquant (Invitrogen) protocol was followed according to manufacturer's protocol. Briefly, a solution of CyQUANT dye in cell lysis buffer was made just prior to each experiment by diluting the CyQUANT dye stock solution into cell lysis buffer according to manufacturers' protocol. To create a standard curve, a cell pellet of known number of cells was thawed at room temperature and 1.0 mL of CyQUANT dye-lysis buffer was added to the pellet. The lysate was resuspended by brief vortexing. A cell dilution series was created in a 96-well cell culture microplate with CyQUANT dye-lysis buffer, in final volumes of 200 μL per well. A control 200 μL well with no cells and CyQUANT dye-lysis buffer only was also prepared. The samples were incubated in darkness for 2 to 5 min at room

temperature. The fluorescence of each sample was measured with a fluorescence microplate reader (FluoroCount, Packard) with 485 nm excitation and 530 nm emission filters. For each experiment, a standard calibration curve was generated by plotting measured fluorescence values in these samples versus cell number, as determined previously from cell suspensions using a hemocytometer. After cells were cultured for one or seven days media was aspirated and cells were carefully washed with PBS. Cells on the tissue culture plate were frozen at -80^{o}C for at least one night before lysing the cells with cyQUANT dye-lysis buffer. Samples were diluted in cyQUANT dye-lysis buffer to ensure absorbance was in the linear range of the standard curve. 200μL of each sample were added to wells in a 96 well microplate. Fluorescence was measured and absorbance was compared to standard curve to determine cell number.

6.2.6 Quantitative PCR analysis of cyclin D1mRNA expression

RNA levels were quantified after one and seven days of culture using a Fast SYBR® Green Cells-to-CT™ Kit (Applied Biosystems, Foster City, CA). Reverse transcription was performed on a Mastercycler S (Eppendorf, Hamburg, Germany). Quantitative PCR was performed using a StepOne Plus (Applied Biosystems, Foster City, CA). The primers used include: GAPDH forward primer 5'-TGGCCTCCAAGGAGTAAGAAAC-3' and reverse 5'-GGGATAGGGCCTCTCTTGCT-3'; and Cyclin D1 forward primer 5'-AGCCAGCTGCAGTGCTGTAG-3' and reverse 5'-CTGGTGGTGCCCGTTTTG-3'. Each sample was analyzed in triplicate, and results were normalized to glyceraldehyde 3-phosphatedehydrogenase (GAPDH) and the no treatment group.

6.2.7 Western blot

Protein levels were determined by Western blot, with detection by HRP conjugated secondary antibodies (Santa Cruz Biotechnology, Inc.) and development using Novex ECL chemiluminescent substrate (Invitrogen). ImageJ was used to determine band intensity levels from the developed blots. All intensity levels were internally normalized to the loading control (α-tubulin) prior to calculating ratios of protein levels.

6.2.8 Statistical Analysis

A statistically significant difference among groups was detected by analysis of variance (ANOVA). Sequential Holm t-tests were then performed to identify differences between specific pairs of conditions.

6.3 Results and Discussion

We created micro devices in the form of microrods made of poly(ethylene glycol) dimethacrylate (PEGDMA) hydrogel with encapsulated MGF-E peptide. Confocal imaging shows that FITC-MGF-E peptide is encapsulated in the microrods after initial washing and after one day in PBS (Figure 6.1 A and B). After seven days in PBS there is some FITC-MGF loaded in the microrods (Figure 6.1 C).

An ELISA method was calibrated using known quantities of natural MGF-E peptide (Figure 6.2). At 2.5 hours, the MGF-E released by elution from microrods was ~1ng per well that was just detectable above background (empty microrods). Overnight, the MGF-E reached ~10ng per well, which was 20.25% of the total quantity loaded into the microrods.

Previously, human mesenchymal stem cells were shown to migrate overnight when MGF-E native peptide (30ng) is provided in the lower migration chamber.[196] The mouse cardiac progenitor (mCP) cells migrate at an even higher rate than the HMSCs at the 30ng dosage of native MGF-E. Microrods containing 30 or 60ng did not result in cell migration but the 120 ng MGF-E dose was effective for mCP migration. This result is consistent with elution profiles determined by the ELISA which showed only 20% MGF-E overnight (20% of 120ng is 24ng). No migration was seen with empty microrods (Fig 6.3).

After one day in culture, C2C12 myoblasts treated with MGF eluting microrods in the insert chamber had increased expression of Cyclin D1 compared to cells with no treatment. MGF peptide alone and empty microrods did not did not have a significant effect on cyclin D1 expression. Additionally when cells are cultured in contact with empty microrods and MGF-loaded microrods an increased on cyclin D1 expression was also observed. This indicates that cells interacting with microrods have increased proliferation even when microrods are empty. When we analyzed cell proliferation using a cyQUANT assay we observed that there was an increased in cell number on the group where cells directly interacted with the MGF-loaded microrods. At day seven mRNA expression follows the same trend as day 1, but there was significant increased cyclinD1 expression and cell number only in the group where myoblasts directly interacted with the MGF loaded microrods. Western blot analysis indicated that myoblasts directly contacting microrods (empty and loaded) had increased cyclin D1 protein expression. Overall our studies indicate that MGF can be encapsulated in the microdevices, the MGF can be protected from degradation for days and the direct cell interation with the microrods can enhance an increase on myoblasts proliferation.

6.5 Conclusion

The microrods protected MGF-E peptide from rapid release and degradation. The custom-made ELISA assay can detect 0.5ng, which is the total MGF-E from 50 microrods with 10pg loaded in each. Twenty percent of the loaded MGF-E was released overnight. The MGF-E eluted overnight by the microrods is bioactive as assessed by induction of stem cell migration and myoblasts proliferation. Interestingly, it was also observed that microrods could enhance the effect of MGF on myoblasts proliferation. The results could be beneficial *in vivo* since our results indicate that loaded microrods could attract stem cells to the site of injury in the first days, and microrods could support proliferation of myoblasts locally.

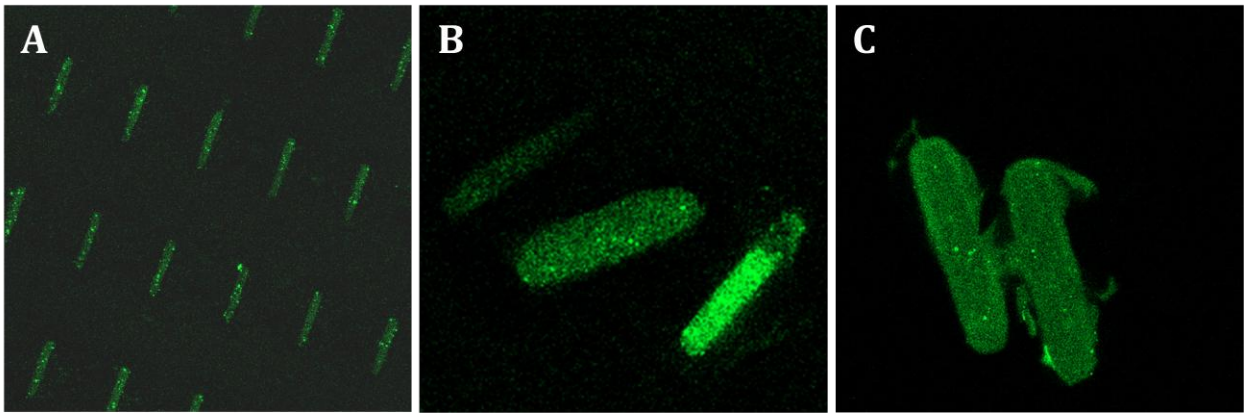

Figure 6.1 FITC-MGF-E loaded in microrods. (A) After initial washing. (B) After one day in PBS. (C) After seven days in PBS.

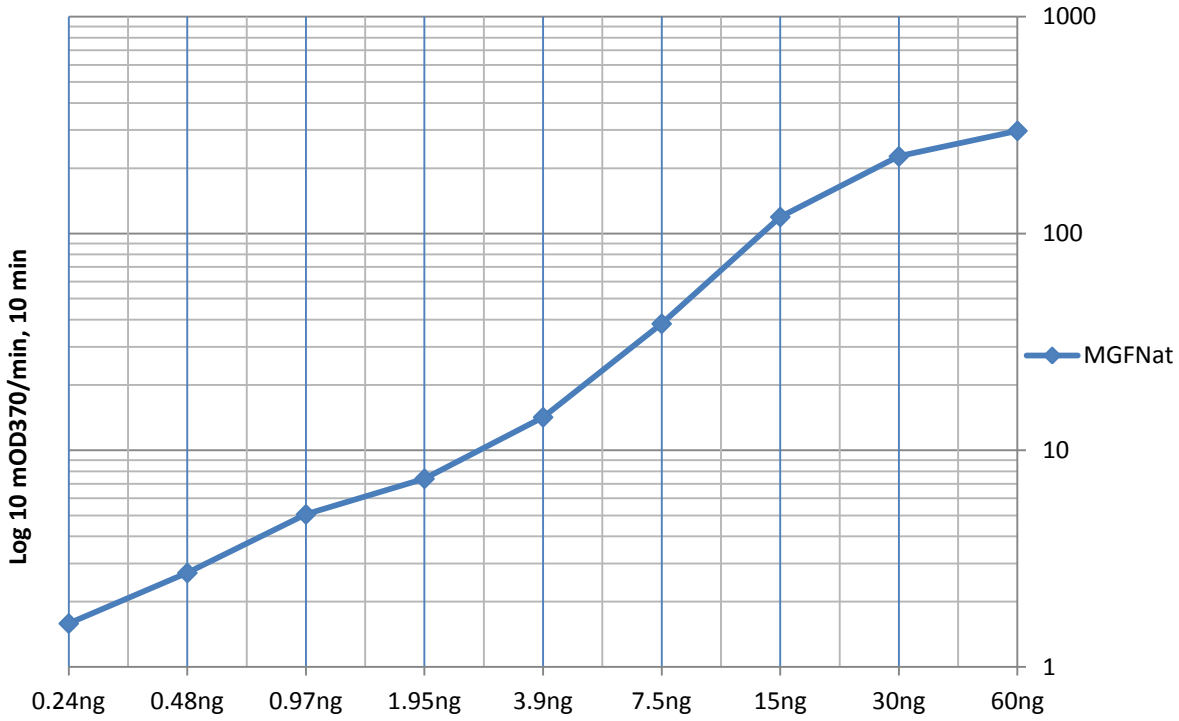

Figure 6.2 ELISA standard curve.

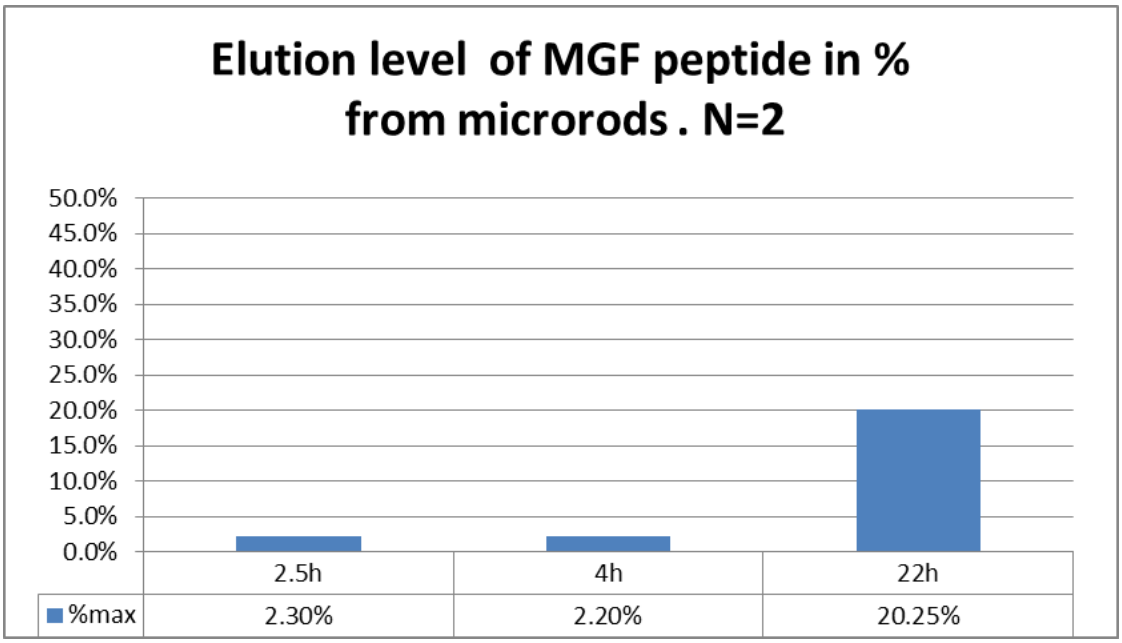

Figure 6.3 Elution of MGF from microrods after 22 hours.

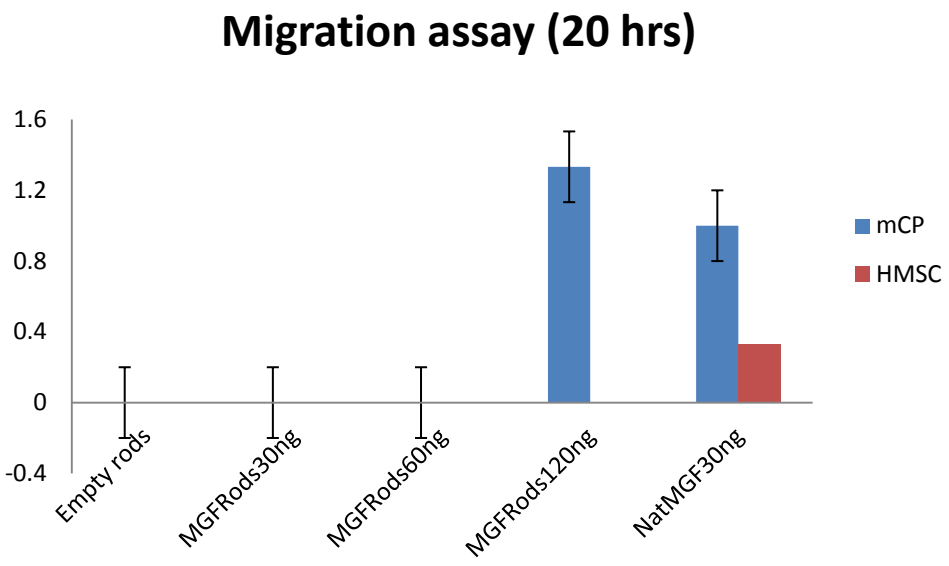

Figure 6.4 Migration assay over 20 hours.

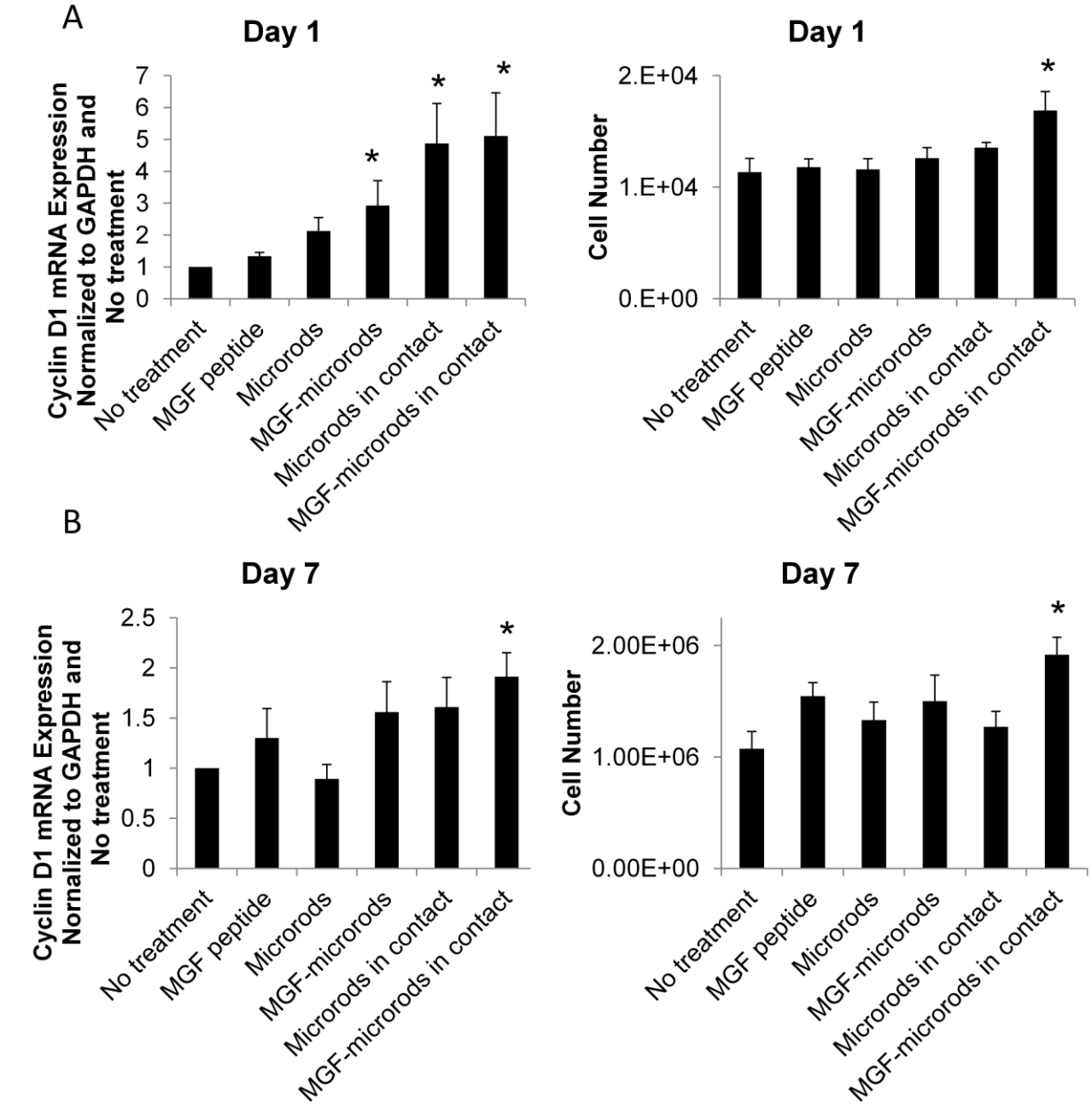

Figure 6.5 C2C12 skeletal myoblasts' proliferation and cyclin D1 mRNA expression (A) Day 1. (B) Day 7. Bars indicate standard error of the mean and (*) indicates $p < 0.05$ compared to control.

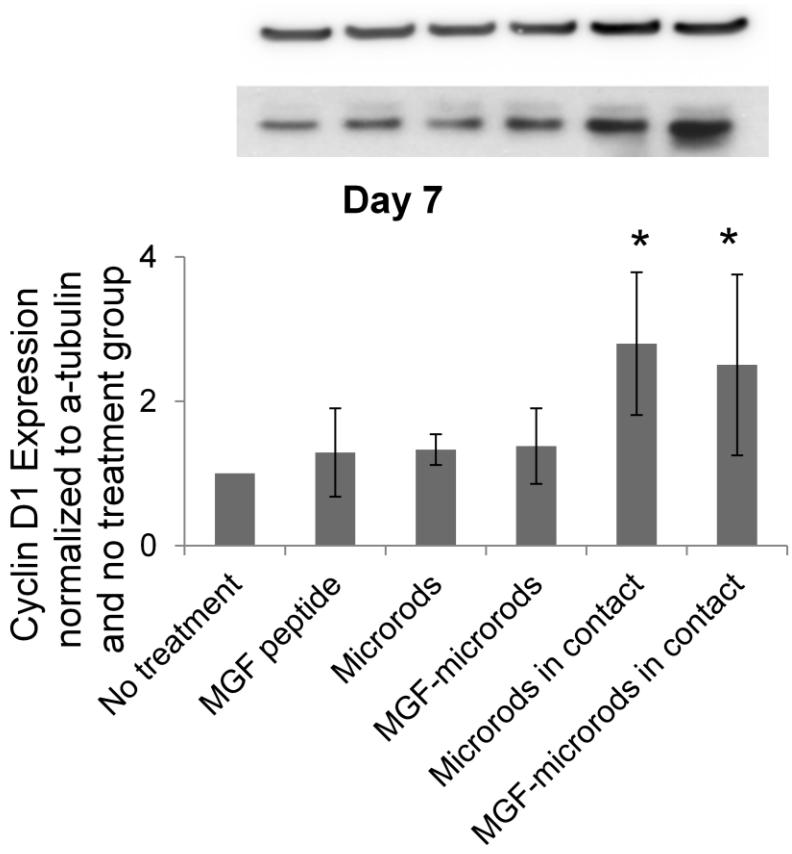

Figure 6.6 C2C12 skeletal myoblasts' cyclin D1 protein expression. Bars indicate standard deviation and (*) indicates $p < 0.05$ compared to control.

Chapter 7. Conclusion and Future Directions

Conclusion

The microdevices developed for this dissertation offer exciting potential for future applications in the fields of cell mechanobiology, tissue engineering, drug delivery and regenerative therapy. This research was focused on the development of discrete polymeric microstructures on 2D and 3D engineered scaffolds, in particular, on analyzing the effect of physical cues on cell mechanotransduction. These studies demonstrated that micro-scale physical cues in the form of stiffness and microtopography could be used to regulate proliferation, phenotype and extracellular matrix production. Additionally, the developed biocompatible tunable microstructures can be used as injectable microscaffolds and as growth factor delivery devices to support tissue regeneration. Together, the results of this work indicate that injectable micro-scale microstructures can support tissue regeneration by influencing cell proliferation and extracellular matrix remodeling *in vitro* and *in vivo*. The results presented in this work could provide researchers with future transplantation technologies which can improve clinical outcomes.

Future Directions

There are many directions that can be taken not only to improve the potential of these microdevices as a therapeutic platform, but also as an in vitro system to study cell behavior or to create engineered tissues. One goal would be to be able to align the microrods at will to investigate mechanobiology questions or to help create organized tissues in vitro. Another goal is to create biodegradable platform therapies for tissue regeneration where the biodegradation of the material occurs in a period of time that allows for the new tissue to grow. The material properties allow for easy conjugation with other materials or proteins that could result on future studies on cell behavior or other in vivo applications.

References

1. Thom, T., *et al.* Heart disease and stroke statistics--2006 update: a report from the American Heart Association Statistics Committee and Stroke Statistics Subcommittee. *Circulation* **113**, e85-151 (2006).
2. Naghavi, M., *et al.* From vulnerable plaque to vulnerable patient: a call for new definitions and risk assessment strategies: Part I. *Circulation* **108**, 1664-1672 (2003).
3. Thygesen, K., Alpert, J.S. & White, H.D. Universal definition of myocardial infarction. *J Am Coll Cardiol* **50**, 2173-2195 (2007).
4. Alpert, J.S., Thygesen, K., Antman, E. & Bassand, J.P. Myocardial infarction redefined--a consensus document of The Joint European Society of Cardiology/American College of Cardiology Committee for the redefinition of myocardial infarction. *J Am Coll Cardiol* **36**, 959-969 (2000).
5. Murry, C.E., Reinecke, H. & Pabon, L.M. Regeneration gaps: observations on stem cells and cardiac repair. *J Am Coll Cardiol* **47**, 1777-1785 (2006).
6. Brown, R.D., Ambler, S.K., Mitchell, M.D. & Long, C.S. The cardiac fibroblast: therapeutic target in myocardial remodeling and failure. *Annu Rev Pharmacol Toxicol* **45**, 657-687 (2005).
7. Mann, D.L. Mechanisms and models in heart failure: A combinatorial approach. *Circulation* **100**, 999-1008 (1999).
8. Cleutjens, J.P., Kandala, J.C., Guarda, E., Guntaka, R.V. & Weber, K.T. Regulation of collagen degradation in the rat myocardium after infarction. *J Mol Cell Cardiol* **27**, 1281-1292 (1995).
9. Sun, Y., Zhang, J.Q., Zhang, J. & Lamparter, S. Cardiac remodeling by fibrous tissue after infarction in rats. *J Lab Clin Med* **135**, 316-323 (2000).
10. Willems, I.E., Havenith, M.G., De Mey, J.G. & Daemen, M.J. The alpha-smooth muscle actin-positive cells in healing human myocardial scars. *Am J Pathol* **145**, 868-875 (1994).
11. Cleutjens, J.P., Verluyten, M.J., Smiths, J.F. & Daemen, M.J. Collagen remodeling after myocardial infarction in the rat heart. *Am J Pathol* **147**, 325-338 (1995).
12. Iyengar, P., *et al.* Adipocyte-derived collagen VI affects early mammary tumor progression in vivo, demonstrating a critical interaction in the tumor/stroma microenvironment. *J Clin Invest* **115**, 1163-1176 (2005).
13. Naugle, J.E., *et al.* Type VI collagen induces cardiac myofibroblast differentiation: implications for postinfarction remodeling. *Am J Physiol Heart Circ Physiol* **290**, H323-330 (2006).
14. Sherman-Baust, C.A., *et al.* Remodeling of the extracellular matrix through overexpression of collagen VI contributes to cisplatin resistance in ovarian cancer cells. *Cancer Cell* **3**, 377-386 (2003).
15. Mollnau, H., Munkel, B. & Schaper, J. Collagen VI in the extracellular matrix of normal and failing human myocardium. *Herz* **20**, 89-94 (1995).
16. Berry, M.F., *et al.* Mesenchymal stem cell injection after myocardial infarction improves myocardial compliance. *Am J Physiol Heart Circ Physiol* **290**, H2196-2203 (2006).
17. Beltrami, A.P., *et al.* Adult cardiac stem cells are multipotent and support myocardial regeneration. *Cell* **114**, 763-776 (2003).
18. Bearzi, C., *et al.* Human cardiac stem cells. *Proc Natl Acad Sci U S A* **104**, 14068-14073 (2007).

19. Urbanek, K., *et al.* Myocardial regeneration by activation of multipotent cardiac stem cells in ischemic heart failure. *Proc Natl Acad Sci U S A* **102**, 8692-8697 (2005).
20. Anversa, P., Kajstura, J., Leri, A. & Bolli, R. Life and death of cardiac stem cells: a paradigm shift in cardiac biology. *Circulation* **113**, 1451-1463 (2006).
21. Durrani, S., Konoplyannikov, M., Ashraf, M. & Haider, K.H. Skeletal myoblasts for cardiac repair. *Regen Med* **5**, 919-932 (2010).
22. Malliaras, K. & Marban, E. Cardiac cell therapy: where we've been, where we are, and where we should be headed. *Br Med Bull* **98**, 161-185 (2011).
23. Strauer, B.E. & Steinhoff, G. 10 years of intracoronary and intramyocardial bone marrow stem cell therapy of the heart: from the methodological origin to clinical practice. *J Am Coll Cardiol* **58**, 1095-1104 (2011).
24. Zhang, F. & Pasumarthi, K.B. Embryonic stem cell transplantation: promise and progress in the treatment of heart disease. *BioDrugs* **22**, 361-374 (2008).
25. Zhang, J., *et al.* Functional cardiomyocytes derived from human induced pluripotent stem cells. *Circ Res* **104**, e30-41 (2009).
26. Christman, K.L. & Lee, R.J. Biomaterials for the treatment of myocardial infarction. *J Am Coll Cardiol* **48**, 907-913 (2006).
27. Wang, H., Zhou, J., Liu, Z. & Wang, C. Injectable cardiac tissue engineering for the treatment of myocardial infarction. *J Cell Mol Med* **14**, 1044-1055 (2010).
28. Tee, R., Lokmic, Z., Morrison, W.A. & Dilley, R.J. Strategies in cardiac tissue engineering. *ANZ J Surg* **80**, 683-693 (2010).
29. Vunjak-Novakovic, G., Lui, K.O., Tandon, N. & Chien, K.R. Bioengineering heart muscle: a paradigm for regenerative medicine. *Annu Rev Biomed Eng* **13**, 245-267 (2011).
30. Formiga, F.R., *et al.* Angiogenic therapy for cardiac repair based on protein delivery systems. *Heart Fail Rev* (2011).
31. Madonna, R. & De Caterina, R. Stem cells and growth factor delivery systems for cardiovascular disease. *J Biotechnol* **154**, 291-297 (2011).
32. Voldman, J., Gray, M.L. & Schmidt, M.A. Microfabrication in biology and medicine. *Annual Review of Biomedical Engineering* **1**, 401-425 (1999).
33. Langer, R. & Vacanti, J.P. Tissue engineering. *Science* **260**, 920-926 (1993).
34. Yurchenco, P.D., Birk, D.E. & Mecham, R.P. (eds.). *Extracellular Matrix Assembly and Structure* 468 (Academic Press, Inc., San Diego, 1994).
35. Gumbiner, B.M. Cell adhesion: the molecular basis of tissue architecture and morphogenesis. *Cell* **84**, 345-357 (1996).
36. Raines, E.W. The extracellular matrix can regulate vascular cell migration, proliferation, and survival: relationships to vascular disease. *Int J Exp Pathol* **81**, 173-182 (2000).
37. Engler, A.J., Sen, S., Sweeney, H.L. & Discher, D.E. Matrix elasticity directs stem cell lineage specification. *Cell* **126**, 677-689 (2006).
38. Gray, D.S., Tien, J. & Chen, C.S. Repositioning of cells by mechanotaxis on surfaces with micropatterned Young's modulus. *J Biomed Mater Res A* **66**, 605-614 (2003).
39. Borenstein, J.T., *et al.* Microfabrication of three-dimensional engineered scaffolds. *Tissue Eng* **13**, 1837-1844 (2007).
40. Choi, N.W., *et al.* Microfluidic scaffolds for tissue engineering. *Nat Mater* **6**, 908-915 (2007).

41. Ryu, W., *et al.* The construction of three-dimensional micro-fluidic scaffolds of biodegradable polymers by solvent vapor based bonding of micro-molded layers. *Biomaterials* **28**, 1174-1184 (2007).
42. Lim, J.Y. & Donahue, H.J. Cell sensing and response to micro- and nanostructured surfaces produced by chemical and topographic patterning. *Tissue Engineering* **13**, 1879-1891 (2007).
43. Khademhosseini, A., Langer, R., Borenstein, J. & Vacanti, J.P. Microscale technologies for tissue engineering and biology. *Proceedings of the National Academy of Sciences of the United States of America* **103**, 2480-2487 (2006).
44. Jung, D.R., *et al.* Topographical and physicochemical modification of material surface to enable patterning of living cells. *Critical Reviews in Biotechnology* **21**, 111-154 (2001).
45. Chen, C.S., Mrksich, M., Huang, S., Whitesides, G.M. & Ingber, D.E. Geometric control of cell life and death. *Science* **276**, 1425-1428 (1997).
46. Khademhosseini, A., Langer, R., Borenstein, J. & Vacanti, J.P. Microscale technologies for tissue engineering and biology. *Proc Natl Acad Sci U S A* **103**, 2480-2487 (2006).
47. Champion, J.A., Katare, Y.K. & Mitragotri, S. Particle shape: a new design parameter for micro- and nanoscale drug delivery carriers. *J Control Release* **121**, 3-9 (2007).
48. Champion, J.A. & Mitragotri, S. Role of target geometry in phagocytosis. *Proc Natl Acad Sci U S A* **103**, 4930-4934 (2006).
49. Martin, F., *et al.* Tailoring width of microfabricated nanochannels to solute size can be used to control diffusion kinetics. *J Control Release* **102**, 123-133 (2005).
50. Desai, T.A., West, T., Cohen, M., Boiarski, T. & Rampersaud, A. Nanoporous microsystems for islet cell replacement. *Advanced Drug Delivery Reviews* **56**, 1661-1673 (2004).
51. Ainslie, K.M., Sharma, G., Dyer, M.A., Grimes, C.A. & Pishko, M.V. Attenuation of protein adsorption on static and oscillating magnetostrictive nanowires. *Nano Letters* **5**, 1852-1856 (2005).
52. Ferrara, L.A., *et al.* An in vivo biocompatibility assessment of MEMS materials for spinal fusion monitoring. *Biomedical Microdevices* **5**, 297-302 (2003).
53. Steeves, C.A., *et al.* Membrane thickness design of implantable bio-MEMS sensors for the in-situ monitoring of blood flow. *Journal of Materials Science-Materials in Medicine* **18**, 25-37 (2007).
54. Desai, T.A., Hansford, D. & Ferrari, M. Characterization of micromachined silicon membranes for immunoisolation and bioseparation applications. *Journal of Membrane Science* **159**, 221-231 (1999).
55. Ma, B., *et al.* A PZT insulin pump integrated with a silicon microneedle array for transdermal drug delivery. *Microfluidics and Nanofluidics* **2**, 417-423 (2006).
56. Santini, J.T., Jr., Cima, M.J. & Langer, R. A controlled-release microchip. *Nature* **397**, 335-338 (1999).
57. Campbell, P.K., Jones, K.E., Huber, R.J., Horch, K.W. & Normann, R.A. A Silicon-Based, 3-Dimensional Neural Interface - Manufacturing Processes for an Intracortical Electrode Array. *Ieee Transactions on Biomedical Engineering* **38**, 758-768 (1991).
58. Chow, A.Y., *et al.* Implantation of silicon chip microphotodiode arrays into the cat subretinal space. *Ieee Transactions on Neural Systems and Rehabilitation Engineering* **9**, 86-95 (2001).

59. Santiesteban, F.M.M., Swanson, S.D., Noll, D.C. & Anderson, D.J. Magnetic resonance compatibility of multichannel silicon microelectrode systems for neural recording and stimulation: Design criteria, tests, and recommendations. *Ieee Transactions on Biomedical Engineering* **53**, 547-558 (2006).
60. Lillis, B., *et al.* Microporous silicon and biosensor development: structural analysis, electrical characterisation and biocapacity evaluation. *Biosensors & Bioelectronics* **21**, 282-292 (2005).
61. Park, I.Y., Li, Z.Y., Li, X.M., Pisano, A.P. & Williams, R.S. Towards the silicon nanowire-based sensor for intracellular biochemical detection. *Biosensors & Bioelectronics* **22**, 2065-2070 (2007).
62. De Stefano, L., *et al.* Porous silicon-based optical microsensor for the detection of L-glutamine. *Biosensors & Bioelectronics* **21**, 1664-1667 (2006).
63. Balarin, A., *et al.* Structure and optical properties of porous silicon prepared on thin epitaxial silicon layer on silicon substrates. *Journal of Molecular Structure* **834**, 465-470 (2007).
64. Chambon, E., Florentin, E., Torchynska, T., Gonzalez-Hernandez, J. & Vorobiev, Y. Optical properties of porous silicon surface. *Microelectronics Journal* **36**, 514-517 (2005).
65. Jelinek, I., *et al.* Nanostructured porous silicon - Optical properties, surface modification and sensor applications. *Chimia* **59**, 222-225 (2005).
66. Natarajan, B., Ramakrishnan, V., Vasu, V. & Ramamurthy, S. Structural and photoluminescence properties of porous silicon: Effect of HF concentration. *Surface Review and Letters* **13**, 351-356 (2006).
67. Peng, K.Q., *et al.* Fabrication of single-crystalline silicon nanowires by scratching a silicon surface with catalytic metal particles. *Advanced Functional Materials* **16**, 387-394 (2006).
68. Reddy, R.R.K., Chadha, A. & Bhattacharya, E. Porous silicon based potentiometric triglyceride biosensor. *Biosensors & Bioelectronics* **16**, 313-317 (2001).
69. Ainslie, K.M., Tao, S.L., Popat, K.C. & Desai, T.A. In vitro Immunogenicity of Silicon Based Micro- and Nano-structured Surfaces. *ACS Nano* **2**, 1076–1084 (2008).
70. Coltro, W.K., Piccin, E., Fracassi da Silva, J.A., Lucio do Lago, C. & Carrilho, E. A toner-mediated lithographic technology for rapid prototyping of glass microchannels. *Lab Chip* **7**, 931-934 (2007).
71. Nagarajan, S., Bosworth, J.K., Ober, C.K., Russell, T.P. & Watkins, J.J. Simple Fabrication of Micropatterned Mesoporous Silica Films Using Photoacid Generators in Block Copolymers. *Chem. Mater.* (Epub: 2007).
72. Brodbeck, W.G., *et al.* Biomaterial surface chemistry dictates adherent monocyte/macrophage cytokine expression in vitro. *Cytokine* **18**, 311-319 (2002).
73. Lu, Y. & Chen, S.C. Micro and nano-fabrication of biodegradable polymers for drug delivery. *Adv Drug Deliv Rev* **56**, 1621-1633 (2004).
74. Weibel, D.B., Diluzio, W.R. & Whitesides, G.M. Microfabrication meets microbiology. *Nat Rev Microbiol* **5**, 209-218 (2007).
75. Xia, Y. & Whitesides, G.M. Soft Lithography. *Angew. Chem. Ed. Engl.* **37**, 550-575 (1998).

76. Takayama, S. Patterning of Cells and Their Environment. in *Principles of Tissue Engineering, 2nd Edition* (eds. Lanza, R.P., Langer, R. & Vacanti, J.) 209-220 (Academic Press, 2000).
77. Madou, M. *Fundamentals of Microfabrication: The Science of Miniaturization*, (CRC Press, New York, NY, 2002).
78. Chaudhury, M.K. & Whitesides, G.M. Direct measurement of interfacial interactions between semispherical lenses and flat sheets of polydimethylsiloxane and their chemical derivatives. *Langmuir* **7**, 1013-1025 (1991).
79. Chaudhury, M.K. & Whitesides, G.M. Correlation between surface free energy and surface constitution. *Science* **255**(1992).
80. Kane, R.S., Takayama, S., Ostuni, E., Ingber, D.E. & Whitesides, G.M. Patterning proteins and cells using soft lithography. *Biomaterials* **20**, 2363-2376 (1999).
81. Takayama, S., *et al.* Patterning cells and their environments using multiple laminar fluid flows in capillary networks. *Proc Natl Acad Sci U S A* **96**, 5545-5548 (1999).
82. Kenis, P.J., *et al.* Fabrication inside microchannels using fluid flow. *Acc Chem Res* **33**, 841-847 (2000).
83. Tan, W. & Desai, T.A. Microscale multilayer cocultures for biomimetic blood vessels. *J Biomed Mater Res A* **72**, 146-160 (2005).
84. Sarkar, S., Dadhania, M., Rourke, P., Desai, T.A. & Wong, J.Y. Vascular tissue engineering: microtextured scaffold templates to control organization of vascular smooth muscle cells and extracellular matrix. *Acta Biomaterialia* **1**, 93-100 (2005).
85. Sarkar, S., Lee, G.Y., Wong, J.Y. & Desai, T.A. Development and characterization of a porous micro-patterned scaffold for vascular tissue engineering applications. *Biomaterials* **27**, 4775-4782 (2006).
86. Tan, W. & Desai, T.A. Layer-by-layer microfluidics for biomimetic three-dimensional structures. *Biomaterials* **25**, 1355-1364 (2004).
87. Sharma, S., Tan, W. & Desai, T.A. Improving the integrity of three-dimensional vascular patterns by poly(ethylene glycol) conjugation. *Bioconjug Chem* **16**, 18-22 (2005).
88. Kulkarni, S.S., Orth, R., Ferrari, M. & Moldovan, N.I. Micropatterning of endothelial cells by guided stimulation with angiogenic factors. *Biosensors & Bioelectronics* **19**, 1401-1407 (2004).
89. Parker, K.K. & Ingber, D.E. Extracellular matrix, mechanotransduction and structural hierarchies in heart tissue engineering. *Philos Trans R Soc Lond B Biol Sci* **362**, 1267-1279 (2007).
90. Khademhosseini, A., *et al.* Microfluidic patterning for fabrication of contractile cardiac organoids. *Biomed Microdevices* **9**, 149-157 (2007).
91. Deutsch, J., Motiagh, D., Russell, B. & Desai, T.A. Fabrication of microtextured membranes for cardiac myocyte attachment and orientation. *Journal of Biomedical Materials Research* **53**, 267-275 (2000).
92. Motlagh, D., Senyo, S., Desai, T.A. & Russell, B. Micro-groove dimensions affect orientation and cell-cell contact. *Journal of Molecular and Cellular Cardiology* **34**, A32-A32 (2002).
93. Boateng, S.Y., *et al.* Inhibition of fibroblast proliferation in cardiac myocyte cultures by surface microtopography. *American Journal of Physiology-Cell Physiology* **285**, C171-C182 (2003).

94. Norman, J.J., Collins, J.M., Sharma, S., Russell, B. & Desai, T.A. Microstructures in 3D Biological Gels Affect Cell Proliferation. *Tissue Eng* (2007).
95. West-Mays, J.A. & Dwivedi, D.J. The keratocyte: corneal stromal cell with variable repair phenotypes. *Int J Biochem Cell Biol* **38**, 1625-1631 (2006).
96. Teixeira, A.I., Abrams, G.A., Bertics, P.J., Murphy, C.J. & Nealey, P.F. Epithelial contact guidance on well-defined micro- and nanostructured substrates. *J Cell Sci* **116**, 1881-1892 (2003).
97. Teixeira, A.I., *et al.* The effect of environmental factors on the response of human corneal epithelial cells to nanoscale substrate topography. *Biomaterials* **27**, 3945-3954 (2006).
98. Berson, E.L. Retinitis pigmentosa. The Friedenwald Lecture. *Invest Ophthalmol Vis Sci* **34**, 1659-1676 (1993).
99. Sieving, P.A., *et al.* Ciliary neurotrophic factor (CNTF) for human retinal degeneration: phase I trial of CNTF delivered by encapsulated cell intraocular implants. *Proc Natl Acad Sci U S A* **103**, 3896-3901 (2006).
100. Dutt, K. & Cao, Y. Engineering Retina from Human Retinal Progenitors (Cell Lines). *Tissue Eng Part A* (2008).
101. Tao, S., *et al.* Survival, migration and differentiation of retinal progenitor cells transplanted on micro-machined poly(methyl methacrylate) scaffolds to the subretinal space. *Lab Chip* **7**, 695-701 (2007).
102. Neeley, W.L., *et al.* A microfabricated scaffold for retinal progenitor cell grafting. *Biomaterials* **29**, 418-426 (2008).
103. Tilles, A.W., Berthiaume, F., Yarmush, M.L., Tompkins, R.G. & Toner, M. Bioengineering of liver assist devices. *J Hepatobiliary Pancreat Surg* **9**, 686-696 (2002).
104. Bhatia, S.N., Balis, U.J., Yarmush, M.L. & Toner, M. Microfabrication of hepatocyte/fibroblast co-cultures: role of homotypic cell interactions. *Biotechnol Prog* **14**, 378-387 (1998).
105. Powers, K.W., *et al.* Research strategies for safety evaluation of nanomaterials. Part VI. Characterization of nanoscale particles for toxicological evaluation. *Toxicol Sci* **90**, 296-303 (2006).
106. Kaihara, S., *et al.* Silicon micromachining to tissue engineer branched vascular channels for liver fabrication. *Tissue Eng* **6**, 105-117 (2000).
107. Wang, J., *et al.* Microfluidics: A new cosset for neurobiology. *Lab Chip* **9**, 644-652 (2009).
108. Huang, Y.C. & Huang, Y.Y. Biomaterials and strategies for nerve regeneration. *Artif Organs* **30**, 514-522 (2006).
109. Kleinfeld, D., Kahler, K.H. & Hockberger, P.E. Controlled outgrowth of dissociated neurons on patterned substrates. *J Neurosci* **8**, 4098-4120 (1988).
110. Oliva, A.A., Jr., James, C.D., Kingman, C.E., Craighead, H.G. & Banker, G.A. Patterning axonal guidance molecules using a novel strategy for microcontact printing. *Neurochem Res* **28**, 1639-1648 (2003).
111. Taylor, A.M., *et al.* A microfluidic culture platform for CNS axonal injury, regeneration and transport. *Nat Methods* **2**, 599-605 (2005).
112. Miller, C., Jeftinija, S. & Mallapragada, S. Micropatterned Schwann cell-seeded biodegradable polymer substrates significantly enhance neurite alignment and outgrowth. *Tissue Eng* **7**, 705-715 (2001).

113. Schmalenberg, K.E. & Uhrich, K.E. Micropatterned polymer substrates control alignment of proliferating Schwann cells to direct neuronal regeneration. *Biomaterials* **26**, 1423-1430 (2005).
114. Thompson, D.M. & Buettner, H.M. Oriented Schwann cell monolayers for directed neurite outgrowth. *Ann Biomed Eng* **32**, 1120-1130 (2004).
115. Khademhosseini, A. & Langer, R. Microengineered hydrogels for tissue engineering. *Biomaterials* **28**, 5087-5092 (2007).
116. Koh, W.G., Itle, L.J. & Pishko, M.V. Molding of hydrogel microstructures to create multiphenotype cell microarrays. *Anal Chem* **75**, 5783-5789 (2003).
117. Koh, W.G., Revzin, A. & Pishko, M.V. Poly(ethylene glycol) hydrogel microstructures encapsulating living cells. *Langmuir* **18**, 2459-2462 (2002).
118. Liu Tsang, V., *et al.* Fabrication of 3D hepatic tissues by additive photopatterning of cellular hydrogels. *Faseb J* **21**, 790-801 (2007).
119. Wong, A.P., Perez-Castillejos, R., Christopher Love, J. & Whitesides, G.M. Partitioning microfluidic channels with hydrogel to construct tunable 3-D cellular microenvironments. *Biomaterials* **29**, 1853-1861 (2008).
120. Itle, L.J., Koh, W.G. & Pishko, M.V. Hepatocyte viability and protein expression within hydrogel microstructures. *Biotechnol Prog* **21**, 926-932 (2005).
121. Zguris, J.C., Itle, L.J., Hayes, D. & Pishko, M.V. Microreactor microfluidic systems with human microsomes and hepatocytes for use in metabolite studies. *Biomed Microdevices* **7**, 117-125 (2005).
122. McBeath, R., Pirone, D.M., Nelson, C.M., Bhadriraju, K. & Chen, C.S. Cell shape, cytoskeletal tension, and RhoA regulate stem cell lineage commitment. *Dev Cell* **6**, 483-495 (2004).
123. Khetani, S.R. & Bhatia, S.N. Microscale culture of human liver cells for drug development. *Nat Biotechnol* **26**, 120-126 (2008).
124. Ulrich, T.A., de Juan Pardo, E.M. & Kumar, S. The mechanical rigidity of the extracellular matrix regulates the structure, motility, and proliferation of glioma cells. *Cancer Res* **69**, 4167-4174 (2009).
125. Curtis, M.W., Sharma, S., Desai, T.A. & Russell, B. Hypertrophy, gene expression, and beating of neonatal cardiac myocytes are affected by microdomain heterogeneity in 3D. *Biomed Microdevices* (2010).
126. Gilbert, P.M., *et al.* Substrate Elasticity Regulates Skeletal Muscle Stem Cell Self-Renewal in Culture. *Science* (2010).
127. Kilian, K.A., Bugarija, B., Lahn, B.T. & Mrksich, M. Geometric cues for directing the differentiation of mesenchymal stem cells. *Proc Natl Acad Sci U S A* **107**, 4872-4877 (2010).
128. Steedman, M.R., Tao, S.L., Klassen, H. & Desai, T.A. Enhanced differentiation of retinal progenitor cells using microfabricated topographical cues. *Biomed Microdevices* **12**, 363-369 (2010).
129. Wan, L.Q., *et al.* Geometric control of human stem cell morphology and differentiation. *Integr Biol (Camb)* **2**, 346-353 (2010).
130. Butcher, D.T., Alliston, T. & Weaver, V.M. A tense situation: forcing tumour progression. *Nat Rev Cancer* **9**, 108-122 (2009).

131. Nelson, C.M. & Bissell, M.J. Of extracellular matrix, scaffolds, and signaling: tissue architecture regulates development, homeostasis, and cancer. *Annu Rev Cell Dev Biol* **22**, 287-309 (2006).
132. Reilly, G.C. & Engler, A.J. Intrinsic extracellular matrix properties regulate stem cell differentiation. *J Biomech* (2009).
133. Discher, D.E., Janmey, P. & Wang, Y.L. Tissue cells feel and respond to the stiffness of their substrate. *Science* **310**, 1139-1143 (2005).
134. Burlew, B.S. & Weber, K.T. Cardiac fibrosis as a cause of diastolic dysfunction. *Herz* **27**, 92-98 (2002).
135. Levental, K.R., *et al.* Matrix crosslinking forces tumor progression by enhancing integrin signaling. *Cell* **139**, 891-906 (2009).
136. Breitbach, M., *et al.* Potential risks of bone marrow cell transplantation into infarcted hearts. *Blood* **110**, 1362-1369 (2007).
137. Boateng, S.Y., *et al.* Inhibition of fibroblast proliferation in cardiac myocyte cultures by surface microtopography. *Am J Physiol Cell Physiol* **285**, C171-182 (2003).
138. Brown, X.Q., Ookawa, K. & Wong, J.Y. Evaluation of polydimethylsiloxane scaffolds with physiologically-relevant elastic moduli: interplay of substrate mechanics and surface chemistry effects on vascular smooth muscle cell response. *Biomaterials* **26**, 3123-3129 (2005).
139. Kim, D.H., *et al.* Guided three-dimensional growth of functional cardiomyocytes on polyethylene glycol nanostructures. *Langmuir* **22**, 5419-5426 (2006).
140. Nelson, C.M., *et al.* Emergent patterns of growth controlled by multicellular form and mechanics. *Proc Natl Acad Sci U S A* **102**, 11594-11599 (2005).
141. Norman, J.J., Collins, J.M., Sharma, S., Russell, B. & Desai, T.A. Microstructures in 3D biological gels affect cell proliferation. *Tissue Eng Part A* **14**, 379-390 (2008).
142. Pelham, R.J., Jr. & Wang, Y. Cell locomotion and focal adhesions are regulated by substrate flexibility. *Proc Natl Acad Sci U S A* **94**, 13661-13665 (1997).
143. Peyton, S.R., Raub, C.B., Keschrumrus, V.P. & Putnam, A.J. The use of poly(ethylene glycol) hydrogels to investigate the impact of ECM chemistry and mechanics on smooth muscle cells. *Biomaterials* **27**, 4881-4893 (2006).
144. Thakar, R.G., *et al.* Contractility-dependent modulation of cell proliferation and adhesion by microscale topographical cues. *Small* **4**, 1416-1424 (2008).
145. Patel, A.A., *et al.* Biophysical mechanisms of single-cell interactions with microtopographical cues. *Biomed Microdevices* **12**, 287-296 (2010).
146. Bouffard, N.A., *et al.* Tissue stretch decreases soluble TGF-beta1 and type-1 procollagen in mouse subcutaneous connective tissue: evidence from ex vivo and in vivo models. *J Cell Physiol* **214**, 389-395 (2008).
147. Langevin, H.M., Bouffard, N.A., Badger, G.J., Iatridis, J.C. & Howe, A.K. Dynamic fibroblast cytoskeletal response to subcutaneous tissue stretch ex vivo and in vivo. *Am J Physiol Cell Physiol* **288**, C747-756 (2005).
148. Poobalarahi, F., Baicu, C.F. & Bradshaw, A.D. Cardiac myofibroblasts differentiated in 3D culture exhibit distinct changes in collagen I production, processing, and matrix deposition. *Am J Physiol Heart Circ Physiol* **291**, H2924-2932 (2006).
149. Wang, J., Seth, A. & McCulloch, C.A. Force regulates smooth muscle actin in cardiac fibroblasts. *Am J Physiol Heart Circ Physiol* **279**, H2776-2785 (2000).

150. Bryant, J.E., *et al.* Cardiac myofibroblast differentiation is attenuated by alpha(3) integrin blockade: potential role in post-MI remodeling. *J Mol Cell Cardiol* **46**, 186-192 (2009).
151. Shamhart, P.E. & Meszaros, J.G. Non-fibrillar collagens: key mediators of post-infarction cardiac remodeling? *J Mol Cell Cardiol* **48**, 530-537 (2010).
152. Camelliti, P., Borg, T.K. & Kohl, P. Structural and functional characterisation of cardiac fibroblasts. *Cardiovasc Res* **65**, 40-51 (2005).
153. Paz, Z. & Shoenfeld, Y. Antifibrosis: To Reverse the Irreversible. *Clin Rev Allergy Immunol* (2009).
154. Polyakova, V., *et al.* Fibrosis in endstage human heart failure: Severe changes in collagen metabolism and MMP/TIMP profiles. *Int J Cardiol* (2010).
155. Hinz, B. Formation and function of the myofibroblast during tissue repair. *J Invest Dermatol* **127**, 526-537 (2007).
156. Sun, Y., Kiani, M.F., Postlethwaite, A.E. & Weber, K.T. Infarct scar as living tissue. *Basic Res Cardiol* **97**, 343-347 (2002).
157. Sun, Y. & Weber, K.T. Infarct scar: a dynamic tissue. *Cardiovasc Res* **46**, 250-256 (2000).
158. Deutsch, J., Motlagh, D., Russell, B. & Desai, T.A. Fabrication of microtextured membranes for cardiac myocyte attachment and orientation. *J Biomed Mater Res* **53**, 267-275 (2000).
159. Collins, J.M., Ayala, P., Desai, T., Russell, B. Three Dimensional Culture with Stiff Microstructures Increases Proliferation and Slows Osteogenic Differentiation of Human Mesenchymal Stem Cells. *Small* (2009).
160. Bhadriraju, K., *et al.* Activation of ROCK by RhoA is regulated by cell adhesion, shape, and cytoskeletal tension. *Exp Cell Res* **313**, 3616-3623 (2007).
161. Biehl, J.K., Yamanaka, S., Desai, T.A., Boheler, K.R. & Russell, B. Proliferation of mouse embryonic stem cell progeny and the spontaneous contractile activity of cardiomyocytes are affected by microtopography. *Dev Dyn* **238**, 1964-1973 (2009).
162. Riento, K. & Ridley, A.J. Rocks: multifunctional kinases in cell behaviour. *Nat Rev Mol Cell Biol* **4**, 446-456 (2003).
163. Totsukawa, G., *et al.* Distinct roles of MLCK and ROCK in the regulation of membrane protrusions and focal adhesion dynamics during cell migration of fibroblasts. *J Cell Biol* **164**, 427-439 (2004).
164. Choma, D.P., Pumiglia, K. & DiPersio, C.M. Integrin alpha3beta1 directs the stabilization of a polarized lamellipodium in epithelial cells through activation of Rac1. *J Cell Sci* **117**, 3947-3959 (2004).
165. Brzoska, E., Bello, V., Darribere, T. & Moraczewski, J. Integrin alpha3 subunit participates in myoblast adhesion and fusion in vitro. *Differentiation* **74**, 105-118 (2006).
166. Borok, Z. Role for alpha3 integrin in EMT and pulmonary fibrosis. *J Clin Invest* **119**, 7-10 (2009).
167. Fazel, S., *et al.* Cardioprotective c-kit+ cells are from the bone marrow and regulate the myocardial balance of angiogenic cytokines. *J Clin Invest* **116**, 1865-1877 (2006).
168. Paul, D., Samuel, S.M. & Maulik, N. Mesenchymal stem cell: present challenges and prospective cellular cardiomyoplasty approaches for myocardial regeneration. *Antioxid Redox Signal* **11**, 1841-1855 (2009).

169. Kawamoto, A., *et al.* CD34-positive cells exhibit increased potency and safety for therapeutic neovascularization after myocardial infarction compared with total mononuclear cells. *Circulation* **114**, 2163-2169 (2006).
170. Discher, D.E., Mooney, D.J. & Zandstra, P.W. Growth factors, matrices, and forces combine and control stem cells. *Science* **324**, 1673-1677 (2009).
171. Ghosh, K., *et al.* Cell adaptation to a physiologically relevant ECM mimic with different viscoelastic properties. *Biomaterials* **28**, 671-679 (2007).
172. Le Bousse-Kerdiles, M.C., Martyre, M.C. & Samson, M. Cellular and molecular mechanisms underlying bone marrow and liver fibrosis: a review. *Eur Cytokine Netw* **19**, 69-80 (2008).
173. Aneja, A., Tang, W.H., Bansilal, S., Garcia, M.J. & Farkouh, M.E. Diabetic cardiomyopathy: insights into pathogenesis, diagnostic challenges, and therapeutic options. *Am J Med* **121**, 748-757 (2008).
174. De Wever, O., Demetter, P., Mareel, M. & Bracke, M. Stromal myofibroblasts are drivers of invasive cancer growth. *Int J Cancer* **123**, 2229-2238 (2008).
175. Collins, J.M., Ayala, P., Desai, T.A. & Russell, B. Three-Dimensional Culture with Stiff Microstructures Increases Proliferation and Slows Osteogenic Differentiation of Human Mesenchymal Stem Cells. *Small* (2009).
176. Kleinman, H.K., *et al.* Basement membrane complexes with biological activity. *Biochemistry* **25**, 312-318 (1986).
177. Kleinman, H.K., *et al.* Isolation and characterization of type IV procollagen, laminin, and heparan sulfate proteoglycan from the EHS sarcoma. *Biochemistry* **21**, 6188-6193 (1982).
178. Diramio, J.A., Kisaalita, W.S., Majetich, G.F. & Shimkus, J.M. Poly(ethylene glycol) methacrylate/dimethacrylate hydrogels for controlled release of hydrophobic drugs. *Biotechnol Prog* **21**, 1281-1288 (2005).
179. Pfister, P.M., Wendlandt, M., Neuenschwander, P. & Suter, U.W. Surface-textured PEG-based hydrogels with adjustable elasticity: Synthesis and characterization. *Biomaterials* **28**, 567-575 (2007).
180. Boontheekul, T., Hill, E.E., Kong, H.J. & Mooney, D.J. Regulating myoblast phenotype through controlled gel stiffness and degradation. *Tissue Eng* **13**, 1431-1442 (2007).
181. Costa-Pinto, A.R., *et al.* Adhesion, proliferation, and osteogenic differentiation of a mouse mesenchymal stem cell line (BMC9) seeded on novel melt-based chitosan/polyester 3D porous scaffolds. *Tissue Eng Part A* **14**, 1049-1057 (2008).
182. Duong, H., Wu, B. & Tawil, B. Modulation of 3D fibrin matrix stiffness by intrinsic fibrinogen-thrombin compositions and by extrinsic cellular activity. *Tissue Eng Part A* **15**, 1865-1876 (2009).
183. Carver, W., Nagpal, M.L., Nachtigal, M., Borg, T.K. & Terracio, L. Collagen expression in mechanically stimulated cardiac fibroblasts. *Circ Res* **69**, 116-122 (1991).
184. Caulfield, J.B. & Janicki, J.S. Structure and function of myocardial fibrillar collagen. *Technol Health Care* **5**, 95-113 (1997).
185. Bashey, R.I., Martinez-Hernandez, A. & Jimenez, S.A. Isolation, characterization, and localization of cardiac collagen type VI. Associations with other extracellular matrix components. *Circ Res* **70**, 1006-1017 (1992).
186. Christman, K.L., Fok, H.H., Sievers, R.E., Fang, Q. & Lee, R.J. Fibrin glue alone and skeletal myoblasts in a fibrin scaffold preserve cardiac function after myocardial infarction. *Tissue Eng* **10**, 403-409 (2004).

187. Huang, N.F., Yu, J., Sievers, R., Li, S. & Lee, R.J. Injectable biopolymers enhance angiogenesis after myocardial infarction. *Tissue Eng* **11**, 1860-1866 (2005).
188. Sievers, R.E., *et al.* A model of acute regional myocardial ischemia and reperfusion in the rat. *Magn Reson Med* **10**, 172-181 (1989).
189. Doursout, M.F., *et al.* Measurement of cardiac function in conscious rats. *Ultrasound Med Biol* **27**, 195-202 (2001).
190. Litwin, S.E., *et al.* Serial echocardiographic-Doppler assessment of left ventricular geometry and function in rats with pressure-overload hypertrophy. Chronic angiotensin-converting enzyme inhibition attenuates the transition to heart failure. *Circulation* **91**, 2642-2654 (1995).
191. Yu, J., *et al.* The use of human mesenchymal stem cells encapsulated in RGD modified alginate microspheres in the repair of myocardial infarction in the rat. *Biomaterials* (2010).
192. Ayala, P., Lopez, J.I. & Desai, T.A. Microtopographical cues in 3D attenuate fibrotic phenotype and extracellular matrix deposition: implications for tissue regeneration. *Tissue Eng Part A* **16**, 2519-2527 (2010).
193. Ayala, P. & Desai, T.A. Integrin alpha3 blockade enhances microtopographical down-regulation of alpha-smooth muscle actin: role of microtopography in ECM regulation. *Integr Biol (Camb)* (2011).
194. Goldspink, G. Impairment of IGF-I gene splicing and MGF expression associated with muscle wasting. *Int J Biochem Cell Biol* **38**, 481-489 (2006).
195. Carpenter, V., *et al.* Mechano-Growth Factor Reduces Loss of Cardiac Function in Acute Myocardial Infarction. *Heart Lung Circ* (2007).
196. Collins, J.M., Goldspink, P.H. & Russell, B. Migration and proliferation of human mesenchymal stem cells is stimulated by different regions of the mechano-growth factor prohormone. *J Mol Cell Cardiol* **49**, 1042-1045 (2010).